A three dimensional level set method for two-phase electrohydrodynamics

Nabila Naz

School of Engineering and Materials Science

Queen Mary University of London

This dissertation is submitted for the degree of

Doctor of Philosophy

February 2023

I would like to dedicate this thesis to my loving family.

Declaration

I hereby declare that except where specific reference is made to the work of others, the contents of this thesis are original and have not been submitted in whole or in part for consideration for any other degree or qualification in this, or any other university. This dissertation is my own work and contains nothing which is the outcome of work done in collaboration with others, except as specified in the text and Acknowledgements.

Nabila Naz

February 2023

Acknowledgements

Completion of this PhD thesis has been an invaluable experience of my life and it would have been possible with the guidance, support and encouragement of many individuals to whom I owe a lot. I would, therefore, like to offer my sincere gratitude and appreciation to all of them.

First and foremost, I would like to take this opportunity to thank my supervisor, Prof. Yi Sui, who inspired me to become what I am today. I am very grateful to him for giving me the opportunity to work in his group, for believing in me, and above all for his heartiest cooperation throughout my PhD. His brilliant supervision and constant feedback help me a lot to progress step by step to achieve this PhD.

In addition to my supervisor, I would like to convey my gratitude to fellow colleagues in Prof. Yi Sui's group, especially to Ruixin Lu, Luoguang Zhao and Dr. Tao Lin for their valuable suggestions regarding various topic of my project. I greatly acknowledge the QMUL PhD Studentship for providing the funding to make my project and my PhD possible. I would also like to acknowledge the computational facility, Apocrita HPC cluster provided by QMUL Research-IT. http://doi.org/10.5281/zenodo.438045 and the ITS research team for their continual support. My special thanks go to Dr. Shubhadeep Mandal, Prof. Haihu Liu, Dr Ahmed Ismail and Dr. Kang Luo for sharing their comprehensive knowledge on electrohydrodynamics.

I would like to express my deepest gratitude to my entire family who have always encouraged me and provided all necessary facilities to elevate my knowledge up to this level,

and without their support and guidance, it would be impossible for me to carry out the thesis work properly.

Last but not the least, I would like to thank almighty Allah, for providing me the guidance, strength and perseverance to complete this thesis through all the trials and tribulation.

Abstract

In this thesis, we have developed a computational method for two-phase electrohydrodynamics (EHD) problem. The method is based on a three dimensional level-set method and the leaky-dielectric EHD model. Level-set method is used for modelling the interface of the two-phase flow system. The electrostatic phenomenon is dealt with the leaky dielectric-leaky dielectric fluid system. In leaky dielectric-leaky dielectric fluid system, both the fluids have small but finite electric conductivity. Upon application of the external electric field, all charges from both fluids accumulate at the interface leaving the bulk free of any charge. At first, we have validated our developed model against existing results from literature. After validation, we have implemented the developed code in a practical application of droplet sorting using non-uniform electric field known as dielectrophoresis (DEP). At present there is no existing computational method on DEP assisted droplet sorting which leads our present analysis a complete novel contribution in this field.

For validation, two classical flow cases are tested: (a) a droplet subjected to a uniform electric field; (b) a droplet subjected to both uniform electric field and shear flow. For both of the cases, results obtained from present computational method show good agreement with the existing results from literature. For droplet subjected to a uniform electric field case, depending on the conductivity (K) and permittivity(Q) ratio of the two fluids, we have obtained three types of droplet deformation namely prolate A, $(PR_A : KQ > 1)$, prolate B$(PR_B : KQ < 1)$, and oblate $(OB : KQ < 1)$ drop. The deformation parameter obtained from the present simulation are quantitatively validated against the existing analytical, numerical

and experimental results. For a droplet subjected to both uniform electric field and shear flow, we have analysed the effect of hydrodynamic capillary number, Ca (ratio of viscous force to and surface tension force) and electric capillary number Ca_E(ratio of electric stress to and surface tension force) on the droplet deformation and breakup. A phase diagram is also established as a function of Ca and Ca_E which depicts that the combined effect of electric stress and shear flow promotes the breakup of the droplet even at smaller Ca which is not possible if there is only shear flow. Results obtained from this case also show good agreement with the numerical results of existing literature.

In the second part, we computationally study the motion of an initially uncharged spherical droplet flowing through a straight rectangular channel with an orthogonal side branch, using a three-dimensional level set method. The spatially non-uniform electric field is created by placing an electrode at the bottom of the channel. We mainly focus on the sorting of the droplet without and with electric field effect as a function of different parameters of the problem namely branch flow ratio, q (ratio of the flow rate in the side branch to the flow rate in the main channel), electric capillary number Ca_E(ratio of electric stress to surface tension), different positions of the electrode, low and high flow Reynolds number Re (ratio of inertia force to and viscous force) and finally different size ratio, λ (ratio of droplet radius to half cross sectional length of the channel). In this research, we mainly investigate the path selection of the droplet when subjected to the above mentioned parameters. Depending on the intensity of the physical parameters, the droplet can flow into either the downstream main channel or it can sort into the orthogonal side branch. The sorting of a droplet is characterized by the critical branch ratio, q_c above which the droplet enters the side branch.

Without electric field, it is obtained that at low Re, the droplet favours the branch which receives higher flow rate. However, inertia has a significant effect on the path selection of droplet. When Re is increased to 20, it has been found that the droplet enters the main channel even when it receives much less flow than the side branch. For spatially non-uniform electric

field, we have considered two different intensities of electric field through the value of electric capillary number Ca_E = 0.4 and 0.9. We obtain that higher the intensity of electric field, larger the electric force which can sort the droplet at a lower value of q_c. We also analyse two electrode positions namely electrode 1 and 2. At electrode 1 position, the electrode is placed closer to the initial position of the droplet compared to the electrode 2 position. It has obtained that with both electrode positions a significant reduction of q_c is achieved. However at electrode 1 position, a greater reduction of q_c is obtained compare to electrode 2 position both at low and high inertia regime.

In addition to it, we investigate different size ratios λ = 0.2, 0.3 and 0.4, on the path selection of the droplet when electrode is placed at position 1 with Ca_E = 0.9 at high inertia regime. It is obtained that larger the value of size ratio (λ), higher the value of dielectrophoresis motion (motion of the droplet due to non-uniform electric field) which promotes the droplet sorting at side branch even at lower branch flow ratio with high inertia effect. Finally, from the present investigation we conclude that electrode at position 1 with Ca_E = 0.9 and λ = 0.4, the critical branch flow ratio is the lowest q_c which is 0.08.

The results and conclusions from the present thesis facilitate the understanding of the fundamental principles and mechanisms of electrohydrodynamics (EHD) based droplet deformation, breakup and sorting of the droplet using dielectrophoresis in microfluidic channel. Therefore present results can have potential usefulness towards the design and development of droplet-based microfluidic devices.

Table of contents

List of figures

Nomenclature

Subscripts

crit Critical state

Acronyms / Abbreviations

ALE Arbitrary Lagrangian–Eulerian

BEM Boundary Element Method

BIM Boundary integral method

CFD Computational Fluid Dynamics

DEP Dielectrophoresis

EHD Electrohydrodynamics

FADS Fluorescence Assisted Droplet Sorting

FDM Finite Difference Method

FEM Finite Element Method

FVM Finite Volume Method

IIM Immersed Interface Method

ITO Indium Tin Oxide

LBM Lattice Boltzmann Method

LD Leaky Dielectric

LES Large Eddy Simulation

nDEP Negative Dielectrophoresis

PC Perfect Conducting

pDEP Positive Dielectrophoresis

PDMS Polydimethylsiloxane

PD Perfect Dielectric

SOR Successive Over Relaxation

WAM Weighted Arithmetic Mean

Chapter 1

Introduction and Literature Review

1.1 Introduction

Electrohydrodynamics which is also known as EHD is an interdisciplinary branch of science which analyses the dynamics of electrically induced fluid flow through the coupling between electric and hydrodynamic forces. Application of electric field on a liquid droplet suspended in another medium leads to some fascinating fluid dynamics due to its ability to deformation, motion and break-up of the droplet. Several industries such as ink jet printing [11], electrospinning [51], atomization of fluids [102], biotechnology [34], material printing [19] involve the precise control of the size and morphology of the droplet when subjected to electric field. Stability of the surface of the fluid can also be maintained by applying electric force. Realizing this fact, EHD has been successfully applied for imitating gravity [47] , mixing and separation of fluids [117, 101], operation of boiling heat exchangers especially under micro-gravity or free space conditions [25, 53, 78, 79]. EHD has also a wide range of applications in micro-pumps in which charged liquid is injected from the blades in order to generate high pressure of fluid flow [57, 61].

Another notable field of EHD is in the droplet based microfluidic devices which are enormously used for cell or particle encapsulation [14], detection and screening of chemicals

[129, 130], protein crystallization [131], reagent mixing [17], and biological assays [41] and so on. Therefore efficient control of droplet generation, shape deformation, transport and manipulation of drops through these micro scale devices is very important in the mentioned applications. In industry, there are many active and passive droplet manipulation techniques. Among them application of external electric fields through microelectrodes is one of the most popular active droplet manipulation techniques [59]. Thus understanding the fundamental principles and mechanism of EHD leading to the motion and deformation of the drops is of utmost importance for the design and development of microfluidic devices [23]. Schematic representation of some industrial application of two phase electrohydrodynamics is illustrated in FIG 1.1.

Realizing the importance of droplet manipulation using electric field in microfluidic devices, we have developed a computational method based on three dimensional level set method and the Melcher–Taylor's leaky-dielectric model for two-phase EHD. The developed method is then implemented to sort the droplet in a rectangular microfluidic channel.

1.2 Fundamentals of Electrohydrodynamics (EHD)

When an initially uncharged droplet suspending in another immiscible fluid is subjected to an electric field following two phenomena happen [115, 67] :

- Molecules of both fluids get polarized and create dipole.
- Movement of free charges from both fluids to the interface through ohmic conduction.

Depending on the above effects, several researchers [83, 12, 58] divided the two phase EHD problem into following three categories:

- Perfect dielectric-perfect dielectric fluid system.
- Perfect conducting-perfect dielectric fluid system..

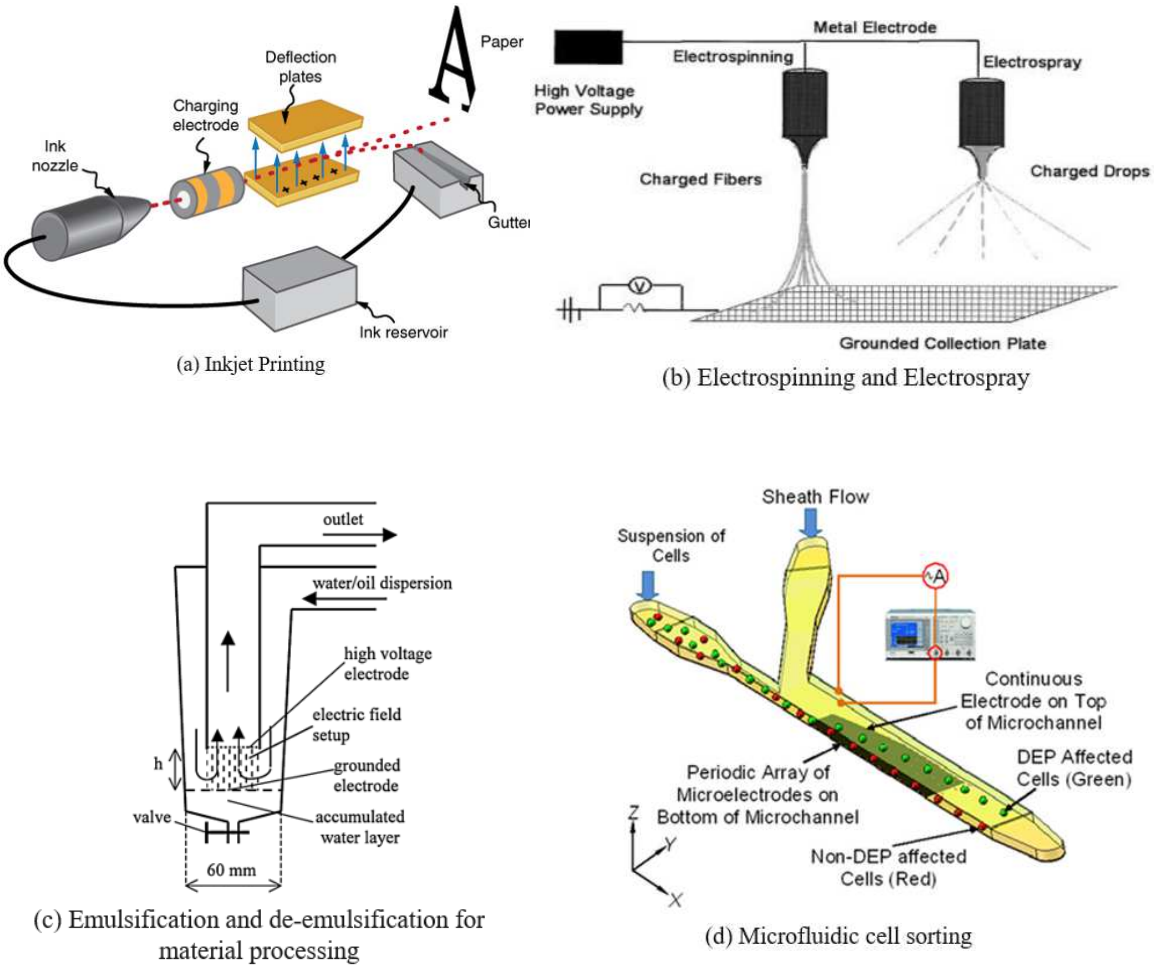

(a) Inkjet Printing

(b) Electrospinning and Electrospray

(c) Emulsification and de-emulsification for material processing

(d) Microfluidic cell sorting

Fig. 1.1 Industry application of two-phase EHD (a) Inkjet Printing [11]; (b) Electrospinning and Electrospray [51]; (c) Emulsification and de-emulsification for material processing [30] , and (d) Microfluidic cell sorting [23]

.

- Leaky dielectric- leaky dielectric fluid system.

Perfect dielectric-perfect dielectric fluid system (PD-PD)

In his fluid system, both of the fluids are considered as perfectly insulating dielectrics without having any free charges. If both of the fluids are homogeneous, the dipoles are balanced everywhere except at the interface. At the interface, the unbalanced dipoles create an electric stress which act only at the normal direction. At the equilibrium state this normal electric stress is balanced by the interfacial tension and both drop and suspending fluid remains motionless. Some examples of perfect dielectric fluid are transformer oil, perfluoroalkanes, and purified water which are all refined by removing the impurities. Although in reality most of the fluids contain some form of impurities and cannot be regarded as perfect dielectric.

Perfect conducting-perfect dielectric fluid system (PC-PD)

In this fluid system, the droplet is considered as highly conductive while the suspending fluid is considered perfectly insulating dielectric. In this case, it this assumed that the free charges migrate instantaneously from the bulk to the fluid interface without any resistivity. Due to the difference in physical properties at interface, a discontinuity of electric stress occurs at the interface. This discontinuity of electric stress also gives rise to a normal electric stress and at equilibrium states both fluids remain motionless. However, perfect conducting fluids are also do not exist in nature, this concept is a useful model when electrical resistance is negligible compared to other effects.

Leaky dielectric- leaky dielectric fluid system (LD-LD)

The most popular fluid system for two-phase EHD is leaky dielectric (LD) fluid system which was first developed by Taylor and Melcher [111–113] for weakly conducting fluid. In leaky dielectric fluid system both of the fluids of the system are weakly conducting

and behave differently from perfect dielectric and perfect conducting fluid system. On the application of an electric field, all free charges accumulate on the drop-fluid surface due to ohmic conduction leaving the bulk free of any charge. A tangential electric field acts on these surface charges generates a shear stress which results in an electrohydrodynamic induced flow both in and around the droplet. Besides, charge at the interface also undergoes an electric displacement. A sketch of the Taylor–Melcher leaky dielectric interface is presented in FIG 1.2. Most common example of LD-LD fluid system is silicone oil drop suspending in castor oil which are widely used by oil, lubricants, ink, pharmaceutical, and medical industries.

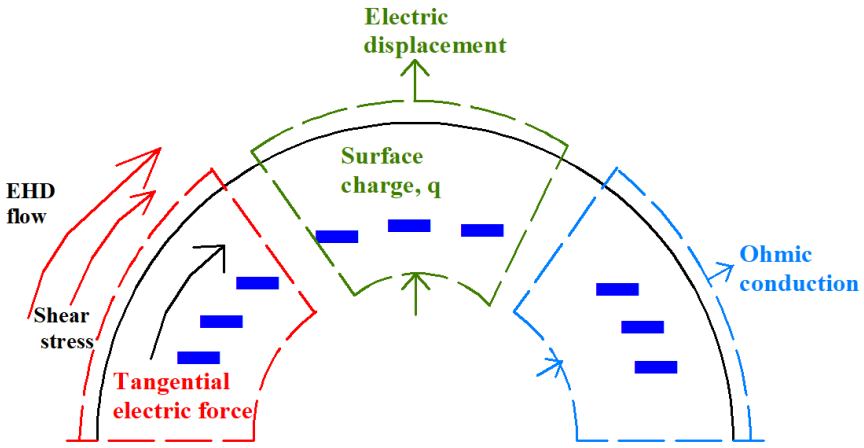

Fig. 1.2 A sketch of the Taylor–Melcher leaky dielectric interface

.

In two-phase fluid system, droplet suspending in another fluid can undergo different types of deformation and breakup when exposed to a uniform electric field. First controlled experiments of two-phase EHD for drops in uniform electric field were done by Allan and Mason [8]. In their experiment they observed two different types of deformation as shown schematically in FIG 1.3. In FIG 1.3 (a) the droplet elongate in the direction of applied uniform electric field which leads to a prolate shape. On the contrary to in FIG 1.3 (b), the droplet elongate in the direction perpendicular to the applied electric field which leads

to an oblate shape. Fundametally, the dynamic response of a drop to an applied electric field is characterized by two physical properties namely the electrical conductivity and the permittivity. A detailed explanation of dynamics of EHD induced droplet deformation is provided at 3.2.2.

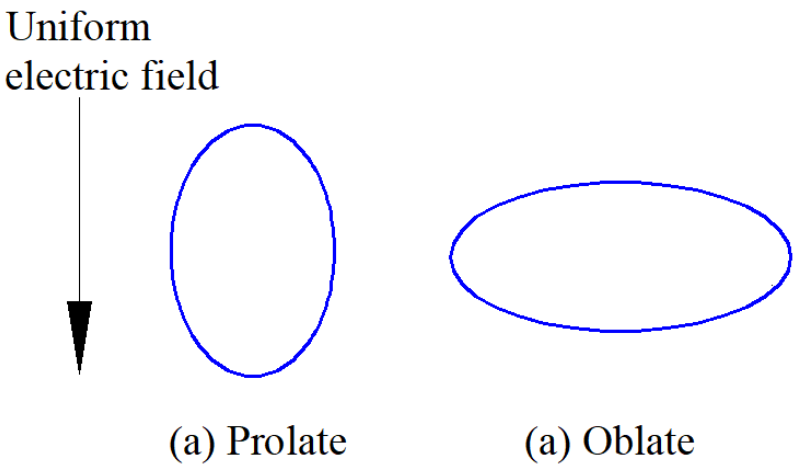

Fig. 1.3 Schematic representation of (a) prolate and (b) oblate drop shapes in the presence of uniform electric field.

1.3 Literature Review

Two-phase electrohydrodynamics (EHD) deals with the dynamics of interfacial flow subjected to electric field. In the present study, two-phase EHD is categorized into following three groups:

- Droplet subjected to uniform electric field.
- Droplet subjected to both uniform electric field and shear flow.
- Droplet sorting using non-uniform electric field.

1.3.1 Droplet subjected to uniform electric field

Earlier studies on two-phase EHD are mainly based on either PD-PD or PC-PD fluid system to simplify the complexity related to EHD. Here, the drop-fluid interface does not experience any tangential electric stresses. Consequently, both fluids remain motionless. Researchers [80, 44] in the earlier studies mentioned that the droplet can only attain a prolate shape as a result of normal electric stress across the interface. However, in a experimental study Allan and Mason [8] observed that normal electric stress can also lead to oblate shape droplet. In his pioneering work, Taylor [112] realized that dielectric fluids can have a very weak conductivity which can carry free charges to the interface through ohmic conduction. The electric field acts on these charges gives rise to tangential electric stress that can generate toroidal circulatory flow both in and around the droplet. By considered this effect, Taylor [113] developed a small-deformation theory. Using his theory Taylor predicted both prolate and oblate shapes depending on the physical properties of the fluid. However as Taylor's leaky dielectric model is based on small deformation theory, it shows greater discrepancy with the experimental results [116, 120, 93] at larger deformation. To improve the discrepancy between theory and experiment, an extensive theoretical [5, 116, 120, 97, 69] researches have been conducted on two-phase EHD. However, all of these theoretical analysis are based on either Stokes flow or inviscid flow with two dimensional domain to simplify the complicated electro-mechanical coupling between electric field and the fluids. Thus, the theoretical prediction is not feasible for most industrial applications which often include complex geometry and droplets can experience large deformation and even breakup.

On the contrary to, numerical approaches have gained popularity over the years due to its ability to deal with large deformation as well as complex interdisciplinary phenomena occurring in complex geometries. A number of numerical approaches have been developed by researchers to simulate two-phase EHD problem. The Boundary Element Method (BEM) is one of the preferred numerical scheme which is used to solve either the electric field

or the flow pattern [100, 48]. However, the BEM is only applicable for inviscid or Stokes flows problems. Finite element method (FEM) is used by several researchers [45, 46, 77] to determine drop deformations of pendant and sessile conducting drops which are subjected to electric field. They have also characterized the equilibrium drop shapes as well as the morphological evolution. But all their works are based on axisymmetric domain. Teigen and Munkejord [114] have presented a sharp-interface approach to simulate two-phase EHD for perfect dielectric model. Tomar et al. [115] have considered perfect dielectric and perfect conducting fluid systems to numerically simulate two-phase EHD using volume-of-fluid (VOF) method. They have shown that the interpolation scheme which is used to smoothen the electric properties (conductivity and permittivity) in the interface transition region has a significant influence on the solution in the bulk; therefore, they have proposed to use weighted harmonic mean (WHM) interpolation scheme rather than the usual weighted arithmetic mean (WAM) scheme in the transition region. Herrera et al. [67] have investigated the influence of WHM interpolation scheme for three limiting cases namely: dielectric-dielectric, conducting-conducting and dielectric-conducting. They have developed a charge conservative EHD code as an extension of the Gerris solver [89]. Zhang and Kwok [127] have done a Lattice Boltzmann study of electrohydrodynamic driven deformations in a 2D drop based on leaky dielectric theory using diffused interfaces. A coupled level set and volume of fluid method have been employed by Welch and Biswas [123] to simulate film boiling of water under the effect of electrostatic forces. Very recently, Poddar et al. [87] have explored the consequences of surfactant coating on the electrohydrodynamics manipulation of a drop motion in a plane Poiseuielle flow. However, they have employed a ‘leaky dielectric model’ with linear dependency of the surface tension on the surfactant concentration. In reality, the relation between surfactant concentration and surface tension is highly nonlinear, therefore their model is not sufficient to represent the real physics behind the two phase flow with surfactant and electric charges. As all of the numerical methods mentioned above are

based on either 2d or axisymmetric domain, we have developed a novel 3d level set method to analyze the dynamics of droplet subjected to uniform electric field

1.3.2 Droplet subjected to both uniform electric field and shear flow

In simple shear flow, the presence of the fluid inside the droplet disturbs the motion of the suspending fluid which induces stress both along the tangential and normal direction at the drop interface. The normal stress gives rise to a pressure difference across the interface which leads to the deformation of the droplet. In addition to it, application of external electric field also induces an electric stress at the interface of the two fluids. Therefore in this case, deformation and equilibrium orientation of the droplet are dependent upon the strength of shear flow, electric field intensity and physical properties of the fluids.

The combined action of hydrodynamic and electric flow field has been explored in a number of experimental, analytical , and numerical studies. Allan and Mason [8] performed experiments on the drop deformation and burst in the combined presence of uniform electric field and simple shear flow. Vlahovska [121] proposed an analytical solution to quantify the small deformations of droplet when subjected to electric field and shear flow in an unconfined domain. Effect of domain confinement on this combined system is analysed analytically by Mandal et. al. [69] and Santra et al. [94]. However their study is only based on small deformations of the droplet. Mahlmann and Papageorgiou [68] numerically investigated the effect of uniform electric field on the deformation and orientation of a drop in shear flow using a two-dimensional level set method . These studies showed that with increase in strength of applied electric field, drop attains more elongated shape with more inclination towards the direction of electric field. Recently Singh et. al.[103] provided a 3d numerical investigation based on lattice Boltzmann and leaky dielectric model for the cumulative effect of EHD and shear flow. In section 3.3.2 we have validated our developed 3d dimensional level set method with the 3d lattice Boltzmann method of Singh et. al.[103]

1.3.3 Droplet sorting using non-uniform electric field

In leaky dielectric fluid system when an initially uncharged droplet, suspending in another fluid is subjected to an external electric field, charges from both fluids accumulates at the interface. If the external electric field is uniform, the accumulated positive and negative charges have equal magnitude and therefore they cancel each other. In this case, the net force on the droplet is zero and the droplet remains stationary. However, if the external electric field is non-uniform, the force on one side is slightly smaller than the other. This unequal forces results in a net force acting on the droplet and it moves it in a particular direction. This movement of the initially uncharged droplet due to nonuniform electric field is known as dielectrophoresis (DEP) motion. The difference between uniform and non-uniform two phase EHD flow is schematically illustrated in FIG 1.4 which is taken from [126].

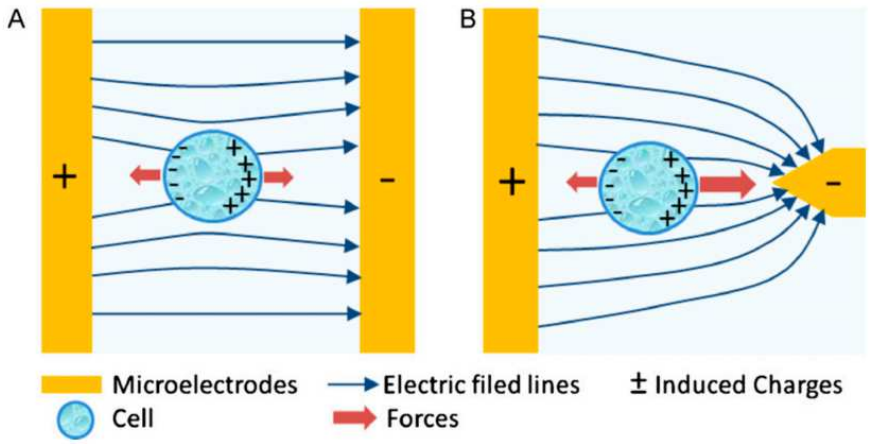

Fig. 1.4 Difference between uniform and non-uniform two-phase EHD [126] : (A) Uniform electric field: symmetric electric force on the particle; (B) Non-uniform electric field: assymmetric electric force on the particle results in DEP motion

.

In droplet based microfluidics, a number of external fields have been implemented for droplet manipulation such as electric [2, 3], magnetic [18, 7], accoustic [85, 64] and pneumatic methods [22, 50]. Among all of the these methods, DEP is the most widely used sorting and separation techniques for microfluidics due to its high speed, efficiency,

sensitivity and selectivity while maintaining a low running cost. DEP is a also label-free method and does not require any modification of sample during the sorting process. DEP is an effective way to trap [38, 96, 122] , separate and sort various types of cells such as breast cancer cells [56], red blood cells [37, 86], viable yeast cells [55] and characterizing micro-organisms [70], DNA [84], virus[40, 26] and bacteria [60, 104, 125].

There are two types of DEP motion: positive DEP and negative DEP. If the particle/droplet has lower permittivity than the suspending fluid ($\varepsilon_p < \varepsilon_m$), it will be attracted to the stronger field regions which is known as positive DEP (pDEP). On the other hand, when the permittivity of the particle/droplet is higher than the suspending fluid ($\varepsilon_p > \varepsilon_m$), it will be repelled from the electric field which is known as negative DEP (nDEP) . The schematic representation pDEP and nDEP is shown in FIG 1.5.

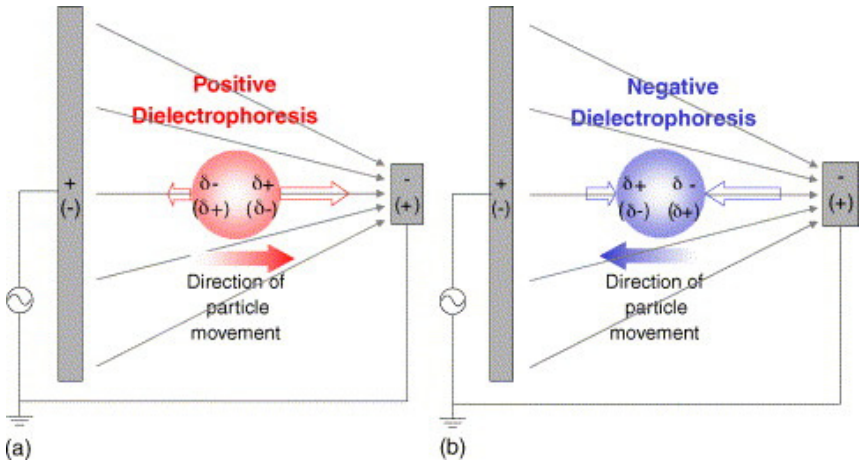

Fig. 1.5 (a) Positive and (b) negative dielectrophoretic response of the particles due to the polarization of the particle [27]

.

The DEP force for an insulating spherical particle was first analytically defined by Pohl [88]. Motivated by the pioneering work of Pohl [88], Feng [32] first analytically computed the DEP velocity of a leaky dielectric drop in the presence of an axisymmetric nonuniform electric field which is generated by combining uniform and quadrupole electric field. In his study Feng [32] concluded that DEP velocity of a drop is governed by the combined

influence of EHD and DEP force. Later, Baret et al. [9] developed a Fluorescence Assisted Droplet Sorting (FADS) device by coupling the fluorescence signal with non-uniform electric field. FADS device depends on laser induced fluorescence to detect the chemical contents within a series of droplets which are continuously passing an excitation light spot. In addition to the fluorescence signal, an electronic sorting unit is placed at the downstream of the channel to steer the droplets into the desired branching channel based on their fluorescence signal intensity . Link et. al. [65] reported an electric droplet manipulation platform based on electrophoresis where the droplet is pre-charged and electrochemical reaction occurs between the droplet and the system. Mhatre and Thaokar [74] investigated the DEP motion of perfectly conducting and leaky dielectric drops in a pin-plate electrode assembly. From their study, they have observed that perfectly conducting drop showed pDEP while leaky dilectric drop showed pDEP or nDEP depending on the electrical properties.

At present most of the researches on droplet sorting using DEP are based on experimental study. In the experimental study [71], the most common material for fabrication of microfluidic devices is polydimethylsiloxane (PDMS). PDMS is a transparent polymer material which can be molded using standard soft lithography techniques [28, 119]. Electric field is incorporated by patterning indium tin oxide (ITO) electrodes on the surface of the glass slide close to the channels. PDMS are strongly hydrophobic and can be directly used to generate water droplet in a suspending oil phase. This facilitates the sorting of droplets and eliminates the cross-contamination caused by surface interactions.

A experimental setup for high-speed droplet sorting device based on dielectrophoresis technology is shown in FIG 1.6. This setup was developed by Ahn et al. [3] where they fabricated microfluidic devices containing microelectrodes underneath PDMS channels that produced a force of more than 10 nN on a water droplet in oil phase, resulting in a sorting rate of higher than 1.6 kHz.

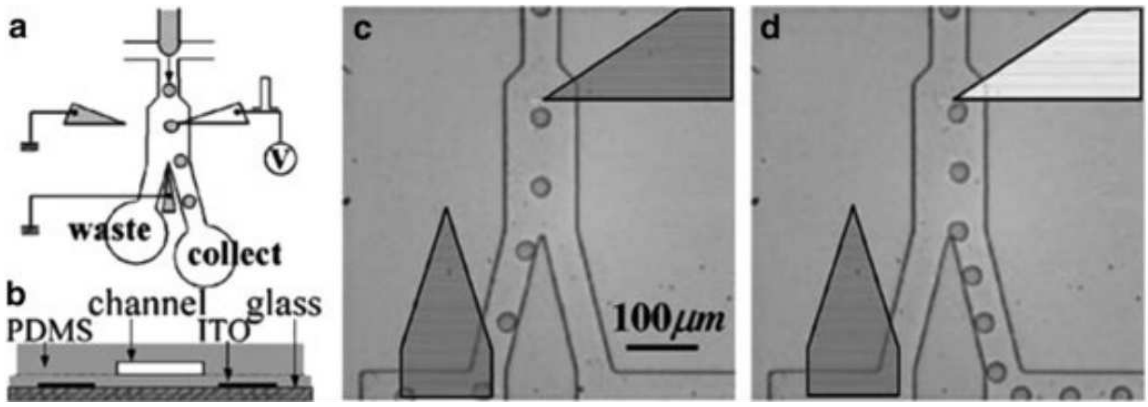

Fig. 1.6 Experimental set-up of a dielectrophoretic droplets sorting device. (a) Schematic view of the device. (b) Schematic cross section of the device. (c) In the absence of an electric field, water droplets flow into the waste channel. (d) Applying an electric field, the droplets are attracted toward the energized electrode and flow into the collection channel. Taken from [3].

The DEP force depends on a number of parameters such as the arrangement of the electrode, electric field distribution, conductivity and permittivity of the droplet with respect to the suspending fluid. However, analysing the effect of these parameters on droplet sorting through experimental investigations are merely difficult, time-consuming, and expensive compared to the numerical analysis. Numerical simulation can analyse the DEP sorting efficiency by changing the relevant parameters in microfluidic environment before performing laboratory experiment. Therefore, computational method can significantly contribute to the design improvement of the microfluidic devices.

Several numerical studies on dielectrophoretic particle-particle interaction and motion have been done using finite element methods (FEM) with an Arbitrary Lagrangian–Eulerian (ALE) algorithm [4, 66] in two-dimensions. However, FEM requires very fine mesh when particles are closely spaced or near the electrode which makes them computationally inefficient. In addition to it, a moving mesh is required to update the particle location for ALE algorithm. A finite volume method (FVM) for predicting particle trajectory in dielectrophoretic motion was proposed by Al-Jarro et al. [6]. A coupled immersed interface–boundary-element

method ((IIM-BEM)) was developed by Le et.al. [62] for dielectrophoretic particle trapping. They used BEM for computing electric field whereas IIM was used to solve viscous fluid flow problem. However, their developed method is based on two-dimensional geometry and not convenient for large systems. There are several other numerical studies which computed the DEP force and particle trajectories in microfluidic channel [39, 63]. The main drawback of these studies is that they did not consider the interfacial phenomena. In this research, we have developed a 3d level set method for two-phase EHD problem. The developed method is also implemented to sort the droplet in microfluidic channel using dielectrophoresis. Upto date, there is no existing computational model for DEP based droplet sorting.

1.4 Deficit in the existing literature and motivation of the present thesis

While cell sorting using an electric field has been the subject of many investigations in the past years, the numerical analysis of droplet sorting has received very little attention. Thus, an accurate fundamental understanding on computational method for DEP assisted droplet sorting either for 2d and 3d geometries is still missing in the literature. This analysis of droplet sorting is of significant importance in the field of microfluidics which involve droplet manipulation using an electric field for biomedical and chemical application. Motivated by this consideration, in the present work we have developed a three dimensional level set method for two-phase electrohydrodynamics. Based on the developed computational method, we have analysed a DEP influenced droplet sorting on microfluidic channel based on several important parameters of the system which can assist the droplet sorting in a microfluidic channel.

1.5 Outline of the thesis

In this research work we have developed a three dimensional level set method for two-phase electrohydrodynamics problem. The developed method is implemented in sorting droplets in microfluidic environment. The structure of the thesis is summarised as follows.

In Chapter 2, at first different computational methods for modelling of the two-phase flow system are briefly presented. After that governing equations of fluid flow and electric field are discussed. Next, important non-dimensional parameters governing the problem are defined. Finally, the numerical procedures applied for solving the problem are briefly outlined.

In Chapter 3, the developed computational method is validated for two problems: (a) Droplet subjected to uniform electric field and (b) Droplet subjected to uniform electric field and simple shear flow. The validation is performed through quantitative comparison of the present results with the existing theoretical, numerical and experimental results of other researchers.

In Chapter 4, the developed computation method is practically implemented for sorting of droplet using electric field. Sorting of droplet without and with electric field are analysed based on different values of branch flow ratio, electric field effect, electrode position, flow inertia and size ratio of the droplet.

In Chapter 5, the major achievements of this thesis are summarised. This chapter ends with a discussion on the scope of further work on two-phase EHD modeling for electrospray printing, droplet/biological cell sorting and encapsulation.

Chapter 2

Numerical method

2.1 Introduction

In two-phase flow system the two fluids are separated by a distinct interface which plays a dominate role in determining the dynamics of the entire flow. When exposed to external electric field droplet can take prolate and oblate shape depending on the interfacial charge distribution. Moreover, the interface could also experience severe topology changes such as break up, conic cusping or tip streaming. One of the challenges in solving two phase EHD problem is to accurately model the interface position. In general, numerical methods to simulate interfacial flows can be broadly divided into two categories: interface-tracking and interface-capturing methods.

Interface tracking methods

Interface-tracking methods, including mainly boundary integral method (BIM), front-tracking method and immersed boundary method. Interface-tracking methods basically implement the Lagrangian approach to explicitly represent the interface. Boundary integral method (BIM) constructs mesh over the modelled surface to track the interface. BIM has been used

by Sherwood [100] to numerically model breakup of fluid droplets in electric and magnetic fields for low Reynolds number. Interaction of two drops in a uniform electric field has been investigated by Baygents et.al. [12] using BIM for leaky dielectric model at low Reynolds number. BIM are also used to solve inviscid electrified jet by Setiawan and Heister [99] and Higuera [48]. From these researches, it is apparent that BIM is only applicable for inviscid or Stokes flows. Front-tracking method tracks the motion of the interface explicitly by connected marker particles, thus the interface curvature and location are provided explicitly and accurately [54]. Front-tracking method has been used by Fern'andez et.al.[35] to examine the effect of an electric field applied to an emulsion of drops flowing through a channel. Bhalla et.al. [15] described an approach to model EHD using an Immersed Boundary (IB) method to determine the effects of rotating electric fields to orient particles and to separate cells using their dielectric properties in a lab-on-a-chip device. In Immersed Boundary method the body is dealt with Lagrangian approach whereas the surrounding fluid is dealt with Eulerian approach. Although interface-tracking methods have been widely used to simulate the dynamics of electrohydrodynamics, they are not suitable for simulating the problem undergoing topological changes such as breakup and coalescence, because in these methods the interface must be manually ruptured based upon some ad-hoc criteria.

Interface capturing methods

Interface-capturing methods use an advection equation to implicitly represent the interface in an Eulerian grid which greatly simplifies gridding, discretization and handling of topological changes. The most popular interface-capturing methods are volume-of-fluid method and level-set method.

Volume of fluid(VOF)method

The volume of fluid method [3, 4, 5] is an implicit approach which uses the volume fraction (C) of the fluid to track the interface position. In the bulk fluid cell, C is equal to zero or unity while in interface cells, it has a value of $0 < C < 1$. The most commonly used VOF method consists of two major steps namely:

- The interface reconstruction step.
- The advection step.

The interface reconstruction step, finds an explicit description of the interface in each multi-fluid cell based on the volume fractions at this time step. The advection step, calculates the distribution of C at the next time step by solving an advection equation using the reconstructed interface and the underlying velocity field. The volume fraction function is purely advected by the velocity field which can be represented by the following equation:

$$\frac{\partial C}{\partial t} + \vec{u} \cdot \nabla C = 0 \tag{2.1}$$

As this equation can suffer discontinuity across the interface, it is important to use sophisticated numerical schemes to solve it. A complex interpolation scheme is required to construct smooth interface. This difficulty can easily be avoided by implementing level set (LS) approach. In LS approach [81, 82, 98] the characteristic functions of the two fluid phases are approximated by the sign of a smooth scalar function, such that the interface is given by the zero-level set of this smooth function. Due to this smooth approximation the computation of curvature is straightforward.

Level Set (LS) Method

In this thesis, we have deveoped a 3d level set method [105, 106] to capture the interface of two-phase EHD problem. In level-set methods, the level-set function $\phi(x,y,z,t)$ is defined as

a signed distance function from the interface and thus the interface is the zero contour of the level set function. The immiscible fluid separated by the interface are named fluid 1 (droplet) and fluid 2 (suspending fluid) as shown in FIG 2.1 and the level-set function is set positive in fluid 1 and negative in fluid 2. Level-set function $\phi(x,y,z,t)$ is defined as a signed distance to the interface and is purely a geometrical variable. This function varies smoothly across the interface, which eliminates the discontinuity problem that occurs in the VOF method. The movement of the interface, however, may lead to a substantial distortion of the level set function over time; i.e., its gradient may become very large or very small near the interface which can adversely effect the stable evaluation of surface tension terms. To overcome this issue a widely used and very successful approach is the reinitialization by a signed distance function, [1, 21, 73, 109]. Such a simple reinitialization technique, however, introduces numerical diffusion to the solution which leads to a deterioration of the volume conservation, i.e. mass conservation in incompressible flow. To this end, several modified reinitialization methods have been developed to improve mass conservation [29, 92, 107] . Sethian [98] level developed a special implementation technique for accurate compliance of mass conservation. The interface tension force in the level set method is modelled using the continuum surface force (CSF) method [16] by using gradient of Heaviside function, H. Similar to the volume fraction function in the VOF method, the level set function used in the LS method is purely transported by the flow velocity. In contrast to the volume fraction, it is just an indicator and has no physical meaning. The advantage of the level-set method is that it handles the topology change of the interface, such as merging and breaking, automatically. It has been proved that when handling problems such as jet breakup caused by Rayleigh-Plateau instability, identical results can be obtained from the level-set method compared to the coupled level-set and volume-of-fluid method which holds better mass conservation [108].

In a two-phase flow system, the local fluid density, ρ, viscosity μ, electric conductivity, K and electric permittivity, ε are functions of ϕ. The smoothed version of the Heaviside

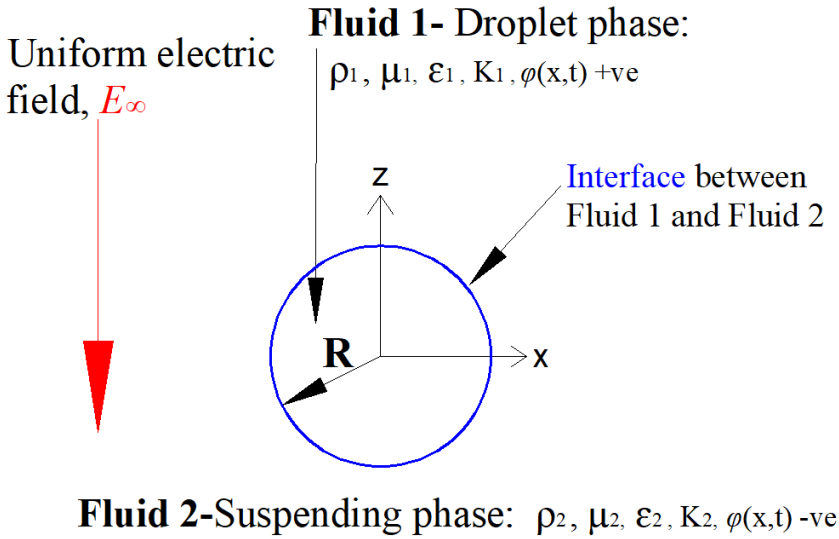

Fig. 2.1 Sketch of the two-phase fluid flow problem subjected to uniform electric field .

function H is applied to smoothly distribute the physical properties across the interface over a thickness of ξ. ξ is usually taken to be 1.5 grid spacing.

$$\rho(\phi) = H(\phi) + (\rho_1/\rho_2)\,[1 - H(\phi)], \tag{2.2}$$

$$\mu(\phi) = H(\phi) + (\mu_1/\mu_2)\,[1 - H(\phi)], \tag{2.3}$$

$$K(\phi) = H(\phi) + (K_1/K_2)\,[1 - H(\phi)], \tag{2.4}$$

$$\varepsilon(\phi) = H(\phi) + (\varepsilon_1/\varepsilon_2)\,[1 - H(\phi)], \tag{2.5}$$

where H is defined as:

$$H(\phi) = \begin{cases} 0, & \phi < -\xi \\ \frac{1}{2}[1 + \phi/\xi + \sin(\pi\phi/\xi)/\pi], & |\phi| \le \xi \\ 1, & \phi > \xi \end{cases} . \tag{2.6}$$

The fluid interface is updated by solving the level-set function which follows the advection equation:

$$\frac{\partial \phi}{\partial t} + \mathbf{u} \cdot \nabla \phi = 0. \tag{2.7}$$

A 'reinitialisation' step is required to ensure that the value of the level-set function adjacent to the interface keeps approximately the signed distance function. For this purpose, the steady-state solution of the following equation was obtained with a few iterations to ensure that the level set function remains the signed distance function:

$$\phi_\tau + S(\phi_0)\left(|\nabla \phi| - 1\right) = 0, \tag{2.8}$$

$$S(\phi_0) = \frac{\varphi_0}{\sqrt{\varphi_0 + \Delta x^2}}, \tag{2.9}$$

where τ is a pseudo time, ϕ_0 represents the value of the level set function before reinitializing, $\Delta x = \Delta y = \Delta z$ is mesh density and S is the smeared out signed function. The level set function is also used to calculate the surface normal vector as:

$$\mathbf{n} = \frac{\nabla \phi}{|\nabla \phi|}, \tag{2.10}$$

where, $\mathbf{n}$ is the normal vector and the interface curvature as:

$$\kappa = -\nabla . \mathbf{n}. \tag{2.11}$$

The surface tension force is incorporated with the momentum equation by a continuous-surface-tension formulation of Brackbill [16]. A finite volume method based on a marker-and-cell (MAC) mesh is employed for the equations of motion. The velocity components are defined at cell faces and scalar variables (e.g. pressure, electric properties and the level-set function) at the cell centres. The details of the numerical steps are provided in section 2.3.

2.2 Governing equations

We have assumed both of the fluids of the system are immiscible and incompressible. Therefore, the continuity Eq. (2.12) and momentum equation Eq. (2.13) in the dimensional form are expressed as:

$$\nabla.\vec{u} = 0, \tag{2.12}$$

$$\rho\left[\frac{\partial\vec{u}}{\partial t}+(\vec{u}.\nabla)\,\vec{u}\right] = -\nabla p+\nabla.\left[\mu\left(\nabla\vec{u}+\nabla\vec{u}^{T}\right)\right]+\sigma\kappa\delta_s\vec{n}+\vec{F}_e, \tag{2.13}$$

where ρ is the fluid density, $\vec{u}$ is the velocity vector, σ is the surface tension coefficient, $\vec{n}$ is the normal to the interface and $\kappa = -\nabla.\mathbf{n}$ is the interface curvature. The surface tension terms only acts on the interface which is represented by the Dirac delta function, δ_s. The effect of electric field is incorporated into the momentum equation by the electrostatic force, $\vec{F}_e$.

2.2.1 Determination of electric force, $\vec{F}_e$

The electric field effects are described using electrostatic model. The essential formulation of EHD problems is based on the Maxwell stress tensor which couples the electrostatic and hydrodynamics [49]. The Maxwell equations are approximated as electroquasistatic [95] in which the effect of magnetic field, $\vec{B}$ is ignored due to small dynamic currents. Therefore, the electric field, $\vec{E}$ is irrotational which can be expressed as follows:

$$\nabla\times\vec{E} = -\frac{\partial\vec{B}}{\partial t} = 0. \tag{2.14}$$

The electric field (E) obeys the Gauss's law which can be expressed as:

$$\Phi_e = \frac{q}{\varepsilon}, \tag{2.15}$$

where Φ_e is the electric flux through a closed surface S enclosing any volume V, and q is the total charge enclosed within V and ε represents permittivity which is the measure of resistance that is encountered when forming an electric field in a particular medium. The electric flux, Φ_e is defined as a surface integral of the electric field:

$$\Phi_e = \oiint_S \vec{E} \cdot d\vec{A}, \tag{2.16}$$

where $d\vec{A}$ is a vector representing an infinitesimal element of area of the surface. From Eq. (2.15) and Eq. (2.16) we can write:

$$\oiint_S \vec{E} \cdot d\vec{A} = \frac{q}{\varepsilon}. \tag{2.17}$$

Using divergence theorem, Eq. (2.16) can be written as:

$$\iiint_V \nabla \cdot \vec{E} \mathrm{d}V = \iiint_V \frac{q}{\varepsilon} \, \mathrm{d}V. \tag{2.18}$$

In order to make this equation simultaneously true for every possible volume V, it is necessary that the integrands are equal everywhere. Therefore, Eq. (2.18) is equivalent to:

$$\nabla \cdot (\varepsilon \vec{E}) = q. \tag{2.19}$$

Electric potential (Φ) is the amount of work needed to move a unit charge from a reference point to a specific point against an electric field $\vec{E}$. If the electric potential is known at every

point in a region of space, the electric field $\vec{E}$ can be defined by the negative gradient of electric potential (Φ) as following:

$$\vec{E} = -\nabla\Phi. \tag{2.20}$$

Charge conservation equation for the surface charge density q_s can be expressed as [67]:

$$\frac{\partial q_s}{\partial t} + \nabla \cdot (q_s\vec{u}) - \nabla \cdot (K\nabla\Phi) = 0. \tag{2.21}$$

At the present work, we have considered the deformation behaviour of a leaky dielectric drop in another leaky dielectric fluid under a static electric field. According this model, in spite of having very small electrical conductivity (K), electric charges always accumulate at the fluid interface almost instantly compared with the time scale of the fluid motion. Thus, the equation for the surface charge (q_s) conservation Eq. (2.21) can be simplified as:

$$\nabla \cdot (K\nabla\Phi) = 0. \tag{2.22}$$

Electric force can be written as the divergence of electrostatic Maxwell stress tensor, $\vec{T}_e$:

$$\vec{T}_e = \varepsilon\left(\vec{E}\vec{E} - \frac{E^2}{2}\mathbf{I}\right), \tag{2.23}$$

by applying the divergence operator:

$$\vec{F}_e = \nabla \cdot \vec{T}_e = q\vec{E} - \frac{1}{2}E^2\nabla\varepsilon. \tag{2.24}$$

In Eq. (2.24), first term of the right hand side represents Coulomb forces due to presence of free charges while the second term represents permittivity gradient force due to the difference in permittivity between two phases. Using the $\vec{F}_e$ term, the governing equation for EHD can

be written as:

$$\rho\left[\frac{\partial\vec{u}}{\partial t}+(\vec{u}.\nabla)\,\vec{u}\right] = -\nabla p+\nabla.\left[\mu\left(\nabla\vec{u}+\nabla\vec{u}^{T}\right)\right]+\sigma\kappa\delta_{s}\vec{n}+(q\vec{E}-\frac{1}{2}E^{2}\nabla\varepsilon). \quad (2.25)$$

2.2.2 Non-dimensional numbers

We non-dimensionalize the governing equations by using the following characteristic scales [43]: length $\rightarrow R$, velocity(u_c) $\rightarrow \varepsilon_e {E_\infty}^2 R/\mu_e$, time $\rightarrow R/u_c$, electric field $\rightarrow E_\infty$, viscous stress $\rightarrow \mu_e u_c/R$, electric stress $\rightarrow \varepsilon_e {E_\infty}^2$. The scale of velocity is obtained by equating the order of magnitude of the viscous stress with the electric stress. Based on the above characteristic scales following non-dimensional numbers and the property ratios are obtained:

- *Reynolds number, Re :* measures the ratio of inertial forces to viscous forces.

$$Re=\frac{\rho_2\varepsilon_2 E_\infty^2 R^2}{\mu_2^2}, \quad (2.26)$$

  where ρ_2, μ_2 are density and viscosity of suspending fluid, R is the droplet radius.

- *Electric Capillary number, Ca_E :* measures the intensity of electric stress over surface tension.

$$Ca_E=\frac{\varepsilon_2 E_\infty^2 R}{\gamma}, \quad (2.27)$$

  where γ is the interfacial tension and E_∞ is the uniform electric field intensity.

- *Electric conductivity ratio, (K)*: It measures the ratio of the conductivity between the droplet (K_1) and suspending fluid (K_2).

$$K=\frac{K_1}{K_2}. \quad (2.28)$$

- *Electric permittivity ratio, (S)*: It measures the ratio of the permittivity between the droplet (ε_1) and suspending fluid (ε_2).

$$S = \frac{\varepsilon_1}{\varepsilon_2}. \tag{2.29}$$

- *Viscosity ratio, (r_v)*: It measures the ratio of the viscosity between the droplet (μ_1) and suspending fluid (μ_2).

$$r_v = \frac{\mu_1}{\mu_2}. \tag{2.30}$$

- *Density ratio, (r_d)*: It measures the ratio of the density between the droplet (ρ_1) and suspending fluid (ρ_2).

$$r_d = \frac{\rho_1}{\rho_2}. \tag{2.31}$$

Based on the dimensionless numbers above, the momentum equation (Eq. 2.13) can be non-dimensionalized as follow:

$$\rho_c \left[\frac{\partial \vec{u}}{\partial t} + (\vec{u}.\nabla)\,\vec{u} \right] = -\nabla p + \frac{1}{Re}\nabla.\left[\mu_c\left(\nabla\vec{u} + \nabla\vec{u}^T\right)\right] + \frac{1}{CaRe}\sigma\kappa\delta_s\vec{n} + \frac{Ca_E}{CaRe}\left(q\vec{E} - \frac{1}{2}E^2\nabla\varepsilon\right). \tag{2.32}$$

2.3 Numerical procedures

In this research we have developed a three dimensional level set method for two phase electrohydrodynamics using Fortran 90. The non-dimensional partial differential equations are discretised using the finite volume method on a staggered grid with velocity and electric field components are defined at the cell faces and scalar variables (e.g. pressure, electric properties and the level-set function) at the cell centres as shown in FIG 2.2.

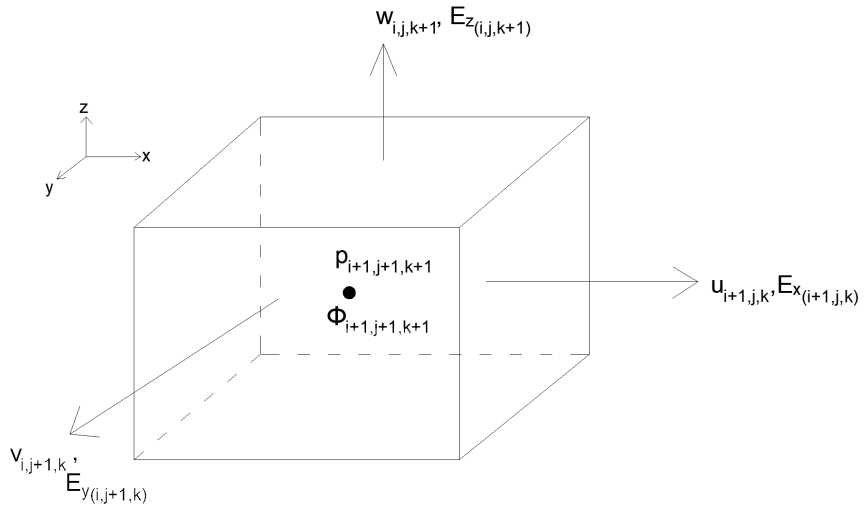

Fig. 2.2 Position of variables in a three-dimensional mesh cell.

The motion of the interface is dependent on the evolution of the velocity field, therefore the advection of the level-set function and the Navier-Stokes equations must be solved in a manner that is temporally matched. In our numerical simulation, the following computational order is followed from time level n to n + 1:

1. Update the level-set function through the advection equation using the velocity field at time level n and n - 1 using Eq. (2.33).

2. Determine the surface tension force at the time level n + 1/2 using the averaged value of the level-set function at time level n and n + 1 using Eq. (2.34).

3. Determine the electric potential at the time level n + 1/2 using Eq. (2.35).

4. The electric field is then straightforwardly computed at the time level n + 1/2 by taking the negative gradient of electric potential at the same time level using Eq. (2.36).

5. Determine the electric charge at the time level n + 1/2 using Eq. (2.37).

6. Determine the electric force term at the time level n + 1/2 using the value of electric field and electric permittivity at the same time level using Eq. (2.38).

7. Update the velocity field for time level n + 1 by solving the momentum and continuity equations with Eq. (2.45).

2.3.1 Updating the level-set function to determine the surface tension force

The update the level-set function at time level n and n - 1 is done through the following advection equation:

$$\phi^{n+1} = \phi^n - \Delta t \left\{ 1.5\mathscr{W}\left[(\mathbf{u}\cdot\nabla\phi)^n\right] - 0.5\mathscr{W}\left[(\mathbf{u}\cdot\nabla\phi)^{n-1}\right] \right\}. \tag{2.33}$$

The Crank-Nicholson method is used for the discretisation of the time-stepping procedure and the Adams-Bashforth method for the advective term. $\mathscr{W}$ is the discrete convection operator where fifth-order weighted essentially non-oscillatory (WENO) scheme is applied. The 'reinitialisation' step is applied after solving the advection equation to make sure that ϕ^{n+1} is kept approximately the signed distance function. Once ϕ^{n+1} is updated, the intermediate value of $\phi^{n+\frac{1}{2}}$ is used to calculate the physical properties of the fluids at the interface and the surface tension forces.

$$\phi^{n+\frac{1}{2}} = \frac{\phi^n + \phi^{n+1}}{2}. \tag{2.34}$$

Determining the electric force

For leaky-dielectric fluids, the electric potential, Φ at the time level n + 1/2 is determined by solving the following equation by successive over-relaxation (SOR) iterative method. SOR method shows a good performance in terms of number of iteration and computational time.

$$\nabla\cdot\left(K_{n+\frac{1}{2}}\nabla\Phi_{n+\frac{1}{2}}\right) = 0. \tag{2.35}$$

Electric field, $\vec{E}_{n+\frac{1}{2}}$ is then determined from following:

$$\vec{E}_{n+\frac{1}{2}} = -\nabla\Phi_{n+\frac{1}{2}}. \tag{2.36}$$

The electric charge, q at the time level n + 1/2 is determined by solving the following equation:

$$\nabla\cdot(\varepsilon_{n+\frac{1}{2}}\nabla\Phi_{n+\frac{1}{2}}) = -(q)_{n+\frac{1}{2}}\,. \tag{2.37}$$

Finally, the electric force, $\vec{F}_{e_{n+\frac{1}{2}}}$ then obtained from following:

$$\vec{F}_{e_{n+\frac{1}{2}}} = \nabla\cdot(\varepsilon_{n+\frac{1}{2}}\nabla\Phi_{n+\frac{1}{2}})\vec{E}_{n+\frac{1}{2}} - \frac{1}{2}E^2\nabla\varepsilon_{n+\frac{1}{2}}. \tag{2.38}$$

E^2 is determined as following:

$$E^2 = {E_x}^2 + {E_y}^2 + {E_z}^2, \tag{2.39}$$

taking the discretization in x- direction:

$$\begin{aligned}
\mathrm{E_x} &= -(\Phi(i+1,j+1,k+1) - \Phi(i,j+1,k+1))/dx,\\
\mathrm{E_y} &= -0.25^*((\Phi(i+1,j+1,k+1) + \Phi(i,j+1,k+1) + \Phi(i+1,j+2,k+1),\\
&\quad + \Phi(i,j+2,k+1)) - (\Phi(i+1,j+1,k+1) + \Phi(i,j+1,k+1)\\
&\quad + \Phi(i+1,j,k+1) + \Phi(i,j,k+1)))/dy\\
\mathrm{E_z} &= -0.25^*((\Phi(i+1,j+1,k+1) + \Phi(i,j+1,k+1) + \Phi(i+1,j+1,k+2)\\
&\quad + \Phi(i,j+1,k+2)) - (\Phi(i+1,j+1,k+1) + \Phi(i,j+1,k+1)\\
&\quad + \Phi(i+1,j+1,k) + \Phi(i,j+1,k)))/dz
\end{aligned} \tag{2.40}$$

2.3.2 Solving the momentum and continuity equations

The projection method [90] is implemented to solve for velocity and pressure field by coupling the momentum equation and the continuity equation. First, the pressure term is removed from the momentum equation and an intermediate velocity $\vec{u}_*$ is obtained through a semi-implicit discretisation and is solved by successive over-relaxation (SOR) iterative method.

$$\rho_{n+\frac{1}{2}}\left[\frac{\vec{u}_*-\vec{u}_n}{\Delta t}\right]=-\left[\frac{3}{2}\mathscr{H}(\vec{u}_n)-\frac{1}{2}\mathscr{H}(\vec{u}_{n-1})\right]+\frac{1}{2Re}\left[\mathscr{L}\left(\vec{u}_n,\mu_{n+1/2}\right)+\mathscr{L}\left(\vec{u}_*,\mu_{n+1/2}\right)\right]+$$

$$\frac{1}{CaRe}\sigma\kappa\delta_(n+\frac{1}{2})\vec{n}+\frac{Ca_E}{CaRe}\vec{F}_{e_{n+\frac{1}{2}}}, \tag{2.41}$$

where $\mathscr{H}$ represents the discrete convection operator and $\mathscr{L}$ denotes the discrete diffusion operator. Taken the discretisation of the equation in x-direction as an example $\mathscr{H}$ and $\mathscr{L}$ are written as equation (2.42) and (2.43).

$$\begin{aligned}\mathscr{H}(\vec{u}) =& u_{ijk}\frac{u_{i+1,j,k}-u_{i-1,j,k}}{2\Delta x}\\ &+v_{i-1/2,j+1/2,k}\frac{u_{i,j+1,k}-u_{i,j-1,k}}{2\Delta y}\\ &+w_{i-1/2,j,k+1/2}\frac{u_{i,j,k+1}-u_{i,j,k-1}}{2\Delta z},\end{aligned} \tag{2.42}$$

$$\begin{aligned}\mathscr{L}(\vec{u},\mu) =& 2\frac{\mu_{i+1,j+1,k+1}\left(u_{i+1,j,k}-u_{i,j,k}\right)-\mu_{i,j+1,k+1}\left(u_{i,j,k}-u_{i-1,j,k}\right)}{\Delta x^2}\\ &+\frac{\mu_{i+1/2,j+2/3,k+1}\left(v_{i,j+1,k}-v_{i-1,j+1,k}\right)-\mu_{i+1/2,j+1/2,k+1}\left(v_{i,j,k}-v_{i-1,j,k}\right)}{\Delta x\Delta y}\\ &+\frac{\mu_{i+1/2,j+2/3,k+1}\left(u_{i,j+1,k}-u_{i,j,k}\right)-\mu_{i+1/2,j+1/2,k+1}\left(u_{i,j,k}-u_{i,j-1,k}\right)}{\Delta y^2}\\ &+\frac{\mu_{i+1/2,j+1,k+2/3}\left(w_{i,j,k+1}-w_{i-1,j,k+1}\right)-\mu_{i+1/2,j+1,k+1/2}\left(w_{i,j,k}-w_{i-1,j,k}\right)}{\Delta x\Delta z}\\ &+\frac{\mu_{i+1/2,j+1,k+2/3}\left(u_{i,j,k+1}-u_{i,j,k}\right)-\mu_{i+1/2,j+1,k+1/2}\left(u_{i,j,k}-u_{i,j,k-1}\right)}{\Delta z^2}.\end{aligned} \tag{2.43}$$

In order to obtain a divergence-free velocity field, the intermediate velocity $\vec{u}_*$ is corrected by:

$$\frac{\vec{u}_{n+\frac{1}{2}}-\vec{u}_*}{\Delta t}=-\frac{\nabla p_{n+\frac{1}{2}}}{\rho_{n+\frac{1}{2}}}. \tag{2.44}$$

Since the velocity field at time level n + 1 is divergence free, we first calculate the pressure field by solving the pressure Poisson equation using the SOR method.

$$\frac{\nabla p_{n+\frac{1}{2}}}{\rho_{n+\frac{1}{2}}}=-\frac{\nabla\cdot\vec{u}_*}{\Delta t}. \tag{2.45}$$

Once the pressure field is obtained, the velocity field at time level n + 1 is calculated with Eq. (2.45).

Chapter 3

Validation of the method

3.1 Introduction

In this thesis, a three dimensional level set method is developed for two phase electrohydrodynamics. In this chapter, the developed method has been validated for two problems which are:

- Droplet subjected to uniform electric field.
- Droplet subjected to both uniform electric field and simple shear flow.

3.2 Droplet subjected to uniform electric field

3.2.1 Problem statement

For this problem, we consider an initially uncharged liquid droplet of radius, R suspending in another immiscible fluid. The two fluids have been considered as leaky dielectric having separate fluid and electric properties such as: densities ρ_1 and ρ_2, viscosities μ_1 and μ_2, electric permittivities ε_1 and ε_1 and conductivities K_1 and K_2. The subscripts 1 and 2 refer to

the physical parameters inside and outside of the droplet respectively. We use the suspending fluid as the reference fluid.

A three dimensional (3d) Cartesian co-ordinate is defined with the x axis along the horizontal direction, y axis along the lateral direction and z axis along the vertical direction. Droplet origin is fixed at the center of the computational domain. The top and bottom walls are separated by a distance 2H and subjected to a uniform electric field of strength E_∞ in the transverse direction. The top wall is connected to the positive electrode of electric potential, $\Phi = HE_\infty$ and the bottom wall is connected to the negative electrode of electric potential, $\Phi = -HE_\infty$ as shown in FIG 3.1. At drop surface the polar angle θ is measured counter clock-wise from negative z-axis. Here, $\theta = 0°, 180°$ are defined as pole region whereas $\theta = 90°$ is defined as equator region.

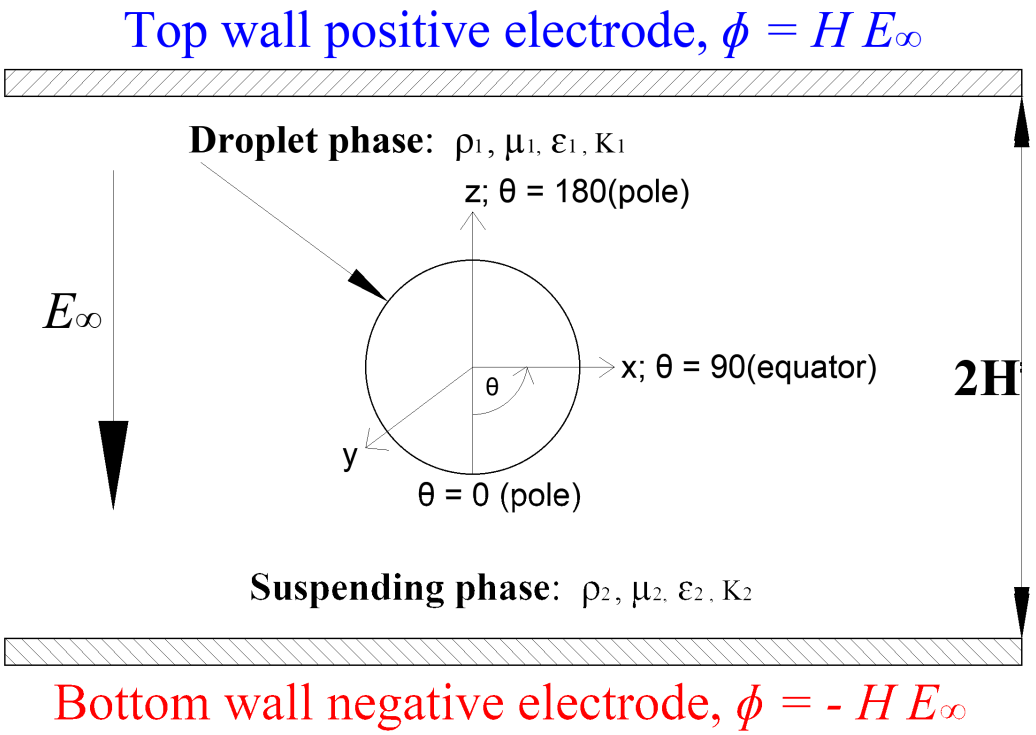

Fig. 3.1 Schematic illustration of a droplet suspended in another fluid and subjected to a uniform electric field, E_∞

.

3.2.2 Dynamics of EHD induced droplet deformation

Based on small perturbation theory, the EHD problem has been solved analytically by Taylor [112] and then by Ajayi [5] to the first and second order in electric capillary number, Ca_E. They characterise the total deformation of a spheroid droplet by means of the parameter D given by the expression:

$$D = \frac{L-B}{L+B}, \tag{3.1}$$

where L and B are the droplet lengths parallel and perpendicular to the electric field, respectively as shown in FIG 3.2. Using a linearised asymptotic analysis and assuming that both fluids are extremely viscous and conducting, Taylor[112] also provided an expression for D as a function of the fluid properties and the electric field intensity:

$$D = \frac{9}{16(2K+1)^2}\left[\frac{3K(3r_v+2)(1-KQ)}{5(r_v+1)} + K^2(1-2Q)+1\right] Ca_E, \tag{3.2}$$

where Ca_E refers to electric capillary number, $K = K_1/K_2$, $Q = \varepsilon_1/\varepsilon_2, r_v = \mu_1/\mu_2$ refer to conductivity, permittivity and viscosity ratio between drop and suspending fluids respectively. Here, subscript 1 refers to drop and subscript 2 refers to suspending medium.

According to Taylor's model, the droplet can deform into either prolate ($D > 0$) or oblate shape ($D < 0$) as shown in FIG 3.2 depending on the ratio conductivity (K) to the permittivity (Q) of the fluid. The relationship between K and Q is defined by a ratio named α which is the ratio of charge relaxation time scale of suspending fluid, (τ_2^E) to the charge relaxation time scale of drop,(τ_1^E). The charge relaxation time scale, (τ_E) represents the time required by the charges to reach the interface by the sole effect of Ohmic conduction.

$$\alpha = \frac{K}{Q} = \frac{\tau_2^E}{\tau_1^E}, \tag{3.3}$$

where, $\tau_1^E = \frac{\varepsilon_1}{K_1}$, $\tau_2^E = \frac{\varepsilon_2}{K_2}$.

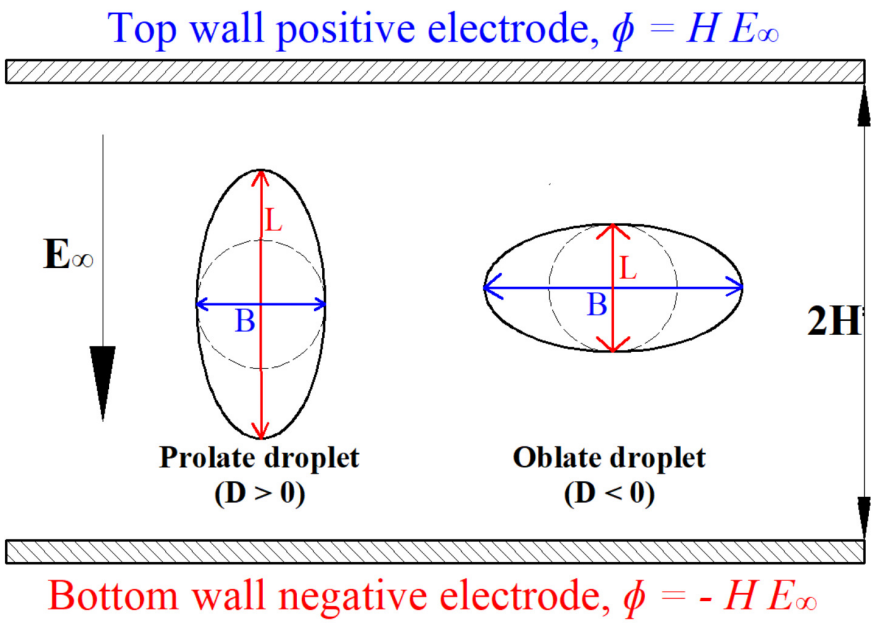

Fig. 3.2 Schematic representation of droplet length L and B at perpendicular and parallel direction of electric field for prolate (D > 0) and oblate (D < 0) droplet.

Different droplet behaviour at different combination of K and Q at $Ca_E << 1$, Re = 0.1, and $r_d = \rho_1/\rho_2 = 1$ (density ratio between drop and suspending fluids), $r_v = \mu_1/\mu_2 = 1$ (viscosity ratio between drop and suspending fluids) is illustrated in FIG 3.3. This figure has been previously presented by several researchers [116, 58, 12] for their EHD study. We have reproduced this figure in order to identify the three fluid system that we used in our validation study. In FIG 3.3, when the values of K and Q fall on the solid curve, the droplet remains spherical which means D = 0. Along the dashed line, $\alpha = 1$. These solid and dashed line divide the parameter space into three regions namely region 1,2 and 3. We have considered three leaky dielectric fluid systems denoted by prolate A (PR_A), prolate B (PR_B) and oblate (OB) which fall into region 1,2, and 3 respectively as shown through three symbols on the FIG 3.3. For PR_A, $\alpha > 1$ whereas for PR_B and OB $\alpha < 1$.

For $\alpha > 1$: The charge relaxation timescale of the drop fluid is faster than suspending fluid ($\tau_1^E < \tau_2^E$) . Therefore, charges from the drop fluid reaches at the equilibrium state much faster than the suspending fluid. As a result, surface charge distribution is mainly controlled

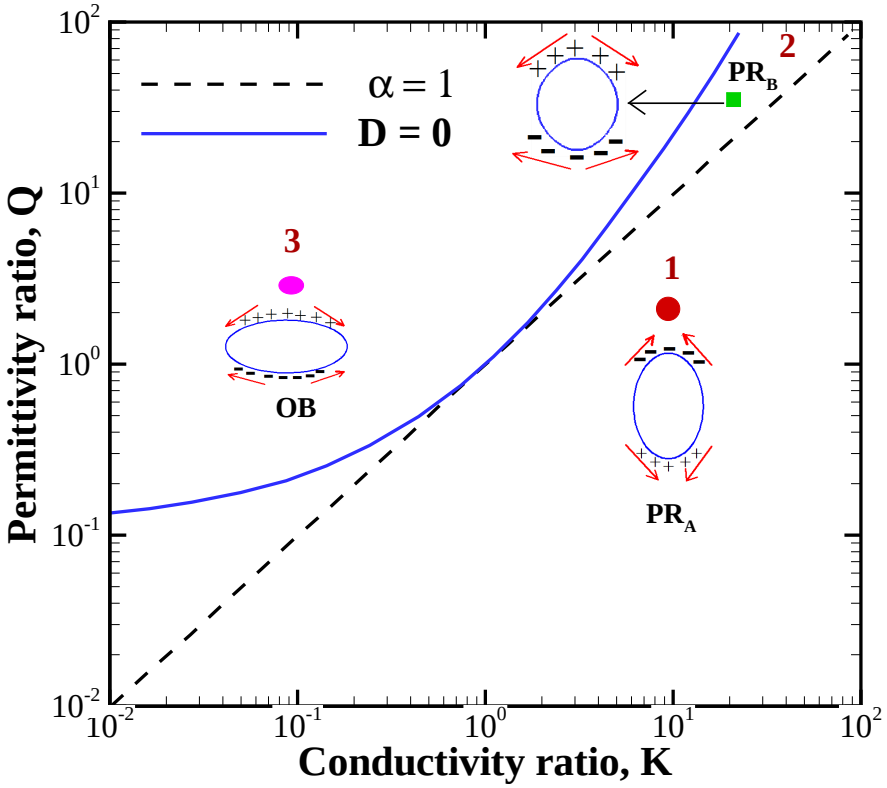

Fig. 3.3 Different droplet behaviour in the K-Q parameter space reproduced from small deformation theory [116, 58]. Here $Ca_E << 1$, Re = 0.1, and $r_d = \rho_1/\rho_2$, $r_v = \mu_1/\mu_2$. The solid line divides the region of prolate (PR) and oblate (OB) drops. The dashed line separates the region of prolate A (PR_A) from prolate B (PR_B) drops. The three symbols on the diagram represent the three systems considered in this study.

by the charges brought from the drop fluid. In this case, the drop dipole moment takes the same direction as the applied electric field and charges at the poles are attracted toward the electrodes and pull the droplet into a prolate, (PR_A) shape [72, 93] as shown schematically in FIG 3.4 (a).

For $\alpha < 1$: the charge relaxation timescale of the suspending fluid is faster than the drop fluid ($\tau_1^E > \tau_2^E$). As a result, charges from the suspending fluid reaches at the equilibrium state much faster than the drop fluid. In this case, surface charge distribution is mainly controlled by the charges brought from the suspending fluid. Consequently, the drop dipole moment takes the opposite direction of applied electric field and charges at the poles are

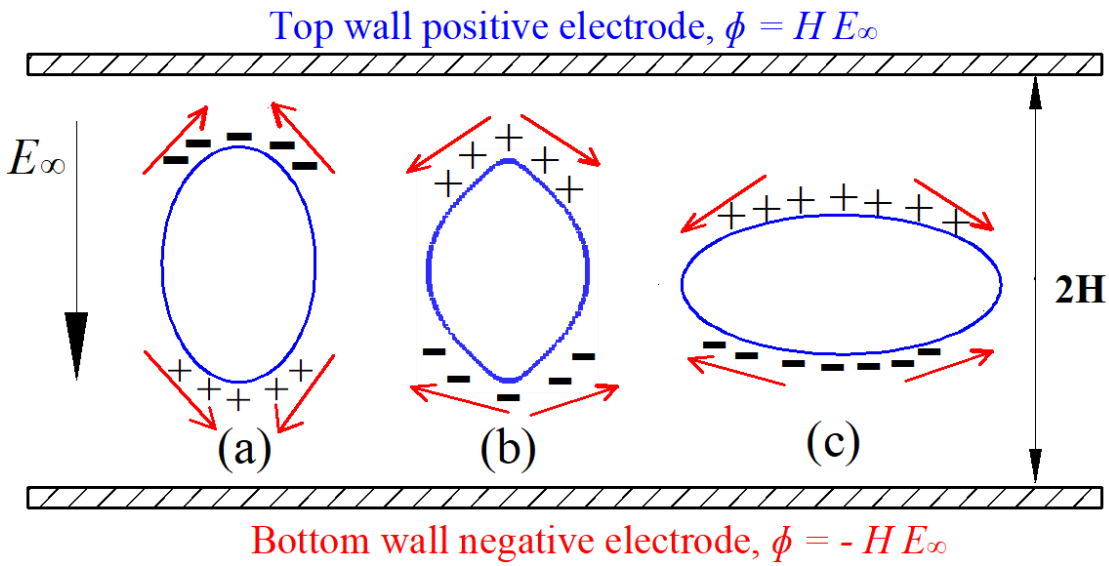

Fig. 3.4 Schematic representation of surface charge distribution and direction of surface electric traction force on a drop in the presence of uniform electric field, E_∞ for (a) $\alpha > 1$, for (b) and (c) $\alpha < 1$

.

repelled from the electrodes and push the droplet into either prolate B or oblate *OB* shape [72, 93] as shown schematically in FIG 3.4(b) and (c) respectively.

3.2.3 Results and discussion

The computational domain used in the present simulation is a cubic box. Due to the symmetry of the problem, only half of the domain is simulated. Symmetric boundary condition is used at x and y directions for both flow field and the electric potential. While at z direction, no-slip boundary condition is used for the flow field and Dirichlet boundary condition are imposed for the electric potential. The uniform rectangular meshes are used to discretize the computational domain. The validation is performed by comparing the present results with the theoretical, numerical and experimental results of other researchers.

Prolate droplet deformation

For prolate deformation, , we have modeled two fluid systems denoted by PR_A and PR_B. For PR_A: (K,Q) = (10.0, 1.37) while for PR_B: (K,Q) = (25.0, 50.0). These fluid systems resemble a real fluid system consisting of silicone oil droplet suspended in castor oil which are also used by several researchers [58, 42] in their experimental and numerical study. Both silicone and castor oil are weakly conductive fluid and have comparable densities but have difference in viscosity. Due to the high viscosity of the suspending castor oil, the silicone drop falls slowly which makes it easier to observe its behaviour. Therefore, the physical properties of the silicone oil drop in castor oil are ideal for modelling a realistic leaky dielectric drop in a leaky dielectric fluid system.

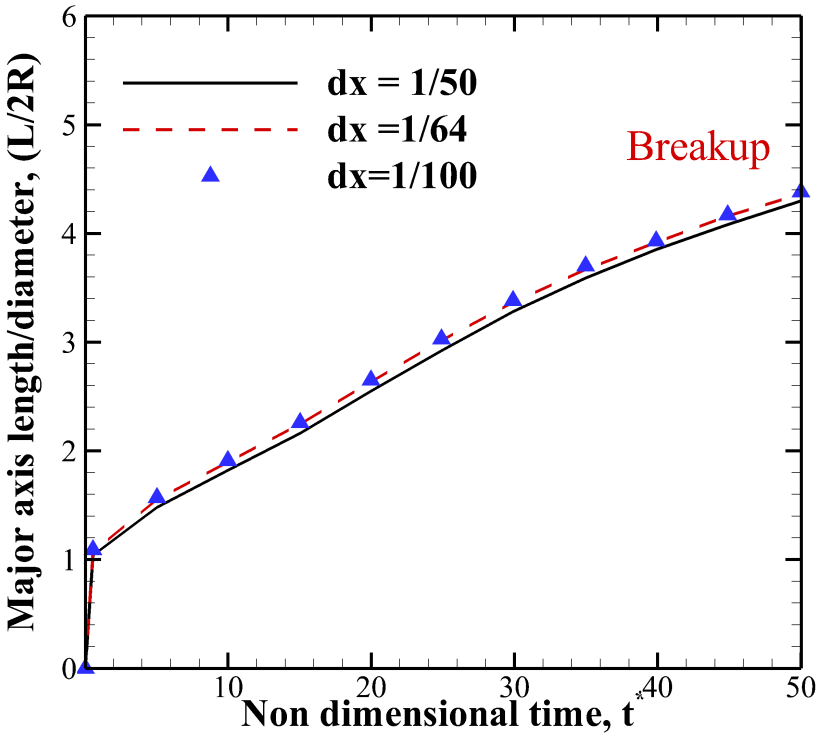

Fig. 3.5 Time evolution of elongation of droplet in uniform electric field with different mesh densities at K =10.0, Q =1.37, Ca_E = 0.35 (where droplet leads to breakup), Re = 0.1, and $r_d = 1$, $r_v = 0.874$.

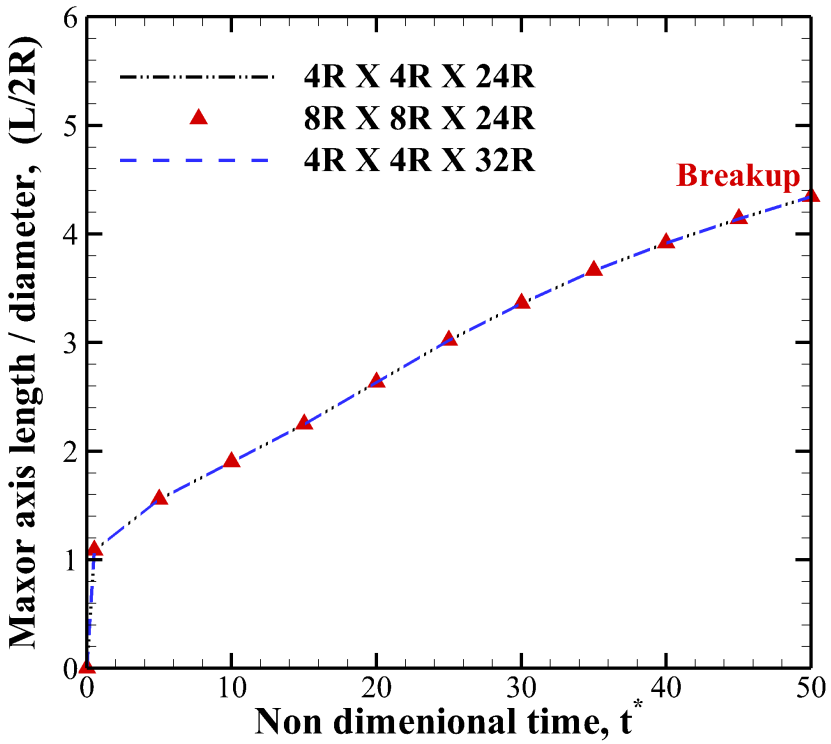

Fig. 3.6 Time evolution of elongation of droplet in uniform electric field with different domain sizes at K =10.0, Q =1.37, Ca_E = 0.35 (where droplet leads to breakup) , Re = 0.1, and $r_d = 1$, $r_v = 0.874$.

.

Before validating the method, a careful mesh-convergence and domain-independence tests have been conducted for prolate droplet to ensure that the reported results do not change with further increasing the mesh density or domain size. The mesh convergency test has been performed for three different mesh densities which are dx = dy = dz = 1/50, 1/64, and 1/100 respectively. We analyse the temporal evolution of the droplets elongation (major axis lengh/diameter) parameter for various mesh densities which has been shown in FIG 3.5. From the result it is seen that the mesh density dx = dy = dz = 1/64 is sufficient to capture the important characteristics. With such a mesh density, we have 33 meshes across the diameter of the droplet and mass of the droplet can also be conserved reasonably well with the relative mass change within 0.7 %.

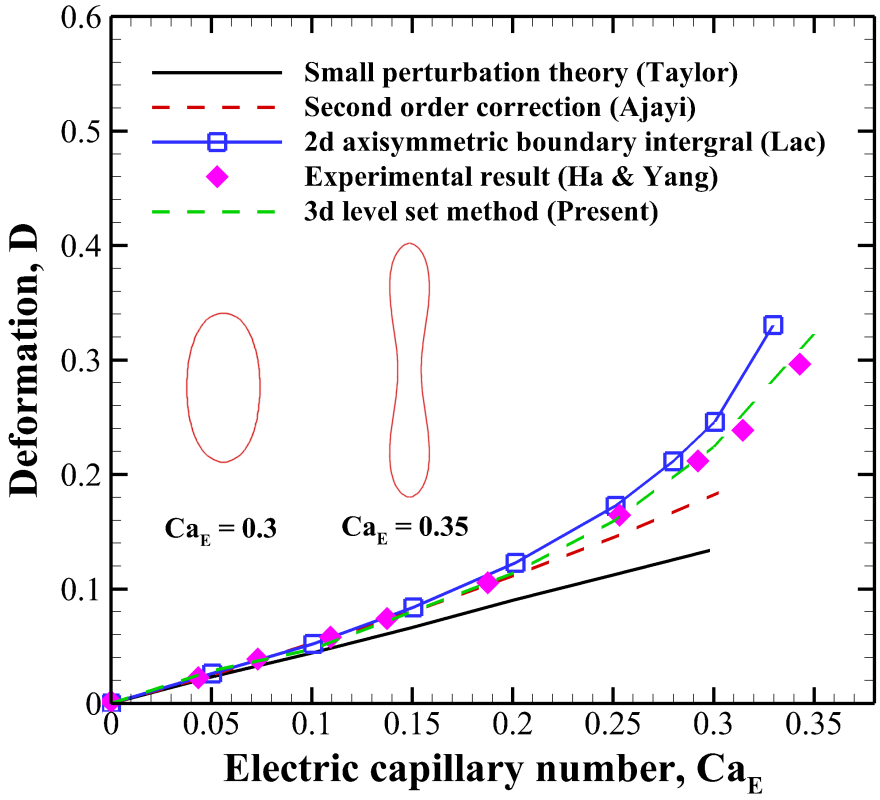

Fig. 3.7 Droplet deformation as a function of electric capillary number, Ca_E, for prolate droplet at K =10.0, Q =1.37, Re = 0.1, and $r_d = 1$, $r_v = 0.874$.

To avoid the boundary effects, a domain independence test has been done with dx = 1/64, for three computational domain sizes with dimensions 4R×4R×24R, 8R×8R×24R, and 4R×4R×32R in x,y and z directions respectively. A time evolution of the droplets Taylor deformation parameter for prolate droplet at $Ca_E = 0.35$ (at which the prolate droplet leads to breakup) has been shown in FIG 3.6 . It is shown that a computational domain with size 4R×4R×24R is large enough to neglect the boundary effect. Therefore the mesh density, dx = 1/64 and computational domain size 4R×4R×24R are used in the validation for the prolate droplet.

When the electric field is applied, the electrical stresses are generated across the drop and suspending fluid interface, which not only leads to deformation of the droplet but also generates an electrohydrodynamic induced flow in and around the droplet. The droplet

deformation is mainly governed by electric capillary number, Ca_E which is the ratio of electric stress to surface tension. With the increase of Ca_E, the intensity of electric stress increases over the surface tension which leads to larger EHD induced droplet deformation.

The quantitative comparisons of Taylor deformation as function of Ca_E for PR_A fluid is shown in FIG 3.7. This figure shows that the droplet deforms into a prolate shape and the magnitude of deformation increase with the increasing value of Ca_E. When Ca_E is increased from 0.3 to 0.35, the electric stress is sufficiently strong to overcome the surface tension which leads to a sudden elongation and break-up of the droplet as shown inset of FIG 3.7. Here, the deformation parameter obtained from present simulation is validated by the existing analytic, numerical and experimental results. For analytical comparison, the present results are compared to the first- and second-order theory of Taylor [112] and Ajayi [5]. Analytical comparison clearly depicts that the deformation curve obtained from present simulation quickly deviates from the first-order theoretical prediction of Taylor [112]. However, the present results show good agreement with second order corrections of Ajayi [5] up to $Ca_E = 0.2$. A reasonable agreement is also obtained among the present results and the axisymmetric boundary integral solution of Lac and Homsy [58] and also with the experimental data provided by Ha and Yang [42].

The quantitative comparisons of Taylor deformation as function of Ca_E for PR_B fluid is shown in FIG 3.8. Here, the deformation parameter obtained from present simulation is validated by the existing analytic, and numerical results. This figure shows that the droplet deforms and forms conical ends at both ends. With the increasing value of Ca_E, the conical ends become more prominent and form Taylor cones. When two Taylor cone develop at its opposing ends, infinitely long thin liquid charged jets start to form from these ends which is known as EHD tip streaming. Inset of FIG 3.8 shows the onset of tip streaming at $Ca_E = 0.45$.

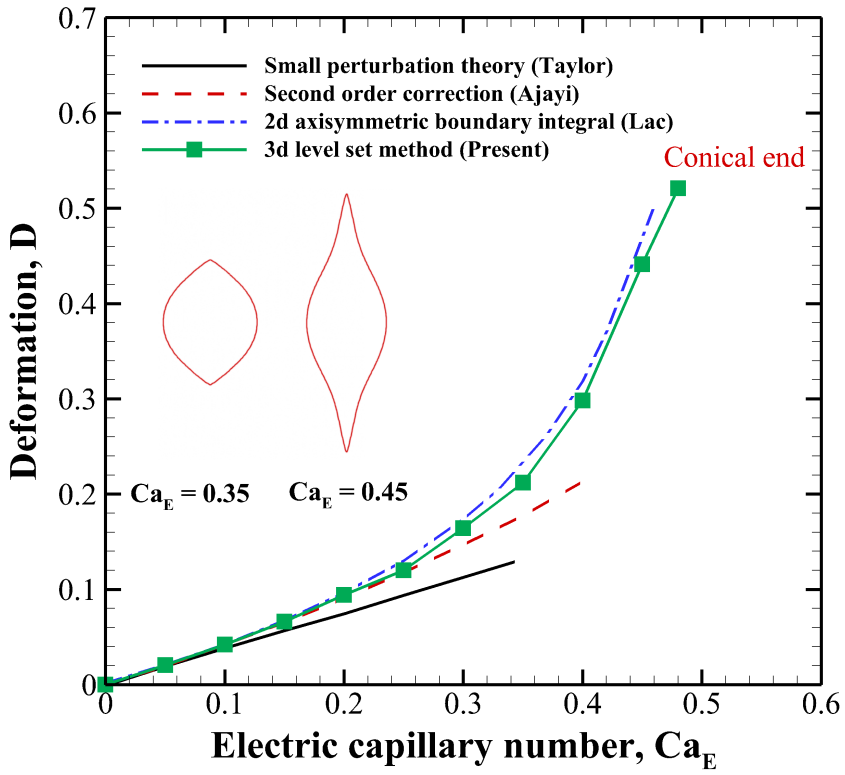

Fig. 3.8 Droplet deformation as a function of electric capillary number, Ca_E, for prolate droplet at K =25.0, Q =50.0, Re = 0.1, and $r_d = 1$, $r_v = 0.874$.

For analytical comparison, the present results are compared to the first- and second-order theory of Taylor [112] and Ajayi [5]. Analytical comparison clearly depicts that the deformation curve obtained from present simulation quickly deviates from the first-order theoretical prediction of Taylor [112]. However, the present results show good agreement with second order corrections of Ajayi [5] up to $Ca_E = 0.25$. A good agreement is also obtained between the present results and the axisymmetric boundary integral solution of Lac and Homsy [58].

Streamline and charge distribution for prolate droplet

When a droplet is subjected to a uniform electric field in leaky dielectric fluid system, all the free charges get accumulated at the interface. Charge density distribution and streamlines of the PR_A droplet at $Ca_E = 0.2, 0.3$ and 0.35 are shown in FIG 3.9. In this case, surface

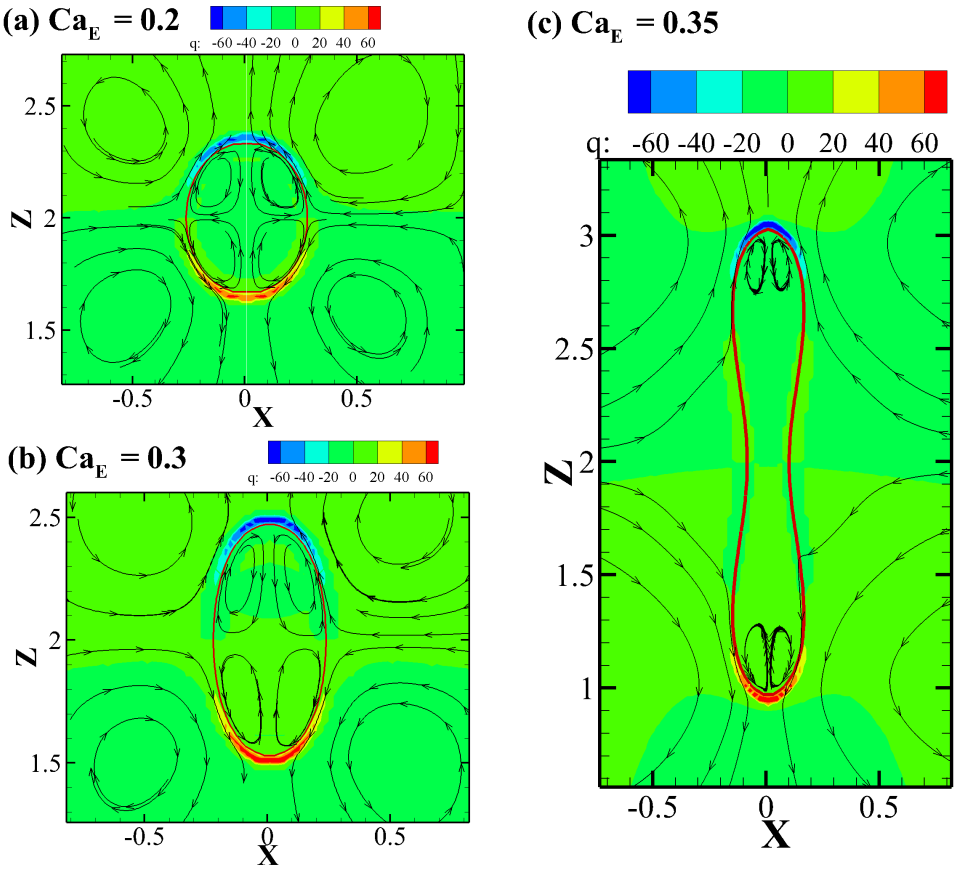

Fig. 3.9 Charge density distribution and streamlines of the prolate droplet at different Ca_E: (a) $Ca_E = 0.2$, (b) $Ca_E = 0.3$; and (c) $Ca_E = 0.35$ for K =10.0, Q =1.37, Re = 0.1, and $r_d = 1$, $r_v = 0.874$.

electric traction force acts in the parallel direction of imposed electric field which results a motion in the surrounding fluid from the equator (θ = 90 °) towards the pole (θ = 0 or 180°). Thus results in a maximum deformation parallel to the electric field and leading to a prolate deformation. In addition to it, for the steady state (at $Ca_E = 0.2, 0.3$), stable counter rotating toroidal vortices are also generated inside the droplet. These flow pattern and direction of toroidal vortices also match with the other established theoretical model [33, 118].

Charge density (q) along the prolate droplet surface as a function of polar angle (θ) at $Ca_E = 0.3$ is shown in FIG 3.10. From the figure, it is apparent that the magnitude of charge density is maximum at two poles at (θ = 0 and 180°) while it reduces to zero at the equator region (θ = 90 °).

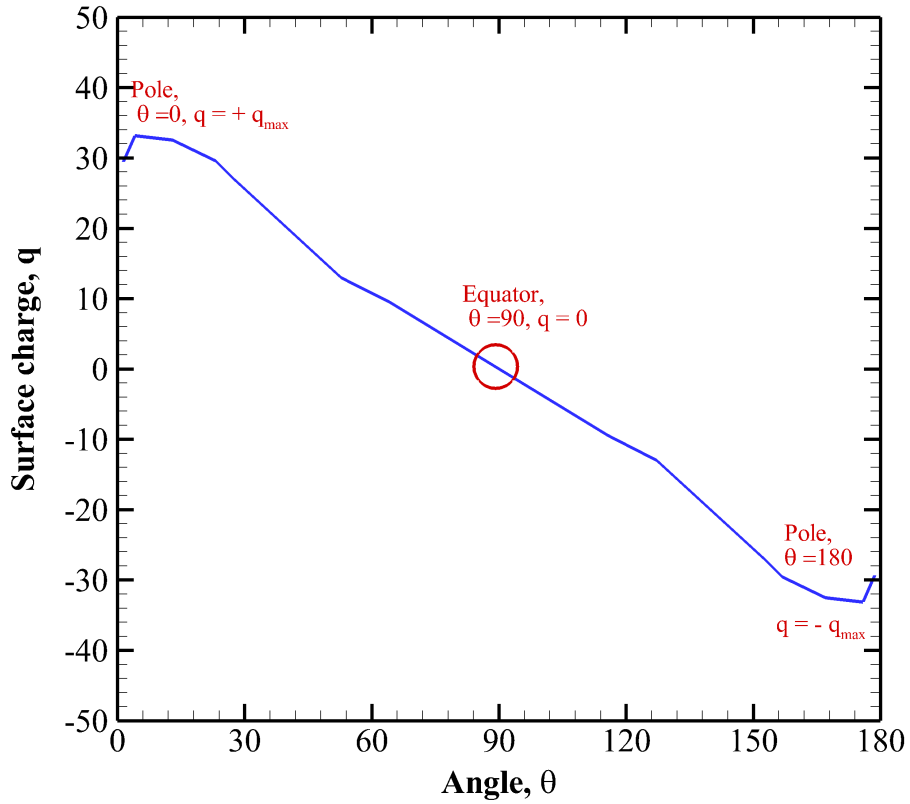

Fig. 3.10 Surface charge distribution (q) as a function of polar angle θ, at $Ca_E = 0.3$, K =10.0, Q =1.37, Re = 0.1, and $r_d = 1$, $r_v = 0.874$.

Oblate droplet deformation

For oblate deformation, we have modeled a fluid system denoted by *OB* with (K,Q) = (0.10, 2.0). This fluid system is also used by Lac and Homsy [58] in their axisymmetrical study of EHD induced droplet deformation.

For oblate deformation, another mesh convergence and domain-independence tests have done for *OB* fluid system. The temporal evolution of the droplets Taylor deformation parameter for three different mesh densities which are dx = dy = dz = 1/50, 1/64, and 1/100 has been shown in FIG 3.11. From the fig, it is obtained that the mesh density dx = dy = dz = 1/64 is sufficient to get convergency. With such a mesh density, we have 33 meshes across the diameter of the droplet and mass of the droplet can also be conserved reasonably well with the relative mass change within 0.7%.

In regards to domain-independence tests three computational domain sizes are taken 12R×12R×4R, 12R×12R×8R, and 16R×16R×4R in x,y and z directions respectively with dx = 1/64. A time evolution of the droplets Taylor deformation parameter for oblate droplet at $Ca_E = 0.35$ (which leads to oblate breakup) has been shown in FIG 3.12 . It is shown that a computational domain with size 12R×12R×4R is large enough to neglect the boundary effect. Therefore the mesh density, dx = 1/64 and computational domain size 12R×12R×4R are used in the validation for the oblate droplet.

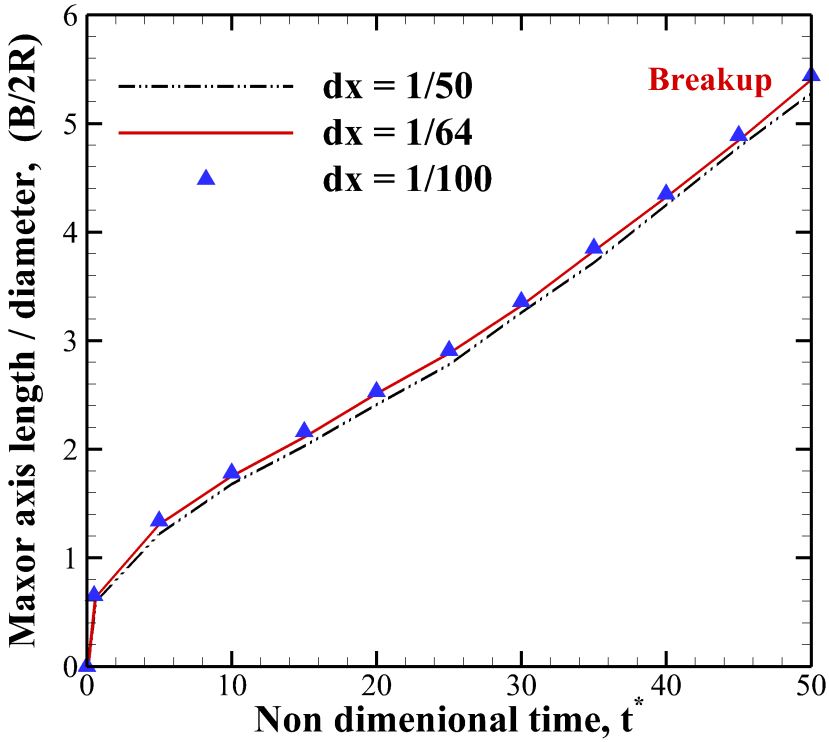

Fig. 3.11 Time evolution of deformation of oblate droplet in uniform electric field with different mesh densities for K =0.10, Q = 2.0 , Ca_E=0.35 (where the droplet does not take steady shape and leads to breakup), Re = 0.1, and $r_d = 1$, $r_v = 0.874$.

Similar to prolate droplet, the deformation of oblate droplet is also controlled by electric capillary number Ca_E. The effect of different electric capillary number (Ca_E) on droplet deformation for *OB* system fluid is shown quantitatively in FIG 3.13. From the fig, it is depicted that the droplet deformation increases with the increase of Ca_E and maximum

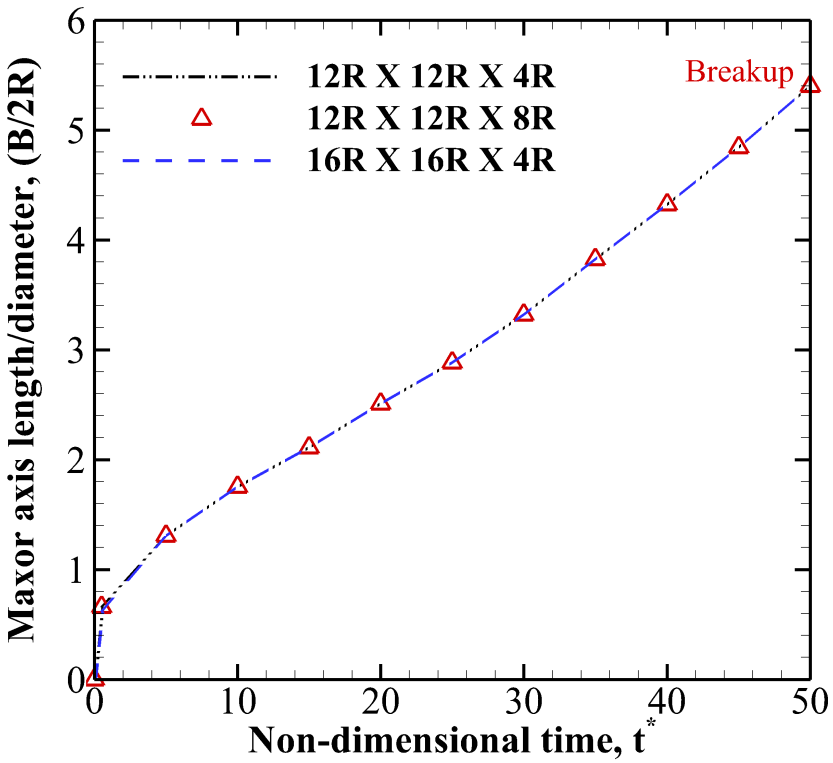

Fig. 3.12 Time evolution of deformation of oblate droplet in uniform electric field with different domain sizes for K =0.10, Q = 2.0 ,Ca = 0.4, Re = 0.1, and $r_d = 1$, $r_v = 0.874$.

deformation occurs at the perpendicular direction of applied field which leads to oblate shape droplet. Here, the droplet reaches the steady shape upto Ca_E = 0.3. After that at Ca_E = 0.35, the droplet no longer takes steady shape and with time it elongates more and more and form bulbous shape at two ends which can lead to breakup as shown inset of FIG 3.13.

The deformation parameter obtained from present simulation for *OB* fluid system is validated by the existing first and second order perturbation theory of Taylor [112] and Ajayi [5] as shown in FIG 3.13. Results obtained from the present simulation deviates from the analytical results after $Ca_E = 0.1$ as analytical results fails to capture larger deformation. However, the present result show a good agreement with the axisymmetric boundary integral solution of Lac and Homsy [58] as shown in FIG 3.13.

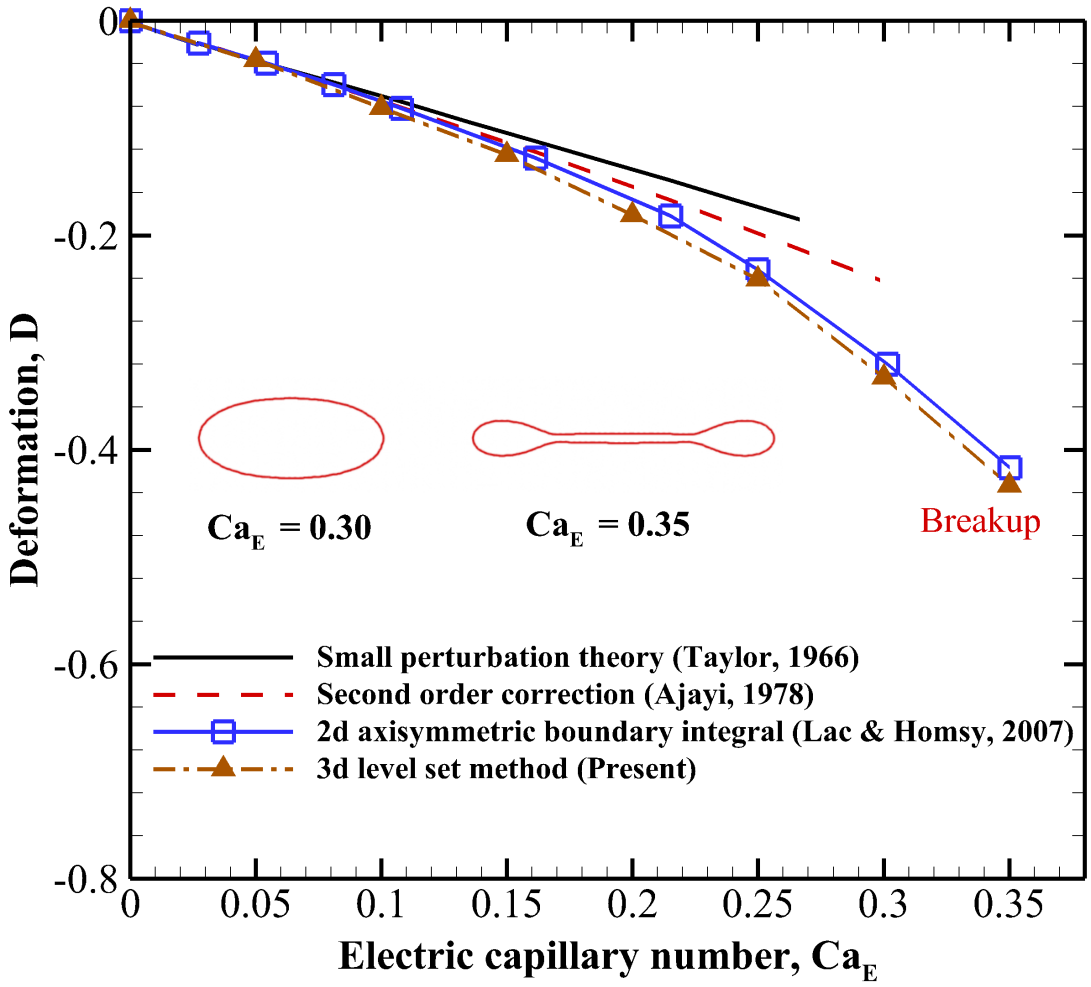

Fig. 3.13 Droplet deformation as a function of electric capillary number, Ca_E, for oblate droplet at K =0.10, Q =2.0, Re = 0.1, and $r_d = 1$, $r_v = 0.874$.

Streamline and charge distribution for oblate droplet

Charge density distribution and streamlines of the oblate droplet at $Ca_E = 0.2, 0.3$ and $Ca_E = 0.35$ are shown in FIG 3.14. In this case, surface electric traction force acts in the perpendicular direction of imposed electric field which results a motion in the surrounding fluid from the pole ($\theta = 0$ or $180°$) towards the equator ($\theta = 90\,°$). Thus results in a maximum deformation perpendicular to the electric field and leading to an oblate deformation. Besides, additional counter-rotating toroidal vortices are also generated inside the droplet for the steady state at Ca_E = 0.2, 0.3. Charge density (q) along the oblate droplet surface as a

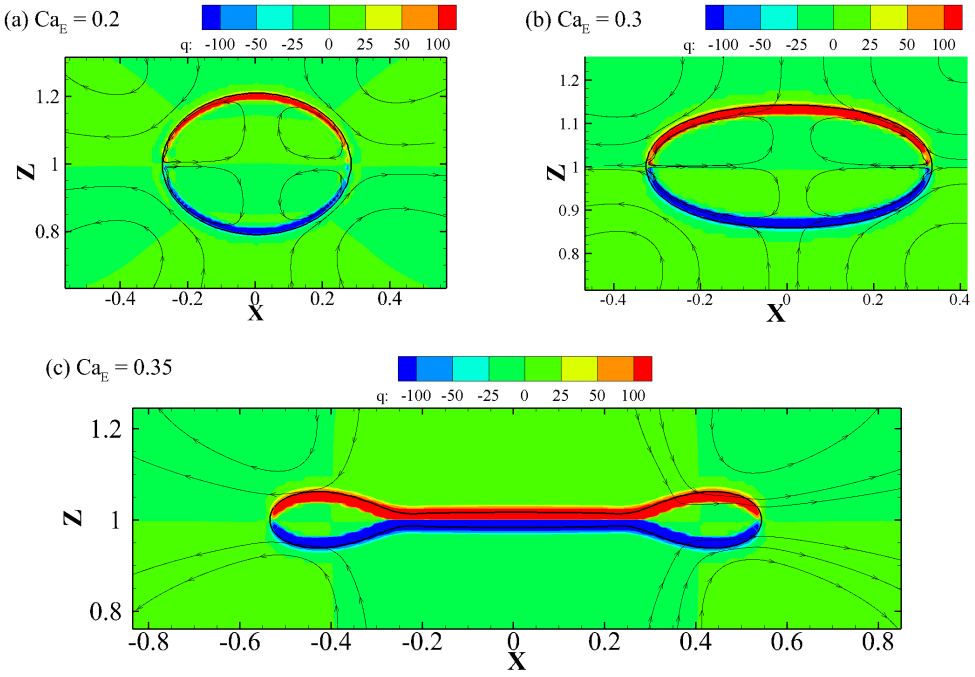

Fig. 3.14 Charge density distribution and streamlines of the oblate droplet at different Ca_E: (a) $Ca_E = 0.2$, (b) $Ca_E = 0.3$; and (c) $Ca_E = 0.35$ for K =10.0, Q = 2.0, Re = 0.1, and $r_d = 1$, $r_v = 0.874$.

function of polar angle (θ) is shown in FIG 3.15. From the figure, it is apparent that the magnitude of charge density is maximum at two poles at (θ = 0 and 180°) while it reduces to zero at the equator region (θ = 90 °).

3.3 Droplet subjected to both uniform electric field and shear flow

When a spherical droplet is subjected to both uniform electric field and simple shear flow, the droplet experiences mainly three types of stresses:

- Viscous stress which always tries to deform the droplet towards the flow direction.
- Electric stress which tries to deform the droplet depending on the value of conductivity and permittivity ratio of the two fluids.

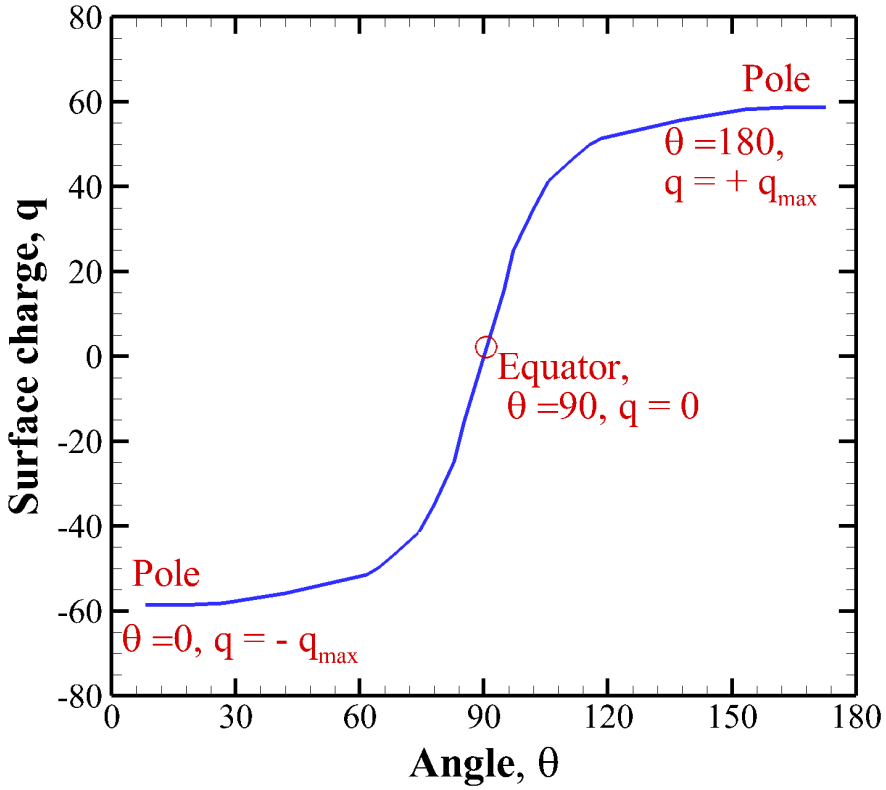

Fig. 3.15 Surface charge distribution for oblate droplet on (a) 3d surface; (b) Charge density (q) as a function of polar angle θ, at $Ca_E = 0.3$, K =10.0, Q = 2.0, Re = 0.1, and $r_d = 1$, $r_v = 0.874$.

- Restoring capillary stress which helps the droplet to maintain its spherical shape.

The relative intensity of viscous stress over capillary stress is denoted by the capillary number ($Ca = \frac{\mu_2 GR}{\gamma}$). Electric capillary number $Ca_E = \frac{\varepsilon_2 E_\infty^2 R}{\gamma}$ measures the relative intensity of electric stress over capillary stress. Therefore, in this case both Ca and Ca_E play significant role in deformation and breakup of the droplet. Another important non-dimensional number is flow Reynolds number, $Re = \frac{\rho_2 GR^2}{\mu_2}$ where G is the shear rate.

3.3.1 Problem statement

In this case, we consider an initially uncharged liquid droplet of radius R which is suspending in another immiscible liquid in a confined Couette flow configuration. The top and bottom

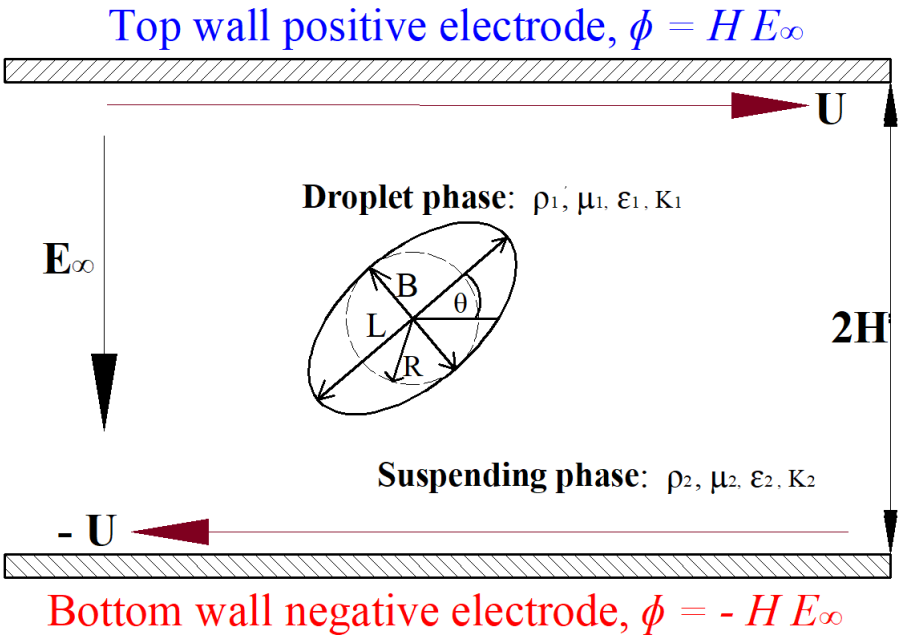

Fig. 3.16 Droplet in shear flow with a uniform electric field.

walls are separated by a distance 2H and subjected to a uniform electric field of strength E_∞ in the transverse direction. The top wall is connected to the positive electrode of electric potential, $\Phi = HE_\infty$ and the bottom wall is connected to the negative electrode of electric potential, $\Phi = -HE_\infty$ as shown in FIG 3.16.

Initially, the drop is spherical which is represented by dashed line. When the droplet is subjected to both uniform electric field and shear flow, the droplet deforms. The deformed profile is represented by a solid line which is inclined at an angle (θ) with the horizontal axis. L and B denote the major and minor axis length after the deformation. Both drop and suspending fluids have been considered as leaky dielectric having separate fluid and electric properties such as: densities ρ_1 and ρ_2, viscosities μ_1 and μ_2, electric permittivity's ε_1 and ε_2 and conductivities K_1 and K_2. The subscripts 1 and 2 refer to the physical parameters inside and outside of the droplet respectively. We use the suspending fluid as the reference fluid.

3.3.2 Results and discussion

The computational domain used in the present simulation is a cubic box. The droplet is placed at the centre of the box. Periodic boundary conditions are used in x and y directions. While at z direction, no-slip boundary condition is used for the flow field and Dirichlet boundary condition are imposed for the electric potential which are illustrated in FIG 3.18.

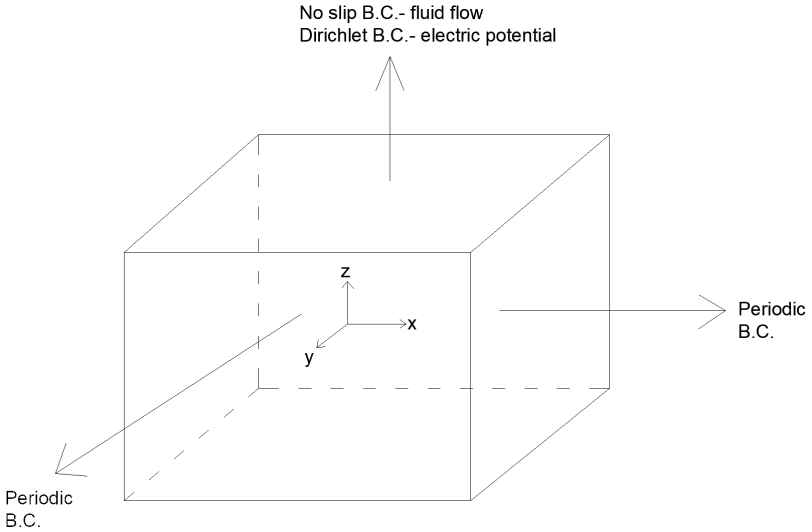

Fig. 3.17 Illustration of boundary conditions for droplet in shear flow case.

The uniform rectangular meshes are used to discretize the computational domain. For this problem, we have modeled a fluid system with K =10, Q = 2, Re = 0.1 , $r_d = r_v = 1$, and different combination of Ca and Ca_E. This fluid system is also used by Singh [103] in their Lattice Boltzmann study of EHD induced droplet deformation.

Before validating the method, a careful mesh-convergence and domain-independence tests have been conducted to ensure that the reported results do not change with further increasing the mesh density or domain size. The mesh convergency test has been performed for three different mesh densities which are dx = dy = dz = 1/40, 1/50, and 1/64 respectively. The temporal evolution of the droplets Taylor deformation parameter for various mesh densities has been shown in FIG 3.18 for Ca = 0.2 and $Ca_E = 0$. From the result it is seen that the mesh density dx = dy = dz = 1/40 is sufficient to capture the important characteristics.

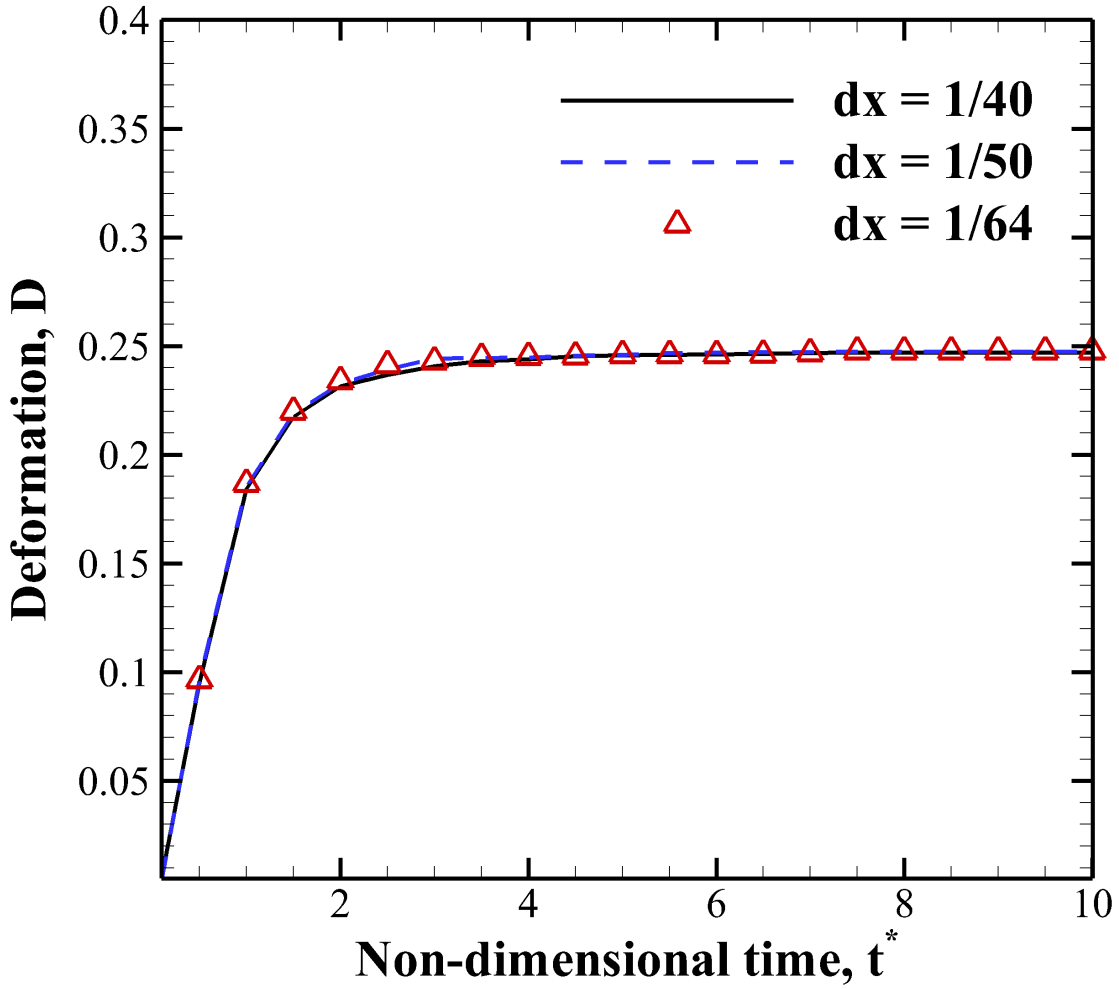

Fig. 3.18 Time evolution of deformation of droplet in shear flow with a uniform electric field with different mesh sizes at K =10, Q =2, Ca=0.2, $Ca_E = 0$, Re = 0.1, and $r_d = r_v = 1$.

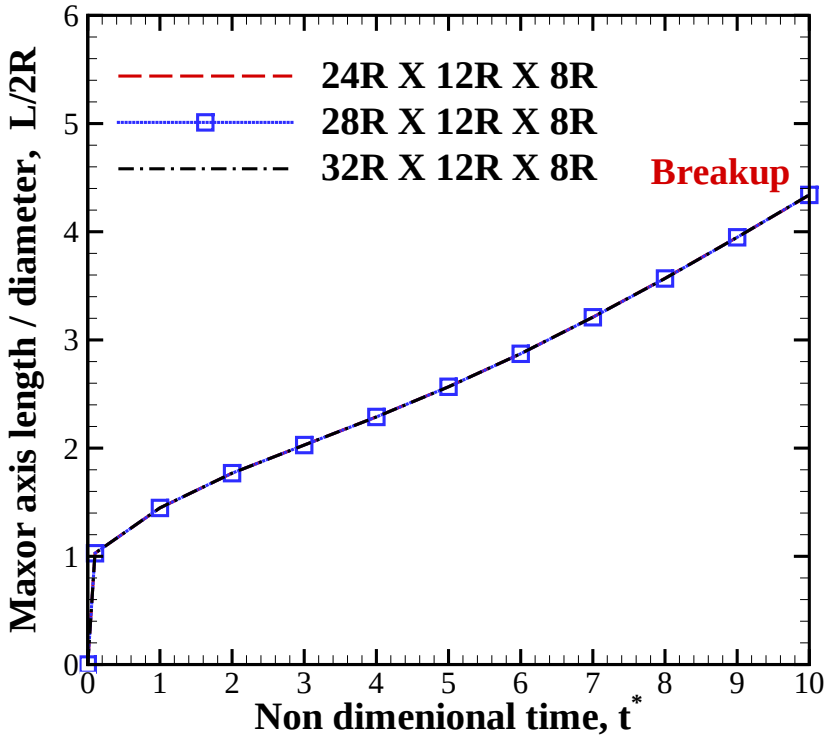

Fig. 3.19 Evolution of droplet elongation subjected to both shear flow and uniform electric field for various computational domain sizes Parameters: Re = 0.1, Ca = 0.2, $Ca_E = 0.4$, K = 10, Q = 2 , $r_d = 1.$, and $r_v = 1$.

To avoid the boundary effects, a domain independence test has also been done for three computational domain sizes 24R×12R×8R, 28R×12R×8R, and 32R×12R×8R in x,y and z directions respectively. A time evolution of the droplet's maximum elongation where the droplet undergoes breakup has been shown in FIG 3.19 for Ca = 0.2 and $Ca_E = 0.4$. Here, the maximum elongation is quantified by major axis length/diameter (L/2R)). It is shown that a computational domain with size 24R×12R×8R is large enough to neglect the boundary effect and capture the breakup phenomenon. Therefore the mesh density, dx = 1/40 and computational domain size 24R×12R×8R are used in the validation for this case.

The time evolution of maximum elongation of the droplet for different Ca_E is shown in FIG 3.20. In this problem, droplet deformation is governed by both Ca and Ca_E. At a fixed Ca, the droplet deformation increases with the increase of Ca_E. This fig depicts that at Ca

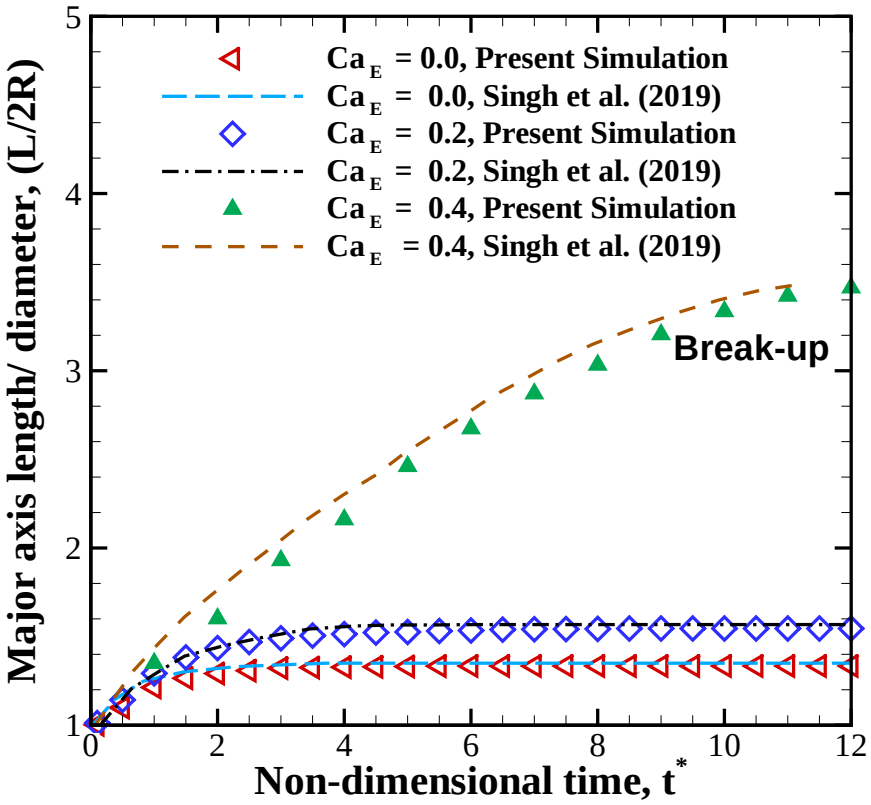

Fig. 3.20 Time evolution of maximum elongation of the droplet for different Ca_E with K =10, Q = 2, Ca = 0.2, Re = 0.1 and $r_d = r_v = 1$.

= 0.2, the droplet takes steady shape for Ca_E = 0.0, 0.2 while it breaks at Ca_E = 0.4. The results from the present simulation show a very good agreement with the numerical results of Singh[103].

FIGs. 3.21 and 3.22 illustrate the droplet fate when subjected to both uniform electric field and shear flow for different Ca_E at Ca = 0.2 and 0.3 respectively. From the figures it is obtained that the value of $Ca_E(crit)$ decreases with increase in Ca. For example, at Ca= 0.2, the droplet breakup occurs at Ca_E = 0.36, whereas for Ca = 0.3 the droplet breakup is observed at Ca_E = 0.2. The small satellite droplets which are formed between the two droplets is not taken into account in this research work.

FIG. 3.23 depicts the fate of the droplet at different combination of Ca_E and Ca for fluid having (K, Q) = (10.0, 0.2) at Re = 0.1. The phase diagram depicts that the value of $Ca_E(crit)$

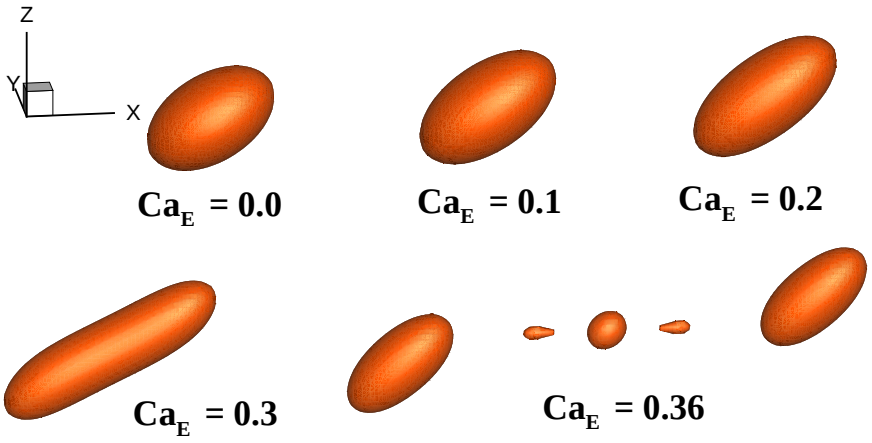

Fig. 3.21 Droplet fate when subjected to both uniform electric field and shear flow for different Ca_E with K =10, Q = 2, Ca = 0.2, Re = 0.1 and $r_d = r_v = 1$.

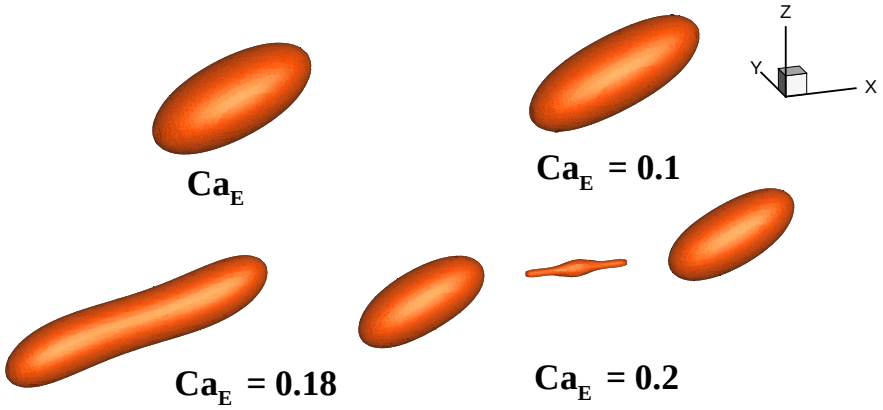

Fig. 3.22 Droplet fate when subjected to both uniform electric field and shear flow for different Ca_E with K =10, Q = 2, Ca = 0.3, Re = 0.1 and $r_d = r_v = 1$.

decreases with the increase of Ca. Therefore, the cumulative effect of electric stress and shear flow promotes the breakup phenomenon even at smaller Ca which is not possible if there is only shear flow.

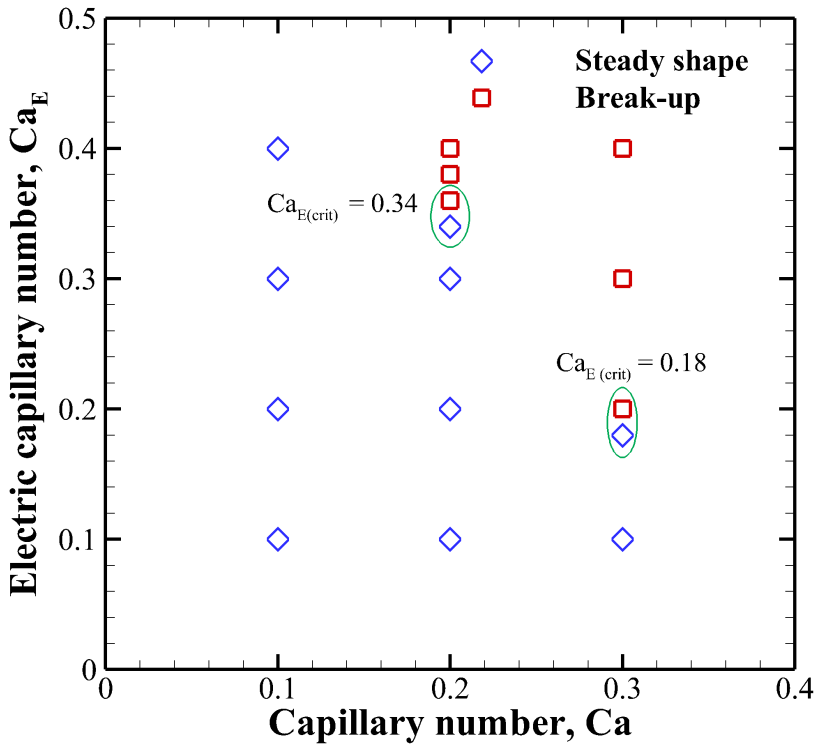

Fig. 3.23 Phase diagram from droplet subjected to both shear flow and unifrom electric field for different Ca and Ca_E at K =10, Q = 2, Re = 0.1 and $r_d = r_v = 1$.

3.4 Conclusions

We have developed a 3d dimensional level set method for two-phase EHD problem. In this chapter we have tested the developed code for two problems namely: (a) Droplet subjected to uniform electric field. (b) Droplet subjected to both uniform electric field and shear flow.

Droplet subjected to uniform electric field

In this problem, we numerically study the electrohydrodynamics of a leaky dielectric drop suspending in another leaky dielectric fluid under the action of a uniform electric field. The aim of this study to obtain the shape deformation of the droplet and validated with the existing analytical, numerical and experimental results. From the results, it is obtained that the droplet deformation increase with the increase of electric stress which is quantified by

electric capillary number, Ca_E. We have obtained three types of droplet deformation namely prolate A (PR_A), prolate B(PR_B), and oblate (OB) drop depending on the conductivity (K) and permittivity (Q) ratio between the two fluids, . If K>Q, the droplet takes (PR_A) shape. However when K<Q, the droplet can take either (PR_B) or (OB) shape.

For (PR_A) and (OB) drops, the droplet takes a steady prolate and oblate shape respectively upto $(Ca_E = 0.3)$. At $(Ca_E = 0.35)$ the droplet elongates more and more and lead to breakup. However, (PR_B) drop behaves very differently from the above two systems. In this system, with the increase of (Ca_E) the deformation increases but the droplet forms conical shape at two ends . At $(Ca_E = 0.45)$, the conical ends results in tip-streaming from two ends. Results obtained from the developed code are qualitatively validated against the existing analytical result of Taylor [112] and Ajayi [5], axisymmetric boundary integral solution of Lac and Homsy [58] and experimental results provided by Ha and Yang [42].

Droplet subjected to both uniform electric field and simple shear flow

In this problem, we consider a leaky dielectric drop suspending in another leaky dielectric fluid and subjected to both uniform electric field and shear flow. In this case, the droplet deformation is governed by both (Ca_E) and (Ca) . The quantitative validation of the present with the numerical results of Singh [103] show very good agreement. In addition to it, a phase diagram is established at different combination of (Ca_E) and (Ca) which depicts that the value of $(Ca_E(crit))$ decreases with the increase of Ca. Therefore, the cumulative effect of electric stress and shear flow promotes the breakup of the droplet even at smaller (Ca) which is not possible if there is only shear flow.

Chapter 4

Application of the method- Droplet sorting using electric field

4.1 Introduction

The sorting of droplets is one of the most important application in microfluidics especially in biological research such as drug delivery [124, 24], biological culture [128, 20, 76] or industrial products such as cosmetics [52, 31] and food additives [75]. Sorting of droplet in a microfluidic channel can be divided into two categories: passive method and active methods. The passive method sorts the droplets based on the characteristics of the droplet and channel geometry. Implementing the passive method, Tan et al. [110] designed a useful and efficient microfilter to sort droplets by sizes. However, this method lacks flexibility as sorting criteria of the passive method cannot be changed after the setting. On the contrary to, active sorting method offers more flexibility in which sorting technique can be controlled at any time. Different active sorting techniques are acoustophoresis, hydrophoresis, magnetophoresis, electrophoresis and dielectrophoresis (DEP). The name of each of these techniques includes two parts, first part indicates the type of the applied force and the second part “phoresis”

means motion. Among all of these techniques, the fastest sorting speeds to date are achieved by dielectrophoresis (DEP) [91, 3, 9].

DEP is the motion of a droplet in a spatially non-uniform electric field .When an initially uncharged drop suspending in another fluid is subjected to a spatially non-uniform electric field, all the free charges from both fluids get accumulated at the interface and the particle get polarized. Due to non-uniformity of the electric field, charges at the interface generate non-equal Columbic forces which causes the DEP motion of the droplet in a particular direction depending on the electrical properties.

For an insulating spherical particle of radius R, in a nonuniform electric field E, the net DEP force is first defined by Pohl [88].

$$\mathbf{F}_{\mathrm{DEP}} = 2\pi R^3 \varepsilon_0 \varepsilon_{\mathrm{m}} \beta \nabla \mathbf{E}^2, \tag{4.1}$$

where R is the droplet radius, ε_{m} is the permittivity of the fluid, $\varepsilon_0 = 8.854 \times 10^{-12}$ F/m is the vacuum permittivity and $\mathbf{E}$ is the electric field intensity. $\beta(\omega)$ is the real part of the frequency-dependent Clausius–Mossotti factor which is given by:

$$\beta(\omega) = \mathrm{Re}\left(\frac{\varepsilon_{\mathrm{p}}^* - \varepsilon_m^*}{\varepsilon_{\mathrm{p}}^* + 2\varepsilon_{\mathrm{m}}^*}\right), \tag{4.2}$$

$\varepsilon_{\mathrm{p}}^*$ and $\varepsilon_{\mathrm{m}}^*$ are the complex permittivity of the drop and the fluid, respectively.

There are two types of DEP motion: positive DEP and negative DEP. If the droplet has lower permittivity than the suspending fluid, it will be attracted to the stronger field regions which is known as positive DEP (pDEP). On the other hand, when the permittivity of the droplet is higher than the suspending fluid, it will be repelled from the electric field which is known as negative DEP (nDEP) . The schematic representation pDEP and nDEP is shown in FIG 1.5.

4.2 Problem statement

We consider an initially uncharged liquid droplet of radius R suspending in another medium flowing through a rectangular channel with an orthogonal side branch as shown in FIG 4.1 (a). Both the straight channel and the side branch have the constant cross section $4l^2$ with a side length of $2l$. The length of the parent channel is $8l$ whereas the length of the two daughter channels are $6l$. Here, the considered length is long enough for the droplet to reach a steady shape before the bifurcation without electric field effect. The fluid motion is governed by the incompressible Navier–Stokes equations. No-slip boundary condition is imposed at the channel wall. Fully developed laminar channel flow profiles are set at the inlet and two outlets with flow rates Q_0, Q_1, Q_2 respectively in a way that $Q_0 = Q_1 + Q_2$. The droplet is initially placed along the centreline of the parent channel at a distance of $2l$ from the inlet. A three-dimensional Cartesian coordinate system is used with x-axis along the axis of the main channel, z-axis along the side branch axis and the origin of the coordinate system is located at the intersection of the two centre lines of two daughter channels. The droplet and suspending medium are considered as water and oil having different physical and electric properties such as: densities ρ_1 and ρ_2, viscosities μ_1 and μ_2, electric permittivities ε_1 and ε_1 and conductivities K_1 and K_2. The subscripts 1 and 2 refer to the physical parameters inside and outside of the droplet respectively. We use the suspending fluid as the reference fluid.

If a spatially non-uniform electric field is generated inside a microchannel which is containing a droplet, the droplet faces DEP motion and moves in a particular direction. In practical DEP applications, the non-uniform can be generated in two ways. One way is to use electrodes of different shapes, size and designs [10] and another way is changing the position of the electrode at different position of the microfluidic channel.

In this research work, we have generated the non-uniform electric field inside the microfluidic channel by placing a rectangular electrode at the bottom of the channel with specific voltage. When a voltage is applied along a device, the electric field creates a linear

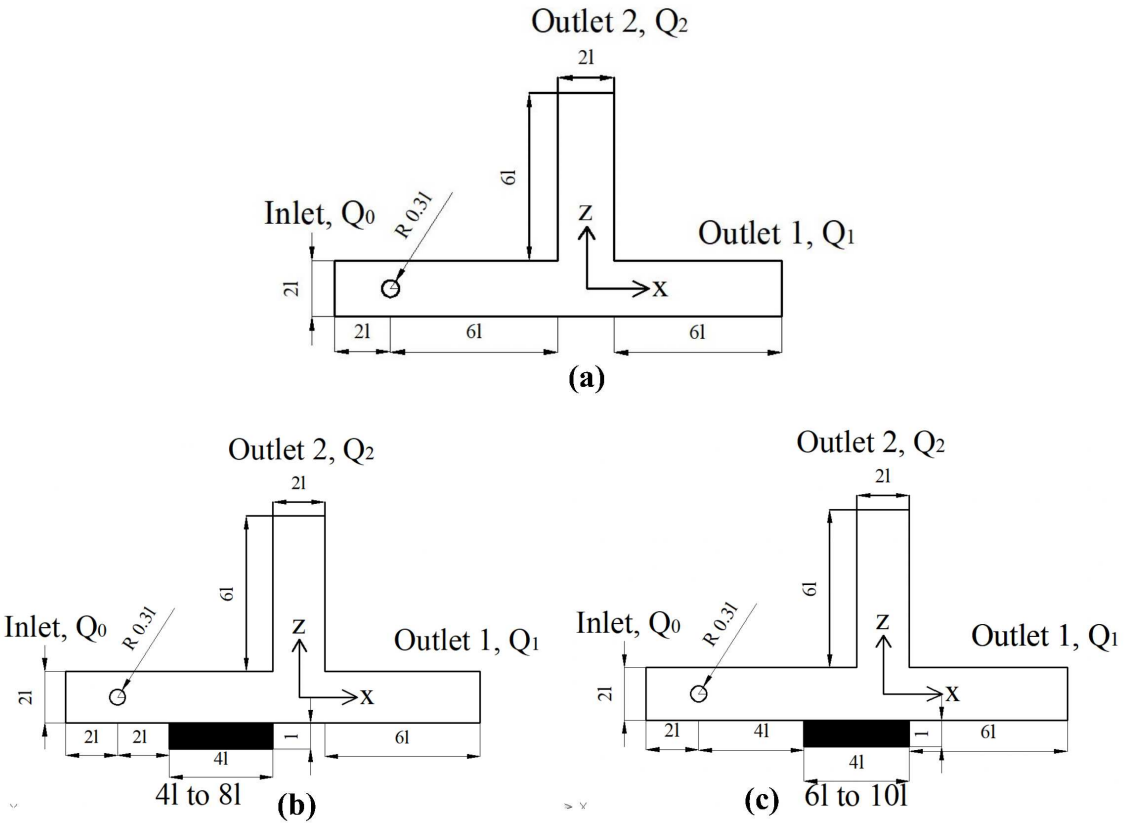

Fig. 4.1 Geometry of the rectangular channel with an orthogonal side branch: (a) without electrode; (b) electrode at position 1; (b) electrode at position 2.

.

gradient which allows the droplet to experience a spatial difference in electric field within the channel. We have considered two electrode positions at a distance of 4l and 6l from the inlet as shown in FIG 4.1 (b) and (c) respectively. The electrode positions are referred as electrode position 1 and electrode position 2. Length, width and height of both electrodes are 4l, 2l and l respectively where l is the half length of the cross-sectional width. With the presence of these electrode positions, electric field intensity is defined by capillary number Ca_E.

Non-dimensional numbers

The problem depends on a number of dimensionless parameters based on the flow configuration, hydrodynamic and electric properties of the drop and suspending fluid.

- *Branch flow ratio, (q)* measures the flow rate ratio of branch channel to main channel.

$$q = \frac{Q_2}{Q_1 + Q_2}, \tag{4.3}$$

where Q_1 and Q_2 are the flow rates in the downstream main channel and in the side channel, respectively, as indicated in FIG 4.1

- *Reynolds number, (Re)* measures the ratio of inertial forces to viscous forces.

$$Re = \frac{\rho_2 u l}{\mu_2}, \tag{4.4}$$

where u is the mean velocity of the Poiseuille flow imposed at the inlet of the main channel and l is the half-cross-sectional dimension of the main channel.

- *Electric conductivity ratio, (K)*: It measures the ratio of the conductivity between the droplet (K_1) and suspending fluid (K_2).

$$K = \frac{K_1}{K_2}, \tag{4.5}$$

- *Electric permittivity ratio, (S)*: It measures the ratio of the permittivity between the droplet (ε_1) and suspending fluid (ε_2).

$$S = \frac{\varepsilon_1}{\varepsilon_2}, \tag{4.6}$$

- *Viscosity ratio, (r_v)*: It measures the ratio of the viscosity between the droplet (μ_1) and suspending fluid (μ_2).

$$r_v = \frac{\mu_1}{\mu_2}, \tag{4.7}$$

- *Density ratio, (r_d)*: It measures the ratio of the density between the droplet (ρ_1) and suspending fluid (ρ_2).

$$r_d = \frac{\rho_1}{\rho_2}, \tag{4.8}$$

- *Hydrodynamic Capillary number, Ca :* measures the intensity of viscous stress over surface tension.

$$Ca = \frac{\mu_2 u}{\gamma}, \tag{4.9}$$

- *Electric Capillary number, (Ca_E)* measures the intensity of electric stress over surface tension.

$$Ca_E = \frac{\varepsilon_2 E^2 l}{\gamma}, \tag{4.10}$$

where γ is the interfacial tension, l is the half-cross-sectional dimension of the main channel. and E is the electric field intensity.

- *Size ratio, (λ)*: It measures the ratio of the droplet radius (R) to the half-cross-sectional dimension of the main channel (l).

$$\lambda = \frac{R}{l}. \tag{4.11}$$

4.3 Path selection of the droplet

In this problem, we have considered leaky dielectric-leaky dielectric fluid system consisting of water droplet suspending in soybean oil. This fluid system is also used in experimental study of Ahn et.al. [3]. The physical properties considered in this research are: K = 0.107, S = 1.34, r_d = 1.09, r_v = 0.018, $\lambda = 0.2, 0.3, 0.4$, Ca = 0.1, Ca_E = 0, 0.4, 0.9, Re = 1, 20 and different branch flow ratios q = 0.1 - 0.7. When this system of fluid is subjected to non-uniform electric field it shows negative DEP motion as permittivity ratio >1 (S>1), which

means that the permittivity of the droplet is higher than the permittivity of the suspending fluid. Therefore the droplet will be repelled from the electric field.

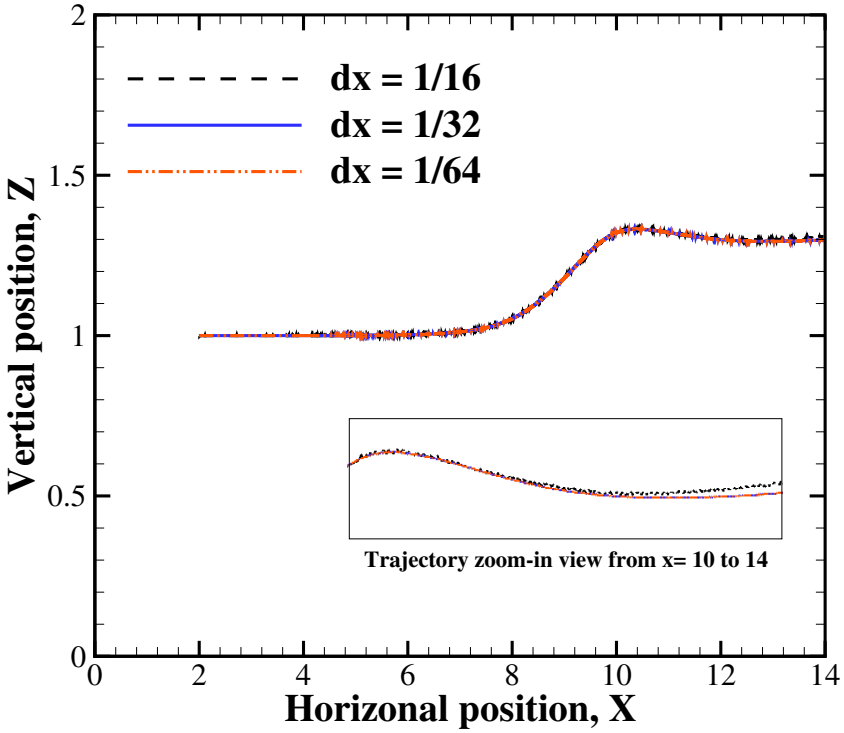

Fig. 4.2 Trajectories of a droplet (R/L = 0.3) flowing in the main channel at Re = 20.0, Ca = 0.1, $Ca_E = 0$, q = 0.3, r_d = 1.09, and r_v = 0.018 with three different mesh sizes

.

At first, we investigate the influence of mesh size on the trajectories of the droplet in x-z plane for three mesh densities which are dx = dy = dz = 1/16, 1/32 and 1/64 . FIG 4.2 shows the influence of different mesh resolution on the trajectories the droplet flowing in the main channel for Re = 20.0, Ca = 0.1, $Ca_E = 0$, q = 0.3 $\lambda = 0.3$, r_d = 1.09, and r_v = 0.018 . It is obtained that the trajectories for dx = 1/32 and 1/64 are almost superimposed on each other. Therefore, we chose dx = 1/32 for the current simulation having around 20 meshes across the diameter of the droplet which is sufficient enough to capture the important characteristics.

The main objective of this research work is to characterize the path selection of the droplet as a function of different physical parameters. A simple way to characterize sorting of a droplet is to define the critical branch ratio, q_c, above which the droplet enters the side

branch. Thus the droplet flows into the main channel after the bifurcation region if $q \leq q_c$ otherwise, it flows into the side branch. In the following section, we have investigated the effect of branch flow ratio (q), electric capillary number (Ca_E), electrode positions, inertia (Re) and size ratio (λ) on the path selection of the droplet. For each case at a fixed value of particular physical properties, we progressively increase q from 0.1 by large steps of $\Delta q = 0.1$ until we find the transition, where the droplet flows into the side branch rather than the main channel. Around the transition region, we then refine the step to $\Delta q = 0.02$.

4.3.1 Effect of branch flow ratio, (q) at Re = 1

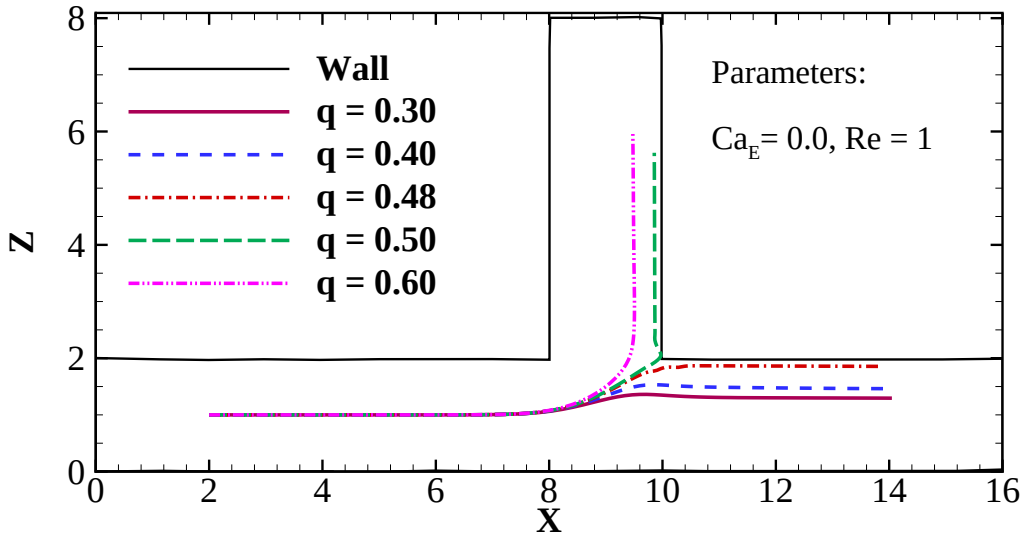

Fig. 4.3 Effect of different branch flow ratio, (q) on the path selection of the droplet without electric field ($Ca_E = 0$). Other parameters, Re = 1.0; Ca = 0.1, $\lambda = 0.3$, $r_d = 1.09$, and $r_v = 0.018$.

In this selection, we have analysed the path selection of the droplet without electric field effect. Without electric field, the droplet sorting is mainly governed by branch flow ratio, q and background flow strength defined by Re. FIG 4.3 presents the trajectories of the droplet's centre of mass for different branch flow ratios at Re =1. From the mass centre trajectory it is depicted that the droplet move along the centre line of the main channel before the bifurcation

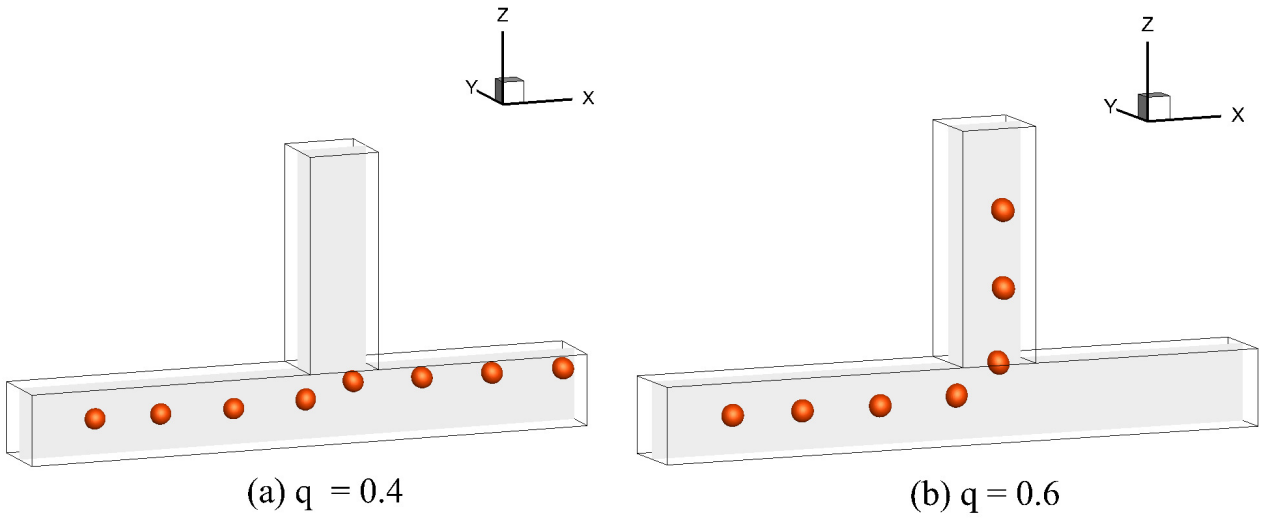

Fig. 4.4 The difference in path selection of the droplet at without electric field ($Ca_E = 0$) for branch flow ratio q = 0.4 and 0.6. Other parameters, Re = 1.0; Ca = 0.1, $\lambda = 0.3$, $r_d = 1.09$, and $r_v = 0.018$

region. When the droplet comes to the bifurcation region, it first attracted by the orthogonal side branch. If the value of $q > 0.48$, the droplet enters to the side branch otherwise, it moves back towards the main channel after passing the bifurcation region. Therefore the critical branch flow ratio without electric field is $q_c = 0.48$ at Re = 1.

The time evolution of the droplet profiles without electric field ($Ca_E = 0$) at Re = 1 are shown in FIG 4.4 for (a) q = 0.4 and (b) q = 0.6 respectively. From the figure it is obtained that the droplet takes the branch which receives the higher flow rate. Consequently it follows into the downstream main channel towards outlet 1 at q = 0.4 where the flow rate of the outlet 2 is lower than the outlet 1. When the flow rate of outlet 2 is increased to 0.6, the droplet enters to the side branch which can be sorted from outlet 2.

4.3.2 Effect of electric field, (Ca_E) at Re = 1

In this section, we have analysed the effect of electric field on the path selection of the droplet at a rectangular microchannel. The electric field effect is incorporated inside the channel by

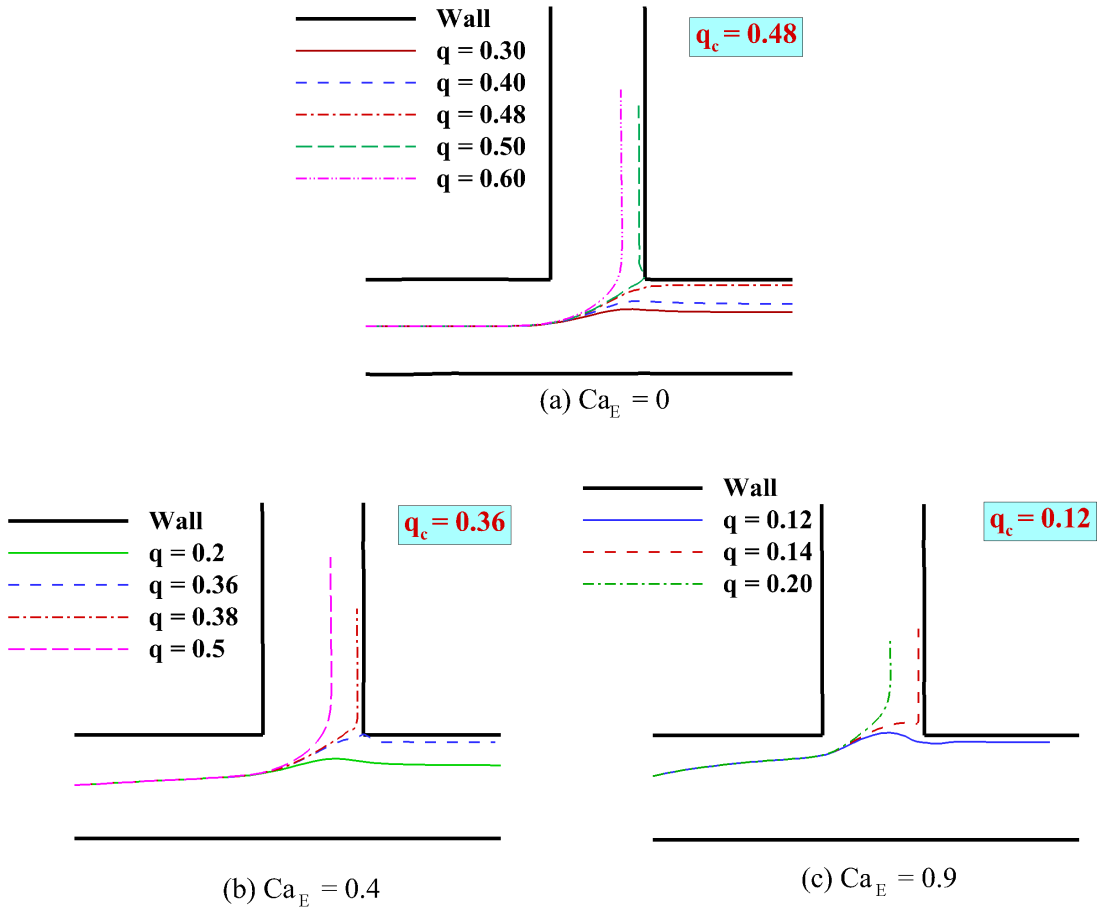

Fig. 4.5 Effect of electric field strength, (Ca_E) on the droplet trajectory at different branch flow ratio, (q). Other parameters, Re = 1.0; Ca = 0.1, $\lambda = 0.3$, $r_d = 1.09$, and $r_v = 0.018$

placing an electrode at the bottom of the channel with a specific voltage. We have considered 2 and 3V electric potential which corresponds to electric capillary number, Ca_E = 0.4 and 0.9 respectively.

FIG 4.5 shows the mass trajectories of the droplet's centre of mass for Ca_E = 0, 0.4, and 0.9. Ca_E is defined as the ratio of electric stress over surface tension. At Ca_E = 0, the electric field is absent and the path selection of the droplet depends on only branch flow ratio, q and Reynolds number, Re. FIG 4.5 (a) shows the trajectory of the droplet at Ca_E = 0 and Re = 1 for different branch flow ratios. In this case, the droplet follows the centre line until the

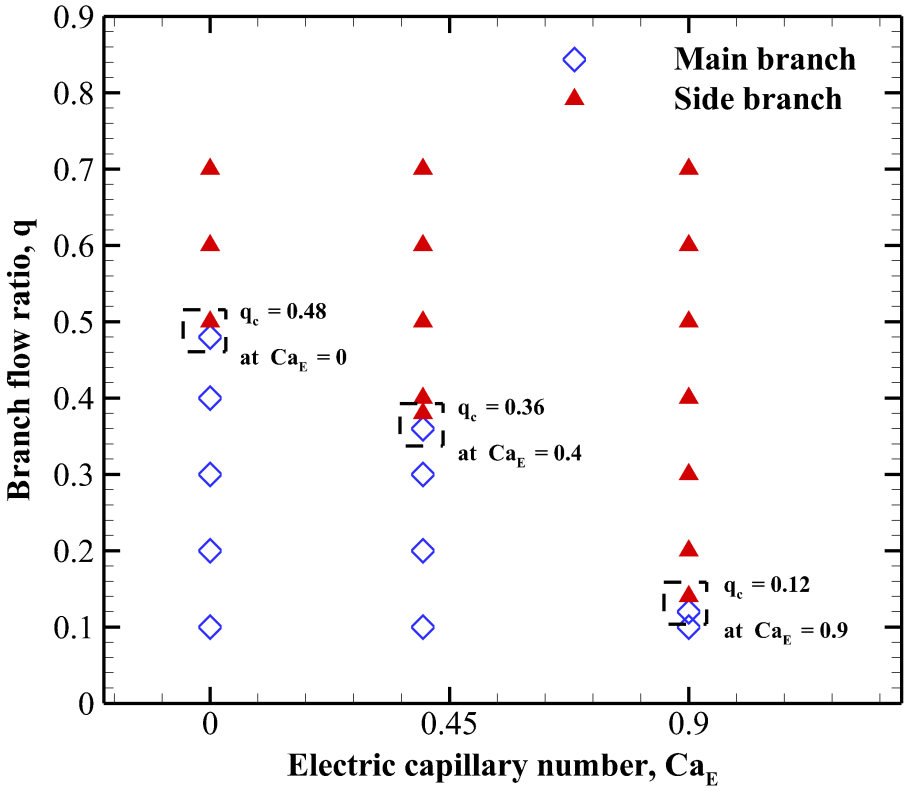

Fig. 4.6 Branch flow ratio as a function of electric capillary number. Other parameters, Re = 1.0; Ca = 0.1, electrode position 1, $\lambda = 0.3$, $r_d = 1.09$, and $r_v = 0.018$.

bifurcation region. After the bifurcation region, it follows into the downstream main channel upto q = 0.48. After that at and above equal branch flow ratio (q = 0.5), it enters into the orthogonal side branch. On the application of electric field with Ca_E = 0.4 and 0.9, it is obtained that the droplet enters the side branch even at lower branch flow ratio. At Ca_E = 0.4, the droplet enters the side branch from q = 0.38 whereas at Ca_E = 0.9, it enters the side branch at very low value of branch flow ratio which is q = 0.14. Therefore, electric field plays a significant role in reducing the value of critical branch flow ratio q_c.

A phase diagram for branch flow ratio (q) as a function of electric capillary number (Ca_E) is shown in FIG 4.6 for a droplet flowing in a microchannel without electric field and with electric field through an electrode at position 1. Without electric field, it is obtained that the q_c = 0.48 for Re = 1. When a non-uniform electric field is introduced through an electrode at

distance of 4l from the inlet (position 1), the obtained q_c = 0.36 and 0.12 for Ca_E = 0.4 and 0.9 respectively. Therefore, electric field can play a significant role in reduction of q_c which can faciliates the sorting of the droplet at desired outlet.

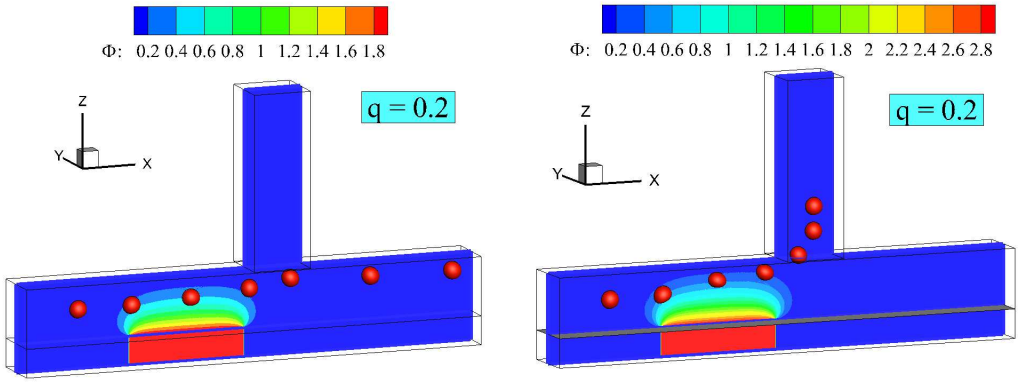

(a) $Ca_E = 0.4$ (b) $Ca_E = 0.9$

Fig. 4.7 The difference in path selection of the droplet at (a) $Ca_E = 0.4$ and (a) $Ca_E = 0.9$ for same branch flow ratio q = 0.2 and electrode position 1 . Other parameters, Re = 1.0; Ca = 0.1, $\lambda = 0.3$, $r_d = 1.09$, and $r_v = 0.018$

The time evolution of droplet profile at q = 0.2 are shown in FIG 4.7 for Ca_E = 0.4, and 0.9 respectively. In this research we have considered water droplet suspending in soybean oil. For this system, permittivity of the droplet is higher than the suspending fluid which gives rise to negative dielectrophoresis (nDEP) motion. Due to nDEP, the droplet starts to repel from the centre of the channel when it comes close to the electrode. Larger the value of Ca_E, larger the repulsive force acts on the droplet which promotes the sorting of the droplet at the side branch even at smaller value of q. Therefore at q = 0.2, the droplet favours the side branch at Ca_E = 0.9 while it flows into the downstream main channel at Ca_E = 0.4.

4.3.3 Effect of electrode position at Re = 1

We have considered two electrode positions at a distance of 4l and 6l from the inlet as shown in FIG 4.8 (a) and (b) respectively. Length, width and height of both electrodes are 4l, 2l and l respectively where l is the half length of the cross-sectional width.

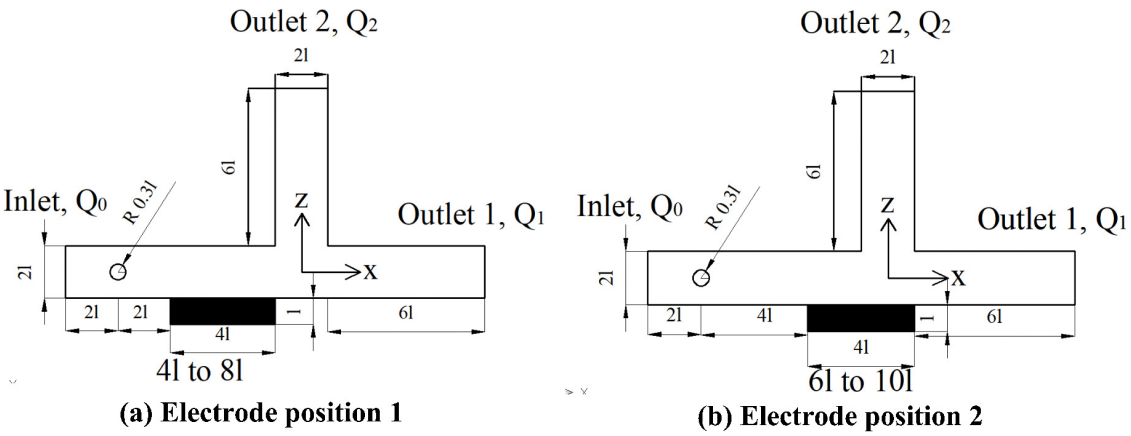

Fig. 4.8 Geometry of the rectangular channel with an electrode of length 4lX2lXl at a distance of 4l (a) (defined as position 1) and 6l (b) (defined as position 2) from the inlet

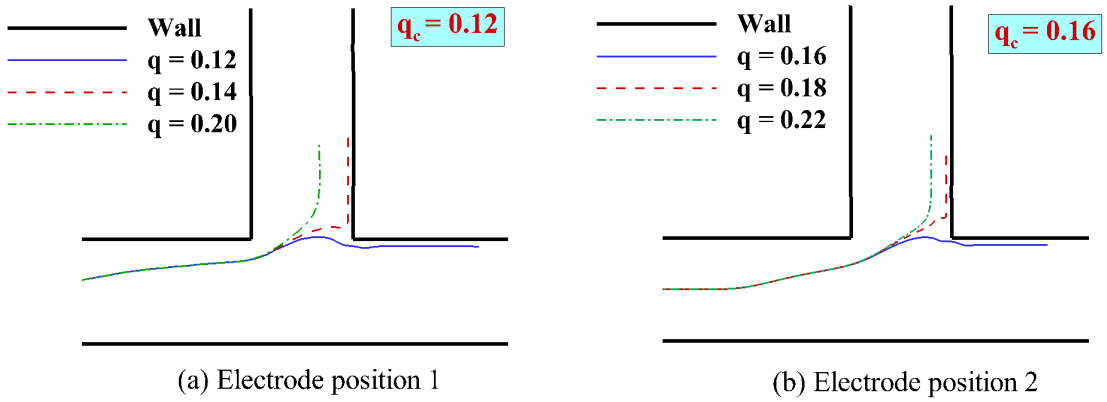

Fig. 4.9 Effect of electrode position on the droplet trajectory at different branch flow ratio, (q). Other parameters, Re = 1.0; Ca = 0.1, $Ca_E = 0.9$, $\lambda = 0.3$, $r_d = 1.09$, and $r_v = 0.018$

FIG 4.9 present the effect of electrode position on the droplet trajectory at different branch flow ratio, (q). From the mass centre trajectory it is depicted that the droplet move along the centre line of the main channel until it comes closer to the electrode. When it comes closer to the electrode due to physical properties of the system, the droplet undergoes a negative dielectrophoresis (nDEP) force and move far away from the centreline and reaches the bifurcation region. At the bifurcation region, it slows down and first attracted by the orthogonal side branch. When the electrode at position 1, the droplet enters to the side

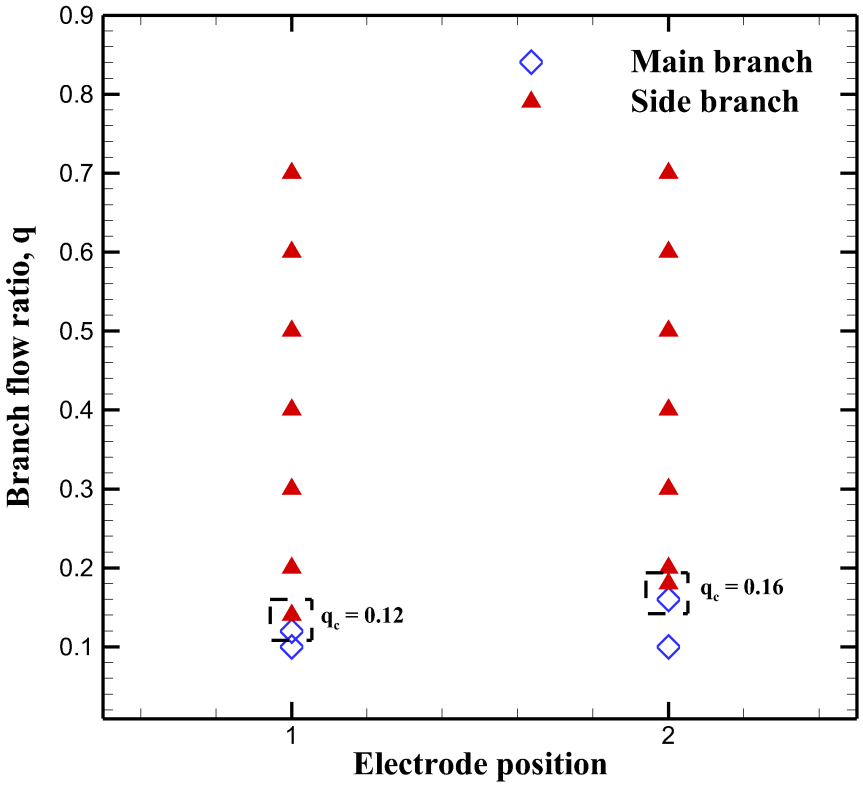

Fig. 4.10 Branch flow ratio as a function of electrode position. Other parameters, Re = 1.0; Ca = 0.1, $Ca_E = 0.9$, $\lambda = 0.3$, $r_d = 1.09$, and $r_v = 0.018$.

branch when $q > 0.12$ otherwise, it moves back towards the main channel after passing the bifurcation region as shown in FIG 4.9(a). However, when we move the electrode from position 1 to 2, it is found that the value of q at which the droplet enters the side branch increases. At this position, the droplet enters into the side branch if $q > 0.16$.

A phase diagram for branch flow ratio (q) as a function of electrode position (1 and 2) is shown in FIG 4.10 for a droplet flowing in a microchannel with electric field having $Ca_E = 0.9$. For electrode position 1, the electrode is placed at a distance of 2l from the droplet's initial position whereas for electrode position 2, the electrode is placed at a distance of 4l from the droplet's initial position.The phase diagram depict that the critical branch flow ratio is $q_c = 0.12 and 0.16$ for electrode position 1 and 2 respectively. Therefore, the closer

the electrode to the droplet initial position, the lower the critical branch flow ratio for sorting is obtained.

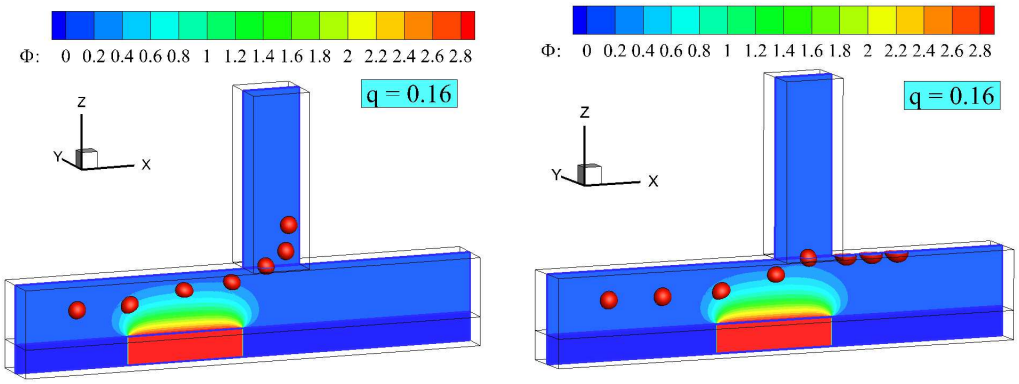

(a) Electrode position 1 (b) Electrode position 2

Fig. 4.11 The difference in path selection of the droplet at two different electrode positions (a) Position 1 and (b) Position 2 at same branch flow ratio, q = 0.16. (q). Other parameters, Re = 1.0; Ca = 0.1, $Ca_E = 0.9$, $\lambda = 0.3$, $r_d = 1.09$, and $r_v = 0.018$

The time evolution of the droplet profiles at q = 0.16 are shown in FIG 4.11 (a) and (b) for electrode position 1 and 2 respectively. From the figure it is obtained that for both electrode positions, the droplet move along the centre line of the main channel until it comes closer to the electrode position which is 4l and 6l position from the inlet for electrode position 1 and 2 respectively. Here both electrodes create a spatially non-uniform electric field with electric potential of 3 volt which corresponds to $Ca_E = 0.9$. When the droplet comes closer to the electrode, it deforms in an oblate shape as conductivity ratio is less than the permittivity ratio, (K<S). In addition to it, the droplet also faces the repulsive electric force due to negative DEP (nDEP). For electrode position 1, this electric repulsive electric force overcome the hydrodynamic force and the droplet enters into the side branch at $q = 0.16$. However for electrode position 2, the droplet can not overcome the hydrodynamic force and it flows back to the main channel at $q = 0.16$.

4.3.4 Effect of inertia, Re

We now investigate the trajectory of the droplet for higher Reynolds number at different branch flow ratios, q. FIG 4.12 presents the trajectories of the droplet's centre of mass for Re = 1 and 20 at different branch flow ratios. Here, other parameters are: Ca = 0.1, $Ca_E = 0.0$, $\lambda = 0.3$, $r_d = 1.09$, and $r_v = 0.018$. The figure illustrates that the mass centre trajectory of the droplet for Re = 20 follows the same pattern as Re = 1. The droplet remains the centerline of the channel before reaching the bifurcation region. When the bifurcation region starts, the droplet first attracted towards the side branch. After passing the bifurcation region at Re = 1, the droplet enters into the side branch at and above equal branch flow ratio (q = 0.5). However with higher inertia effect (Re = 20), it is obtained that the droplet takes the path towards the main branch if $q \leq 0.62$, otherwise it enters to the side branch.

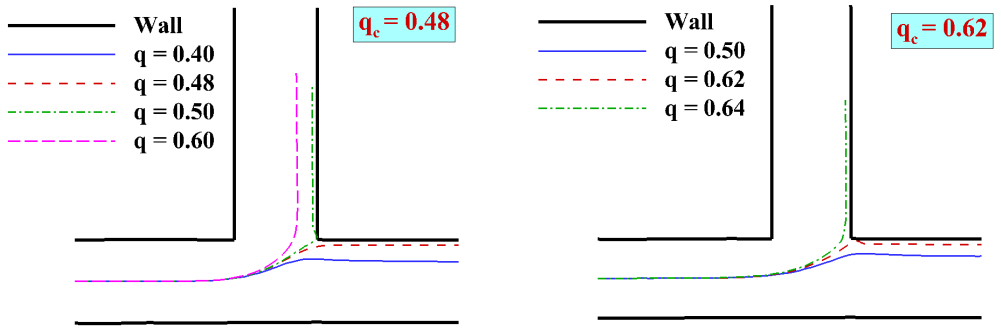

Fig. 4.12 Effect of inertia on the droplet trajectory at different branch flow ratios, (q). Other parameters, Ca = 0.1, $Ca_E = 0.0$, $\lambda = 0.3$, $r_d = 1.09$, and $r_v = 0.018$

A phase diagram for branch flow ratio (q) as a function of Reynolds number (Re = 1 and 20) is shown in FIG 4.13 for a droplet flowing in a microchannel without electric field ($Ca_E = 0.$). Here at Re = 1, obtained q_c is 0.48; however, when then the inertia effect is increased to Re = 20, the value of q_c is also increased to 0.62. The time evolution of the droplet profiles without electric field ($Ca_E = 0$) at q = 0.5 are shown in FIG 4.14 for (a) Re = 1 and (b) Re = 20 respectively. From the figure it is obtained that at equal branch flow ratio,

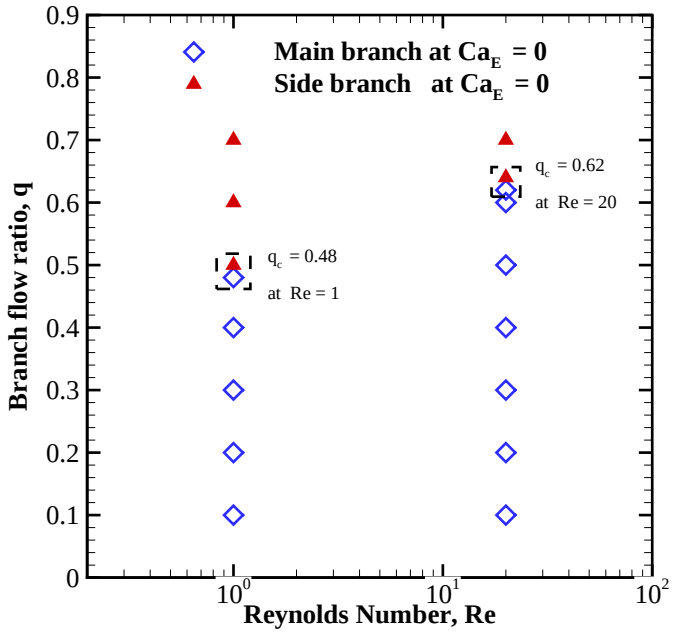

Fig. 4.13 Branch flow ratio as a function of flow Reynolds number with $Ca_E = 0.0$, $\lambda = 0.3$, $r_d = 1.09$, and $r_v = 0.018$.

the droplet selects the path towards the orthogonal side branch at Re = 1 whereas it goes back to the main channel when inertia effect is increased to Re = 20.

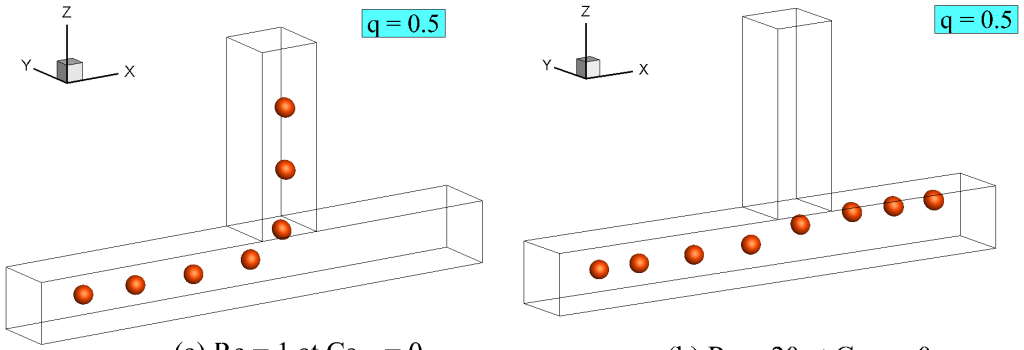

(a) Re = 1 at $Ca_E = 0$ (b) Re = 20 at $Ca_E = 0$

Fig. 4.14 The difference in path selection of the droplet at (a) Re = 1 and (b) Re = 20 at same branch flow ratio, q = 0.5. (q). Other parameters, Ca = 0.1, $Ca_E = 0.0$, $\lambda = 0.3$, $r_d = 1.09$, and $r_v = 0.018$

Therefore it is found that when the flow is governed only by poiseuille flow, the inertia plays an important role on critical branch flow ratio (q_c) above which sorting can be achieved.

In most practical application, sorting will be delayed where inertia effect is significant. Here it comes the necessity of droplet manipulation for rapid sorting. In the following section, we will study how non-uniform electric field can facilitate the droplet sorting even at higher Re.

FIG 4.15 shows the combined effect of inertia (Re = 1 and 20) and electric field (Ca_E = 0.9) on the droplet trajectory at different branch flow ratios (q) with electrode positions 1 (a,b) and electrode positions 2 (c,d). From the figure it is obtained that when the electrode is at position 1, the droplet takes the side branch when q> 0.12 both for Re =1 and 20. However at electrode position 2, the droplet takes the side branch at q> 0.16 and q> 0.22 for Re =1 and 20 respectively.

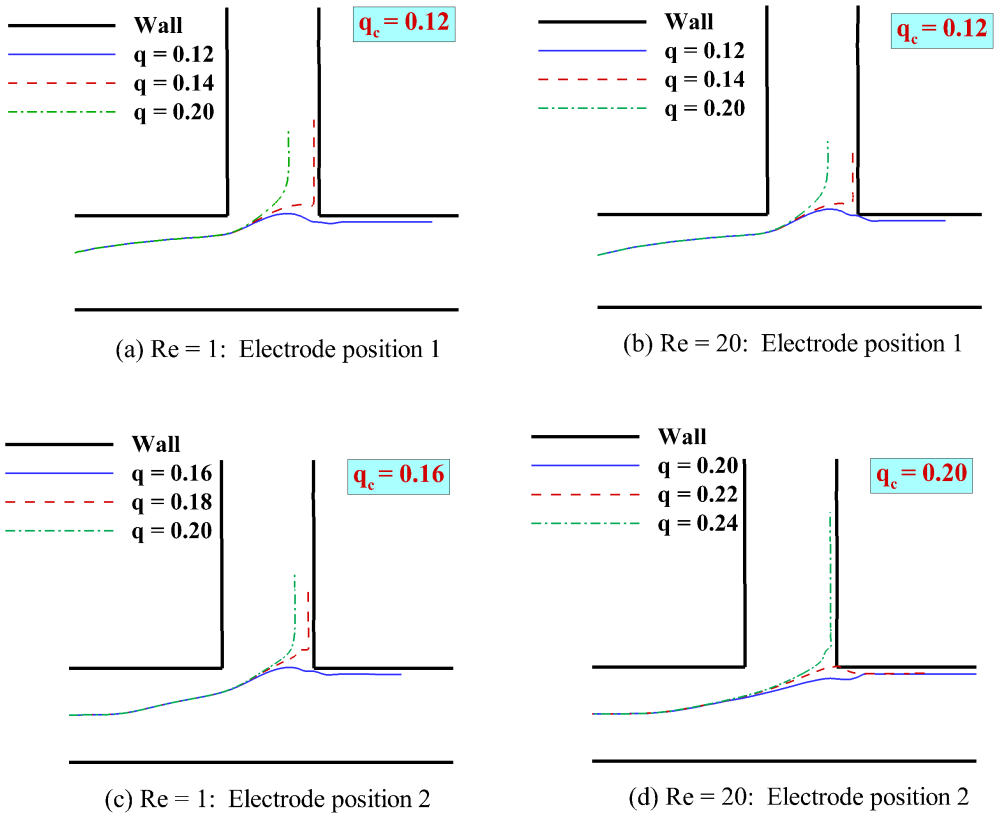

Fig. 4.15 Effect of electrode position on the droplet trajectory at different branch flow ratio, (q). Other parameters, Re = 1.0; Ca = 0.1, $Ca_E = 1.09$, $\lambda = 0.3$, $r_d = 1.09$, and $r_v = 0.018$

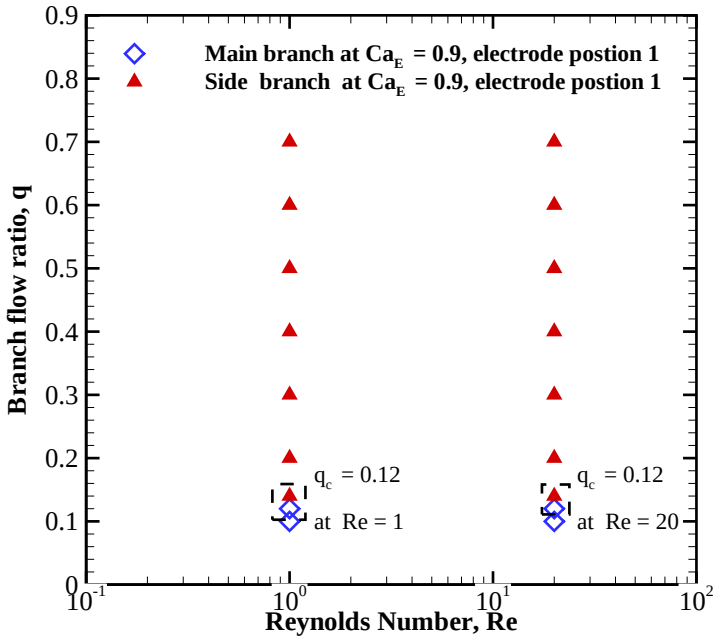

Fig. 4.16 Branch flow ratio as a function of flow Reynolds number at electrode position 1 with $Ca_E = 0.9$, $\lambda = 0.3$, $r_d = 1.09$, and $r_v = 0.018$.

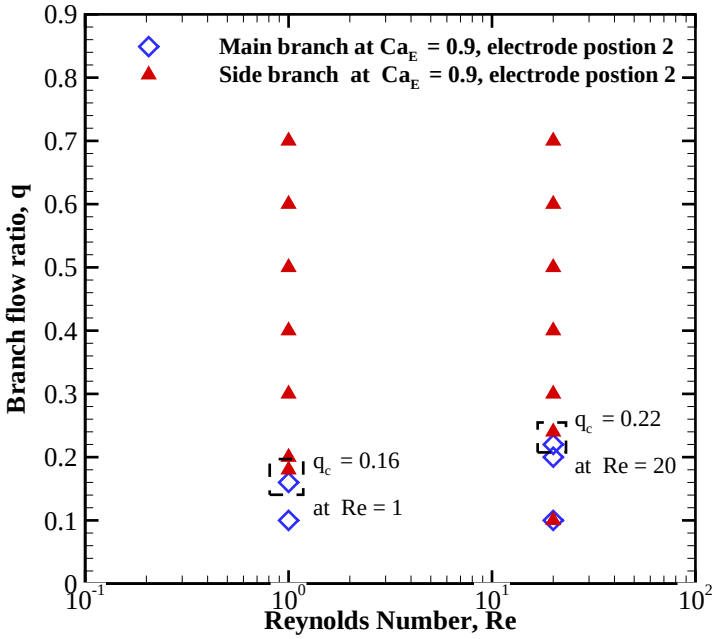

Fig. 4.17 Branch flow ratio as a function of flow Reynolds number at electrode position 2 with $Ca_E = 0.9$, $\lambda = 0.3$, $r_d = 1.09$, and $r_v = 0.018$.

A phase diagram is also established illustrating the value of critical branch flow ratio q_c as a function of Re for electrode position 1 and 2 are shown in FIG 4.16 and FIG 4.17 respectively. Phase diagram depicts that critical branch ratio q_c = 0.12 both for Re = 1 and 20 at electrode position 1. For electrode position 2, q_c = 0.16 at Re = 1 and q_c = 0.22 at Re = 20. For both electrode positions, the presence of electric field promotes the droplet sorting at lower branch flow ratio (q) even at higher inertia regime which can not be obtained without electric field effect. Moreover at electrode position 1, we get the same value of q_c for both lower and higher inertia effect. Therefore, in practical application where inertia is significant, placing an electrode closer to the droplet with sufficient electric potential can speed up the sorting process with a lower value of q_c.

The time evolution of the droplet profiles at q = 0.2 are shown in FIG 4.18 which shows the effect of inertia for electrode position 1 (a,b) and 2 (c, d). From the figure it is obtained that at q = 0.2, the droplet takes the path to the side branch for both Re = 1 and 20 when electrode at position 1. However when the electrode at position 2, the droplet favours the main branch when Re =20.

4.3.5 Effect of size ratio, λ at Re = 20

In this section we have investigated the effect of droplet size ratio ($\lambda = R/l$), with Re = 20, electrode at position 1 and $Ca_E = 0.9$. We have considered three different size ratios, λ = 0.2,0.3, and 0.4 as shown in FIG 4.19. The trajectories of the droplet's centre of mass and a phase diagram for different branch flow ratios are shown in FIG 4.20 and FIG 4.21 for different branch flow ratios at λ = 0.2,0.3, and 0.4. From the figures, it is observed that at a given value of other parameters, the size ratio, λ has significant effect on the path selection of the droplet. At λ = 0.2, after passing the bifrcation region the droplet follows the path towards the straight channel upto q = 0.28 after that it enters into the side branch. Therefore, the critical branch ratio, q_c = 0.28 at λ = 0.2. When the increase the size ratio to λ = 0.3,

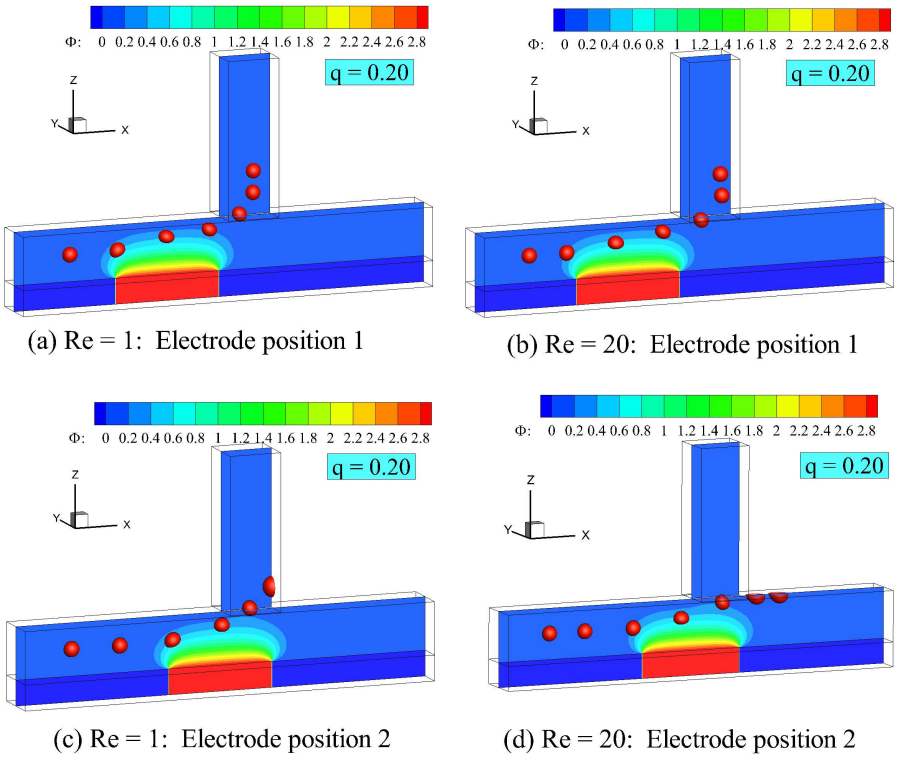

(a) Re = 1: Electrode position 1

(b) Re = 20: Electrode position 1

(c) Re = 1: Electrode position 2

(d) Re = 20: Electrode position 2

Fig. 4.18 The difference in path selection of the droplet at low (Re = 1) and high (Re = 20) inertia regime with electrode position 1 (a,b) and electrode position 2 (c,d) at same branch flow ratio, q = 0.2. Other parameters: Ca = 0.1, $Ca_E = 0.9$, $\lambda = 0.3$ $r_d = 1.09$, and $r_v = 0.018$

q_c is reduced to 0.12. Further increase of size ratio to λ = 0.4 leads to further reduction of q_c which is 0.08. This reduction of the value of q_c as a function of λ is also illustrated in FIG 4.21 through a phase diagram.

The time evolution of the droplet profiles at q = 0.10 are shown in FIG 4.20 (a) and (b) for λ = 0.2 and 0.4 respectively. From the figure it is obtained that when the side branch receives very small flow rate, (q = 0.1), the droplet takes path to the side branch for larger size ratio, λ = 0.4. However, at smaller size ratio λ = 0.2, the droplet favours the main channel. As dielectrophoresis force is proportional to the droplet radius, larger droplet undergoes higher dielectrophoresis force which promotes the droplet sorting at the side branch even at the lower value of branch flow ratio.

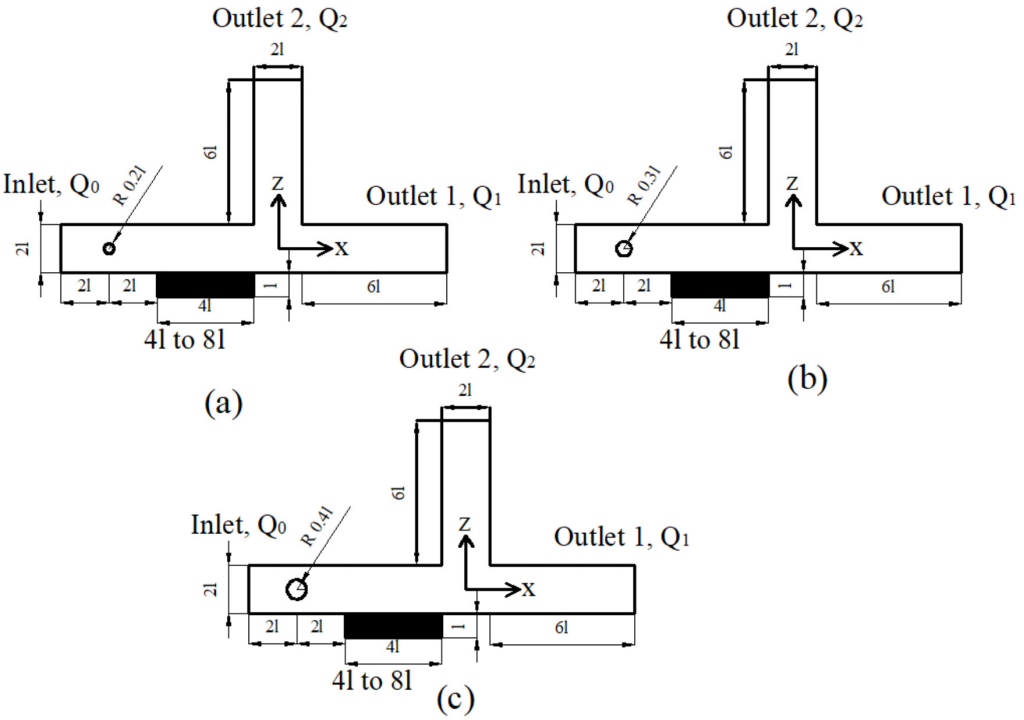

Fig. 4.19 Three different size ratios at electrode position 1: (a) $\lambda = 0.2$; (b) $\lambda = 0.3$; and (c) $\lambda = 0.4$.

4.4 Conclusions

We have implemented our developed 3d level set code to solve a practical engineering problem of droplet sorting in microfluidics. At present there is no existing computational method on DEP assisted droplet sorting either for 2d and 3d geometries which leads our present analysis a novel contribution to numerical simulation of droplet sorting. In this chapter, we have performed a parametric study on the path selection of the droplet by varying branch flow ratio (q), electric capillary number (Ca_E), electrode position, inertia (Re), and size ratio (λ). From the above discussed results the following conclusions can be drawn:

- Without any electric field effect, the path selection of the droplet depends only on branch flow ratio (q) and flow inertia (Re). At low Re, the droplet favours the branch which receives higher flow rate. At high inertia, the droplet can flow into the downstream main channel even when it receives much less flow rate than the side branch.

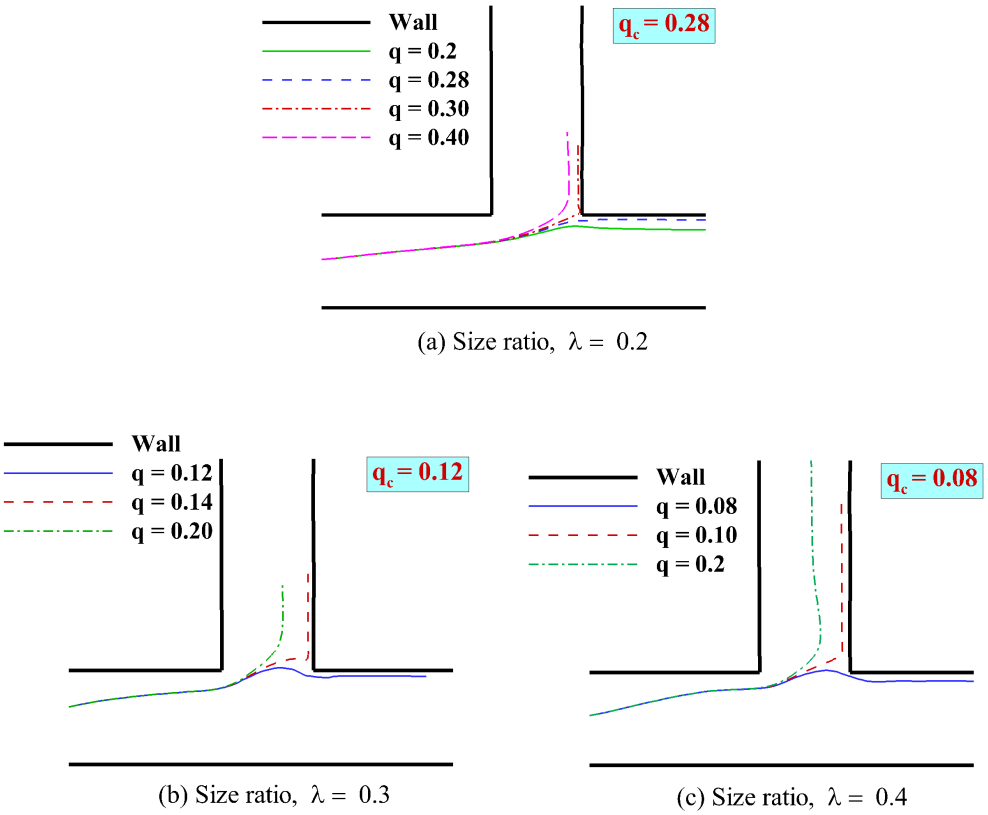

(a) Size ratio, λ = 0.2

(b) Size ratio, λ = 0.3

(c) Size ratio, λ = 0.4

Fig. 4.20 Effect of droplet size on the droplet trajectory at different branch flow ratio, (q). Other parameters, Re = 20.0; Ca = 0.1, $Ca_E = 0.9$, electrode position 1, $r_d = 1.09$, and $r_v = 0.018$

- The larger the magnitude of electric field i.e., higher the value of Ca_E, the lower the value of critical branch flow ratio (q_c), above which the droplet enters into side branch. The closer the position of the electrode from the initial position of the droplet, the lower the value of critical branch flow ratio (q_c).

- In practical application with higher inertia effect, active droplet sorting using non-uniform electric field can facilitate the sorting even a lower flow rate of the side branch. Larger the size ratio (λ), the larger the value of dielectrophoresis force which promotes the droplet sorting at side branch at lower branch flow ratio.

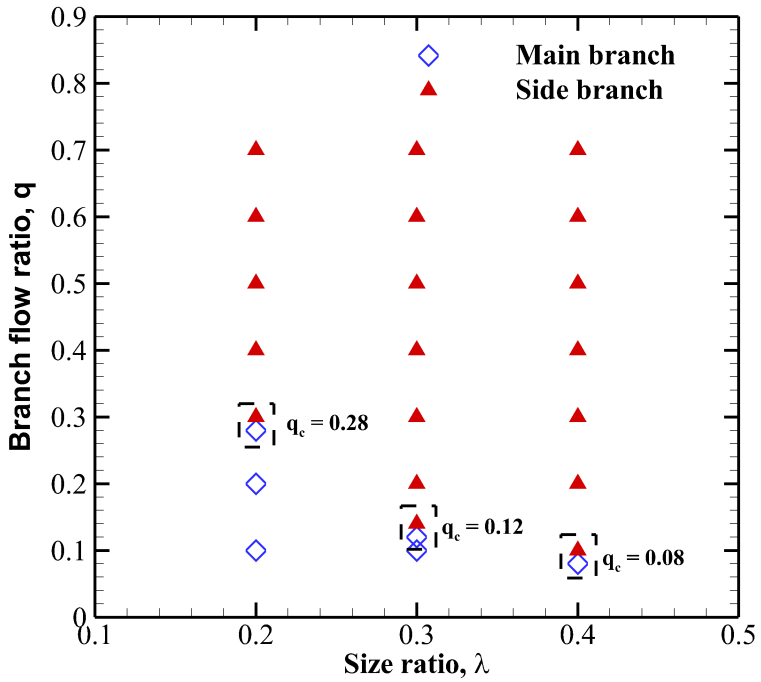

Fig. 4.21 Branch flow ratio as a function of size ratio. Other parameters, Re = 20.0; Ca = 0.1, $Ca_E = 0.9$, electrode position 1, $r_d = 1.09$, and $r_v = 0.018$.

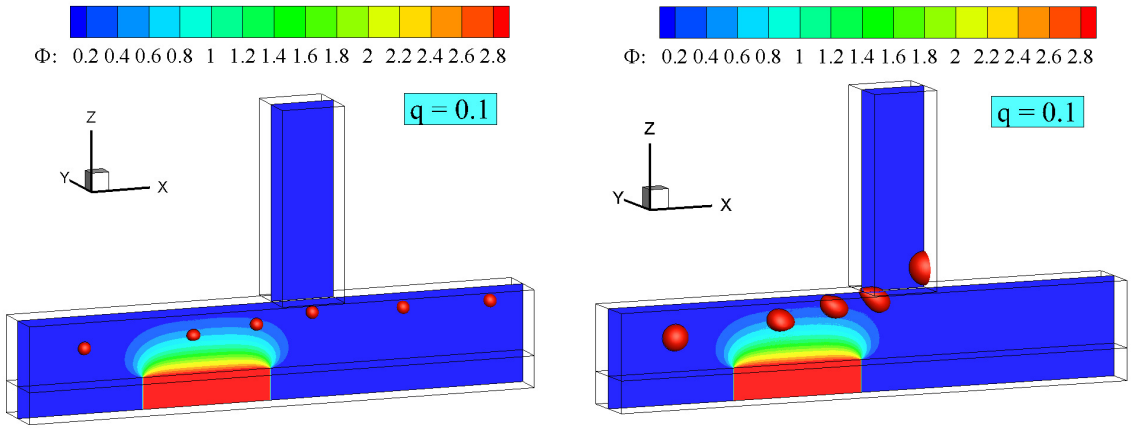

(a) Size ratio, $\lambda = 0.2$ (b) Size ratio, $\lambda = 0.4$

Fig. 4.22 The difference in path selection of the droplet at two different size ratio, λ (a) 0.2 and (b) 0.4 at same branch flow ratio, q = 0.1. Other parameters, Re = 20.0; Ca = 0.1, $Ca_E = 0.9$, Electrode position 1, $r_d = 1.09$, and $r_v = 0.018$

- Finally from the present investigation we have observed that electrode at position 1 with $Ca_E = 0.9$ and $\lambda = 0.4$, the critical branch flow ratio is the lowest which is $q_c = 0.08$.

Chapter 5

Conclusions and Future work

5.1 Conclusions

In this thesis, we have developed a 3d dimensional level set model for two-phase EHD problem. The developed model has been implemented to solve a practical engineering problem of droplet sorting in microfluidics. At present there is no existing computational method on DEP assisted droplet sorting either for 2d and 3d geometries which leads our present analysis a complete novel contribution. The key findings and conclusions from the presented thesis are summarized below:

First of all, the developed code is validated for two problems namely: (a) Droplet subjected to uniform electric field. (b) Droplet subjected to both uniform electric field and shear flow.

Droplet subjected to uniform electric field

In this problem, we consider a leaky dielectric drop suspending in another leaky dielectric fluid and subjected to uniform electric field. After observing the effect of electric capillary number (Ca_E), conductivity (K) and permittivity ratio (Q), we have reached to the following conclusions:

i) Three types of droplet deformation namely prolate A (PR_A), prolate B(PR_B), and oblate (OB) drop is obtained depending on the conductivity (K) and permittivity (Q) ratio between the two fluids, . If K>Q, the droplet takes PR_A shape. However when K<Q, the droplet can take either PR_B or OB shape.

ii) When K>Q, surface electric force acts in the parallel direction of imposed electric field which results a motion in the surrounding fluid from the equator towards the pole and maximum deformation occurs parallel to the electric field. On the other hand when K<Q, surface electric force acts in the perpendicular direction of imposed electric field which results a motion in the surrounding fluid from the pole towards the equator and maximum deformation occurs perpendicular to the electric field.

iii) The magnitude of droplet deformation increases with the increase of Ca_E. For PR_A and OB, the droplet takes a steady prolate and oblate shape respectively upto $Ca_E = 0.3$. At $Ca_E = 0.35$, the droplet elongates more and more and ultimately leads to breakup both for PR_A and OB droplet . However, PR_B droplet behaves very differently from the above two system. With the increase of Ca_E the deformation increases but the droplet forms conical shape at two ends . At $Ca_E = 0.45$, the conical ends results in tip-streaming from two ends.

iv) The results obtained from the present simulation show good agreement with the existing analytical result of Taylor [112] and Ajayi [5], axisymmetric boundary integral solution of Lac and Homsy [58] and experimental results provided by Ha and Yang [42].

Droplet subjected to both uniform electric field and simple shear flow

In this problem, we consider a leaky dielectric drop suspending in another leaky dielectric fluid and subjected to both uniform electric field and shear flow. The main findings from this study are summarized as below:

i) The droplet deformation is governed by both electric capillary number, (Ca_E) and hydrodynamic capillary number, (Ca) . With the increase of Ca_E and Ca, the droplet elongation increases with an increase in electric field which leads to the breakup of the droplet into smaller droplets beyond a critical value.

ii) A phase diagram is established at different combination of Ca_E and Ca which depicts that at $Ca = 0.2$, $Ca_E(crit) = 0.34$. When Ca is increased to 0.3, $Ca_E(crit)$ reduces to 0.18. Therefore, the cumulative effect of electric stress and shear flow promotes the breakup of the droplet even at smaller Ca which is not possible if there is only shear flow.

iii) The validation of the present results with the numerical results of Singh [103] is performed through time evolution of maximum elongation of the droplet for different value of Ca_E at $Ca = 0.2$. This graph shows that the droplet takes steady shape at $Ca_E = 0.0$ and 0.2 while it leads to breakup at $Ca_E = 0.4$. The present results also show very good agreement with the numerical results of Singh [103].

Droplet sorting using non-uniform electric field

The developed 3d level set code for two-phase EHD is implemented to study the droplet sorting in a microfluidic channel. At present there is no existing computational method on droplet sorting using non-uniform electric field either for 2d and 3d geometries which leads our present analysis a novel contribution in this field.

In this study, we consider a water droplet suspending in soybean oil and flowing through a rectangular channel with an orthogonal side branch. Fully developed laminar channel flow profiles are set at the inlet and two outlets. We investigate the trajectory of the droplet by changing the various parameters such as branch flow ratio (q), electric capillary number (Ca_E), two electrode positions, Reynolds number (Re), and different size ratios (λ). Based on these parameters, the droplet can either sorted to outlet 1 (downstream main channel)

or 2 (orthogonal side branch). Main findings from the present analysis are summarized as follows:

i) Without any electric field effect, the droplet trajectory is mainly governed by the value of q and Re. At low value of inertia, the droplet favours the outlet which receives higher flow rate. However when inertia effect is significant, the droplet takes the outlet 1 even it receives lower flow rate until q_c is achieved.

   From the present analysis, we find q_c for droplet sorting are 0.48 and 0.62 for Re = 1 and 20 respectively which implies that the inertia has a leading role on increasing the value of q_c.

ii) The spatially non-uniform electric field is created by placing a single electrode at the bottom of the microchannel. Electric field intensity is represented by electric capillary number, (Ca_E). We have investigated trajectory of the droplet for different branch flow ratios (q) for two different values of Ca_E which are 0.4 and 0.9 and compared it to the result without electric field effect (Ca_E = 0) . It has been observed that higher the value of Ca_E, higher the reduction of critical branch flow ratio (q_c) is observed.

   At $Ca_E = 0$, the critical branch flow ratio is q_c = 0.48 at low inertia (Re = 1). However, at Ca_E =0.4 and 0.9, the branch flow ratio reduces to q_c = 0.36 and 0.12 at the same inertia (Re = 1). Therefore, spatially non-uniform electric field can play a significant role in droplet sorting at desired outlet.

iii) Next, we study the effect of electrode positions on the path selection of the droplet. Two electrode positions are considered namely electrode 1 and electrode 2 which are placed at a distance of 4l and 6l from the inlet of the channel. At electrode position 1, q_c = 0.12 at Re = 1. When electrode is move to position 2, a slight increase of critical branch ratio is obtained which is q_c = 0.16 at the same Re. Therefore the closer the electrode is placed from the intial position of the droplet, smaller the branch flow ratio.

iv) After that, we studied the effect on inertia by increasing the value of Re from 1 to 20. When there is no electric field effect (Ca_E = 0.0), it has been obtained that the value of q_c = 0.62 at Re = 20 whereas it is 0.48 at Re = 1. Therefore, without any electric field the droplet can flow into the downstream main channel even when it receives lesser flow rate than the side branch.

However when electric field is applied at higher inertia, it is still possible to sort the droplet at side branch at lower value of q_c. For example at electrode position 1, we have obtained q_c = 0.12 both for Re = 1 and 20. For electrode position 2, q_c is increased from 0.16 to 0.22 when Re is increased from 1 to 20 which is still lower than the value of q_c without electric field at high inertia . Therefore with electric field, the droplet can be manipulated to sort at the side branch even at a higher inertia with smaller value of q_c

v) Finally we analyse the effect of size ratio (λ) on the path selection of the selection when electrode is placed at position 1 with Ca_E = 0.9 and Re =20. We consider three different value of λ which are 0.2, 0.3 and 0.4. It is obtain that with the increase of the value of λ, a reduction of the value of q_c is obtained. When we increase the value of λ from 0.2 to 0.3, we obtain the reduction of q_c = 0.28 to 0.12. After that when we further increase the value of λ to 0.4, a very small value of q_c is obtained which is 0.08. Larger the size ratio (λ), the larger the value of dielectrophoresis force acting on the droplet which promotes the droplet sorting at side branch even at lower branch flow ratio with high inertia effect.

vi) To conclude, from the present investigation we have observed that electrode at position 1 with Ca_E = 0.9 and λ = 0.4, the critical branch flow ratio is the lowest q_c which is 0.08.

5.2 Future work

In the present work a three dimensional level set method is developed for two-phase electro-hydrodynamics (EHD) problem which opens a myriad of scope for future studies. In chapter

4, we study the dielectrophoresis assisted droplet sorting for rectangular microchannel with cartesian grids. Therefore the present model can be improved to deal with complex geometry for example microchannel with Y-bifurcation as shown in FIG 1.6. Additionally further parametric analysis can be performed to elucidate the effect of other parameters such as multiple number of droplets and electrodes, complex interactions between the droplet themselves, or more interestingly different geometry of the microchannel including a series of successive bifurcations.

Two relevant future works which can be undergone along the direction of this research are briefly described below:

i) **Multiphase modeling of electrospray printing technology**

In chapter 3 for PR_B droplet, we observe a conical surface at two ends of droplet at Ca_E = 0.45. If we further increase the value of Ca_E to 0.5, a Taylor cone is formed due to accumulation of charges on both ends as shown in FIG 5.1 . When this taylor cone becomes unstable and the droplet forms liquid jet from both ends. This phenomenon is known a tip streaming. In this research work, we observe the onset of tip streaming for PR_B droplet. This tip streaming phenomenon can further be studied to develop a numerical model for electrospray printing technology. FIG 5.2 shows the schematic diagram of electrospray printing mechanism.

In electrospraying printing, electric fields are used to create liquid streams and drops. When a sufficiently high potential difference is applied between a liquid in a nozzle and a nearby plate, a Taylor cone is formed and liquid can jet from its tip. In electrospraying, a competition is generated between Coulomb forces of surface charges and cohesive forces inside the droplet. Once the applied Coulomb forces overcome the cohesive ones, the droplet will undergo breakup into smaller droplets in the micro-scale to nanoscale [19]. The developed 3d level set code from this thesis can easily be implemented to model the two phase electrospray printing.

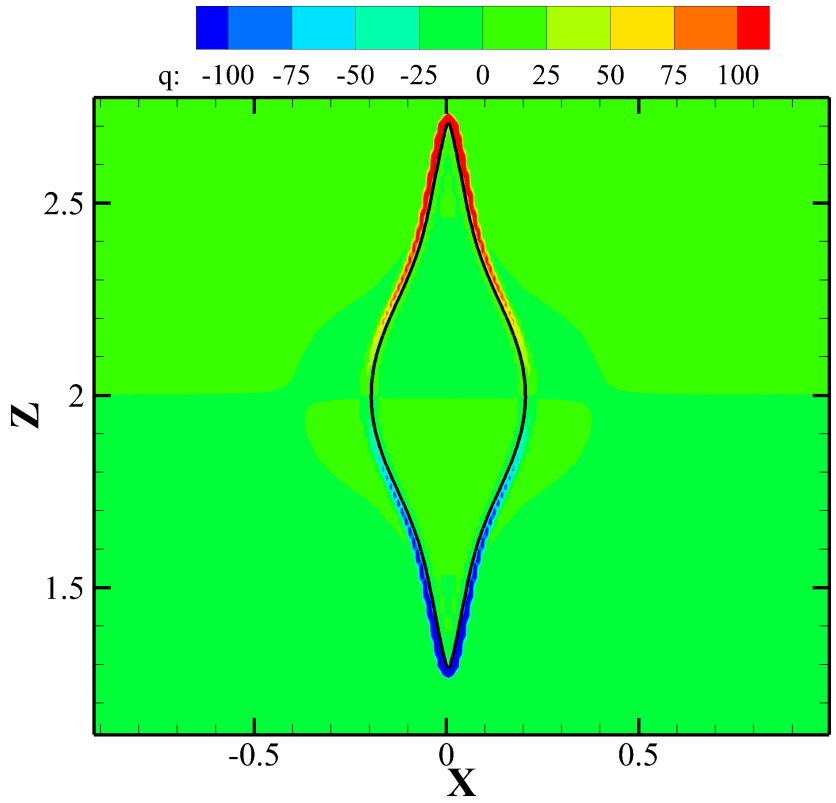

Fig. 5.1 Formation of Taylor cone and tip streaming phenomenon for prolate B droplet at K =25.0, Q =50.0, Re = 0.1, Ca_E = 0.5 and $r_d = 1$, $r_v = 0.874$.

ii) **Multiphase modeling of cell encapsulation and sorting for biological applications**

The present research work can be extended to numerically study the dynamics of single cells encapsulated in water-in-oil emulsions. The encapsulate cell can be subjected to positive or negative dielectrophoresis (pDEP/nDEP) force to sort at desired location based on their biomechanical properties. FIG 5.3 shows schematic modeling of cell encapsulation in a microfluidic device. Single cell encapsulation inside a droplet promotes the delivery of therapeutic molecules at a fixed rate which can give rise to greater physiological concentrations [13].

Therefore present work opens a door for a myriad of research work related to droplet manipulation in microfluidics, numerical modeling of complex printing technology, droplet and cell encapsulation for biological applications.

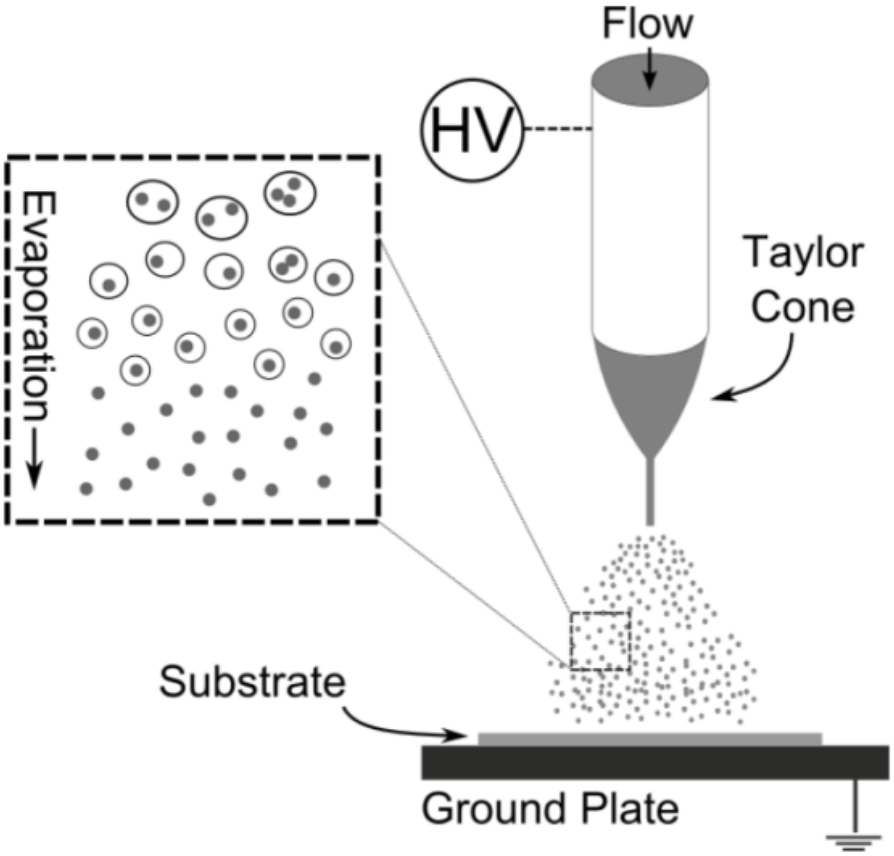

Fig. 5.2 Electrospray printing of colloidal dispersions [19].

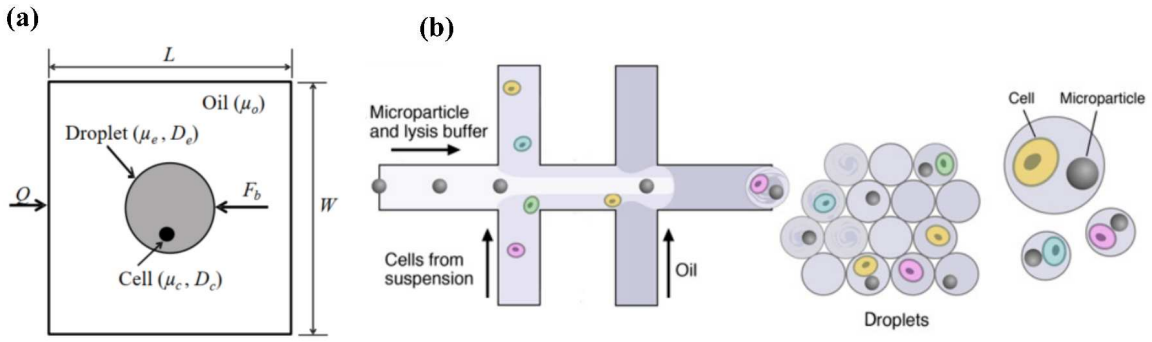

Fig. 5.3 Schematic of (a) modeling of flow of a single cell encapsulated inside an droplet [13]; (b) cell droplet encapsulation in a microfluidic device [36] .

References

[1] Adalsteinsson, D. and Sethian, J. A. (1995). A fast level set method for propagating interfaces. *Journal of computational physics*, 118(2):269–277.

[2] Agresti, J. J., Antipov, E., Abate, A. R., Ahn, K., Rowat, A. C., Baret, J.-C., Marquez, M., Klibanov, A. M., Griffiths, A. D., and Weitz, D. A. (2010). Ultrahigh-throughput screening in drop-based microfluidics for directed evolution. *Proceedings of the National Academy of Sciences*, 107(9):4004–4009.

[3] Ahn, K., Kerbage, C., Hunt, T. P., Westervelt, R., Link, D. R., and Weitz, D. A. (2006). Dielectrophoretic manipulation of drops for high-speed microfluidic sorting devices. *Applied Physics Letters*, 88(2):024104.

[4] Ai, Y. and Qian, S. (2010). Dc dielectrophoretic particle–particle interactions and their relative motions. *Journal of colloid and interface science*, 346(2):448–454.

[5] Ajayi, O. (1978). A note on taylor's electrohydrodynamic theory. *Proceedings of the Royal Society of London. A. Mathematical and Physical Sciences*, 364(1719):499–507.

[6] Al-Jarro, A., Paul, J., Thomas, D., Crowe, J., Sawyer, N., Rose, F., and Shakesheff, K. (2006). Direct calculation of maxwell stress tensor for accurate trajectory prediction during dep for 2d and 3d structures. *Journal of Physics D: Applied Physics*, 40(1):71.

[7] Ali-Cherif, A., Begolo, S., Descroix, S., Viovy, J.-L., and Malaquin, L. (2012). Programmable magnetic tweezers and droplet microfluidic device for high-throughput nanoliter multi-step assays. *Angewandte Chemie*, 124(43):10923–10927.

[8] Allan, R. and Mason, S. (1962). Particle behaviour in shear and electric fields i. deformation and burst of fluid drops. *Proceedings of the Royal Society of London. Series A. Mathematical and Physical Sciences*, 267(1328):45–61.

[9] Baret, J.-C., Miller, O. J., Taly, V., Ryckelynck, M., El-Harrak, A., Frenz, L., Rick, C., Samuels, M. L., Hutchison, J. B., Agresti, J. J., et al. (2009). Fluorescence-activated droplet sorting (fads): efficient microfluidic cell sorting based on enzymatic activity. *Lab on a Chip*, 9(13):1850–1858.

[10] Barrett, L. M., Skulan, A. J., Singh, A. K., Cummings, E. B., and Fiechtner, G. J. (2005). Dielectrophoretic manipulation of particles and cells using insulating ridges in faceted prism microchannels. *Analytical chemistry*, 77(21):6798–6804.

[11] Basaran, O. A., Gao, H., and Bhat, P. P. (2013). Nonstandard inkjets. *Annual Review of Fluid Mechanics*, 45:85–113.

[12] Baygents, J. C., Rivette, N., and Stone, H. A. (1998). Electrohydrodynamic deformation and interaction of drop pairs. *Journal of Fluid Mechanics*, 368:359–375.

[13] Beshay, P. E., Ibrahim, A. M., Jeffrey, S. S., Howe, R. T., and Anis, Y. H. (2021). Encapsulated cell dynamics in droplet microfluidic devices with sheath flow. *Micromachines*, 12(7):839.

[14] Bhagat, A. (2010). Bow h. hou hw tan sj han j. lim ct med. biol. *Eng. Comput*, 48:999–1014.

[15] Bhalla, A. P. S., Bale, R., Griffith, B. E., and Patankar, N. A. (2014). Fully resolved immersed electrohydrodynamics for particle motion, electrolocation, and self-propulsion. *Journal of Computational Physics*, 256:88–108.

[16] Brackbill, J. U., Kothe, D. B., and Zemach, C. (1992). A continuum method for modeling surface tension. *Journal of computational physics*, 100(2):335–354.

[17] Bringer, M. R., Gerdts, C. J., Song, H., Tice, J. D., and Ismagilov, R. F. (2004). Microfluidic systems for chemical kinetics that rely on chaotic mixing in droplets. *Philosophical Transactions of the Royal Society of London. Series A: Mathematical, Physical and Engineering Sciences*, 362(1818):1087–1104.

[18] Brouzes, E., Kruse, T., Kimmerling, R., and Strey, H. H. (2015). Rapid and continuous magnetic separation in droplet microfluidic devices. *Lab on a Chip*, 15(3):908–919.

[19] Brown, N. A., Gladstone, J. N., and Chiarot, P. R. (2014). Materials printing using electrospray. In *ASME 2014 International Mechanical Engineering Congress and Exposition*, pages V02BT02A049–V02BT02A049. American Society of Mechanical Engineers.

[20] Chang, C. B., Wilking, J. N., Kim, S.-H., Shum, H. C., and Weitz, D. A. (2015). Monodisperse emulsion drop microenvironments for bacterial biofilm growth. *Small*, 11(32):3954–3961.

[21] Chen, S., Merriman, B., Osher, S., and Smereka, P. (1997). A simple level set method for solving stefan problems. *Journal of Computational Physics*, 135(1):8–29.

[22] Cheng, S. and Chandra, S. (2003). A pneumatic droplet-on-demand generator. *Experiments in fluids*, 34(6):755–762.

[23] Chiarot, P. R., Sullivan, P., and Mrad, R. B. (2011). An overview of electrospray applications in mems and microfluidic systems. *Journal of Microelectromechanical Systems*, 20(6):1241–1249.

[24] Datta, S. S., Abbaspourrad, A., Amstad, E., Fan, J., Kim, S.-H., Romanowsky, M., Shum, H. C., Sun, B., Utada, A. S., Windbergs, M., et al. (2014). 25th anniversary article: Double emulsion templated solid microcapsules: Mechanics and controlled release. *Advanced Materials*, 26(14):2205–2218.

[25] Di Marco, P., Grassi, W., Memoli, G., Takamasa, T., Tomiyama, A., and Hosokawa, S. (2003). Influence of electric field on single gas-bubble growth and detachment in microgravity. *International Journal of Multiphase Flow*, 29(4):559–578.

[26] Docoslis, A., Tercero Espinoza, L. A., Zhang, B., Cheng, L.-L., Israel, B. A., Alexandridis, P., and Abbott, N. L. (2007). Using nonuniform electric fields to accelerate the transport of viruses to surfaces from media of physiological ionic strength. *Langmuir*, 23(7):3840–3848.

[27] Doh, I., . C. Y. H. (2005). A continuous cell separation chip using hydrodynamic dielectrophoresis (dep) process. *Sensors and Actuators A: Physical*, 121(1):59–65.

[28] Duffy, D. C., McDonald, J. C., Schueller, O. J., and Whitesides, G. M. (1998). Rapid prototyping of microfluidic systems in poly (dimethylsiloxane). *Analytical chemistry*, 70(23):4974–4984.

[29] Enright, D., Fedkiw, R., Ferziger, J., and Mitchell, I. (2002). A hybrid particle level set method for improved interface capturing. *Journal of Computational physics*, 183(1):83–116.

[30] Eow, J. S. and Ghadiri, M. (2002). Electrostatic enhancement of coalescence of water droplets in oil: a review of the technology. *Chemical Engineering Journal*, 85(2-3):357–368.

[31] Feczkó, T., Kokol, V., and Voncina, B. (2010). Preparation and characterization of ethylcellulose-based microcapsules for sustaining release of a model fragrance. *Macromolecular research*, 18(7):636–640.

[32] Feng, J. Q. (1996). Dielectrophoresis of a deformable fluid particle in a nonuniform electric field. *Physical Review E*, 54(4):4438.

[33] Feng, J. Q. (1999). Electrohydrodynamic behaviour of a drop subjected to a steady uniform electric field at finite electric reynolds number. *Proceedings of the Royal Society of London. Series A: Mathematical, Physical and Engineering Sciences*, 455(1986):2245–2269.

[34] Fenn, J. B., Mann, M., Meng, C. K., Wong, S. F., and Whitehouse, C. M. (1989). Electrospray ionization for mass spectrometry of large biomolecules. *Science*, 246(4926):64–71.

[35] Fernández, A., Tryggvason, G., Che, J., and Ceccio, S. L. (2005). The effects of electrostatic forces on the distribution of drops in a channel flow: Two-dimensional oblate drops. *Physics of Fluids*, 17(9):093302.

[36] Giuliano, C. B. (2020). Droplets encapsulation for biological applications: a review. *Elveflow*.

[37] Gordon, J. E., Gagnon, Z., and Chang, H.-C. (2007). Dielectrophoretic discrimination of bovine red blood cell starvation age by buffer selection and membrane cross-linking. *Biomicrofluidics*, 1(4):044102.

[38] Green, N. G., Morgan, H., and Milner, J. J. (1997). Manipulation and trapping of sub-micron bioparticles using dielectrophoresis. *Journal of Biochemical and Biophysical Methods*, 35(2):89–102.

[39] Green, N. G., Ramos, A., and Morgan, H. (2002). Numerical solution of the dielectrophoretic and travelling wave forces for interdigitated electrode arrays using the finite element method. *Journal of Electrostatics*, 56(2):235–254.

[40] Grom, F., Kentsch, J., Müller, T., Schnelle, T., and Stelzle, M. (2006). Accumulation and trapping of hepatitis a virus particles by electrohydrodynamic flow and dielectrophoresis. *Electrophoresis*, 27(7):1386–1393.

[41] Guo, M. T., Rotem, A., Heyman, J. A., and Weitz, D. A. (2012). Droplet microfluidics for high-throughput biological assays. *Lab on a Chip*, 12(12):2146–2155.

[42] Ha, J.-W. and Yang, S.-M. (2000). Deformation and breakup of newtonian and non-newtonian conducting drops in an electric field. *Journal of Fluid Mechanics*, 405:131–156.

[43] Halim, M. A. and Esmaeeli, A. (2013). Computational studies on the transient electrohydrodynamics of a liquid drop. *Fluid Dyn. Mater. Process*, 9(4):435–460.

[44] Harris, F. E. and O'Konski, C. T. (1957). Dielectric properties of aqueous ionic solutions at microwave frequencies. *The journal of physical chemistry*, 61(3):310–319.

[45] Harris, M. T. and Basaran, O. A. (1993). Capillary electrohydrostatics of conducting drops hanging from a nozzle in an electric field. *Journal of colloid and interface science*, 161(2):389–413.

[46] Harris, M. T. and Basaran, O. A. (1995). Equilibrium shapes and stability of nonconducting pendant drops surrounded by a conducting fluid in an electric field. *Journal of colloid and interface science*, 170(2):308–319.

[47] Hart, J. E., Glatzmaier, G. A., and Toomre, J. (1986). Space-laboratory and numerical simulations of thermal convection in a rotating hemispherical shell with radial gravity. *Journal of Fluid Mechanics*, 173:519–544.

[48] Higuera, F. (2007). Emission of drops from the tip of an electrified jet of an inviscid liquid of infinite electrical conductivity. *Physics of Fluids*, 19(7):072113.

[49] Hua, J., Lim, L. K., and Wang, C.-H. (2008). Numerical simulation of deformation/motion of a drop suspended in viscous liquids under influence of steady electric fields. *Physics of Fluids*, 20(11):113302.

[50] Huang, C., Fang, W., Ke, M., Chou, H., and Yang, J. (2014). A biocompatible open-surface droplet manipulation platform for detection of multi-nucleotide polymorphism. *Lab on a Chip*, 14(12):2057–2062.

[51] Huang, Z.-M., Zhang, Y.-Z., Kotaki, M., and Ramakrishna, S. (2003). A review on polymer nanofibers by electrospinning and their applications in nanocomposites. *Composites science and technology*, 63(15):2223–2253.

[52] Jacquemond, M., Jeckelmann, N., Ouali, L., and Haefliger, O. P. (2009). Perfume-containing polyurea microcapsules with undetectable levels of free isocyanates. *Journal of applied polymer science*, 114(5):3074–3080.

[53] Johnson, R. (1968). Effect of an electric field on boiling heat transfer. *AIAA journal*, 6(8):1456–1460.

[54] Juric, D. and Tryggvason, G. (1996). A front-tracking method for dendritic solidification. *Journal of computational physics*, 123(1):127–148.

[55] Kadaksham, J., Singh, P., and Aubry, N. (2005). Dielectrophoresis induced clustering regimes of viable yeast cells. *Electrophoresis*, 26(19):3738–3744.

[56] Kang, Y., Li, D., Kalams, S. A., and Eid, J. E. (2008). Dc-dielectrophoretic separation of biological cells by size. *Biomedical microdevices*, 10(2):243–249.

[57] Kazemi, P. Z., Selvaganapathy, P. R., and Ching, C. Y. (2009). Electrohydrodynamic micropumps with asymmetric electrode geometries for microscale electronics cooling. *IEEE Transactions on Dielectrics and Electrical Insulation*, 16(2):483–488.

[58] Lac, E. and Homsy, G. (2007). Axisymmetric deformation and stability of a viscous drop in a steady electric field. *Journal of Fluid Mechanics*, 590:239–264.

[59] Lapizco-Encinas, B. H. (2014). Applications of dielectrophoresis in microfluidics. *Microfluidics in Detection Science; RSC Publishing: Cambridge, UK*, 24:192–223.

[60] Lapizco-Encinas, B. H., Simmons, B. A., Cummings, E. B., and Fintschenko, Y. (2004). Insulator-based dielectrophoresis for the selective concentration and separation of live bacteria in water. *Electrophoresis*, 25(10-11):1695–1704.

[61] Laser, D. J. and Santiago, J. G. (2004). A review of micropumps. *Journal of micromechanics and microengineering*, 14(6):R35.

[62] Le, D. V., Rosales, C., Khoo, B. C., and Peraire, J. (2008). Numerical design of electrical-mechanical traps. *Lab on a Chip*, 8(5):755–763.

[63] Li, H. and Bashir, R. (2004). On the design and optimization of micro-fluidic dielectrophoretic devices: a dynamic simulation study. *Biomedical microdevices*, 6(4):289–295.

[64] Li, S., Ding, X., Guo, F., Chen, Y., Lapsley, M. I., Lin, S.-C. S., Wang, L., McCoy, J. P., Cameron, C. E., and Huang, T. J. (2013). An on-chip, multichannel droplet sorter using standing surface acoustic waves. *Analytical chemistry*, 85(11):5468–5474.

[65] Link, D. R., Grasland-Mongrain, E., Duri, A., Sarrazin, F., Cheng, Z., Cristobal, G., Marquez, M., and Weitz, D. A. (2006). Electric control of droplets in microfluidic devices. *Angewandte Chemie International Edition*, 45(16):2556–2560.

[66] Liu, Y., Liu, W. K., Belytschko, T., Patankar, N., To, A. C., Kopacz, A., and Chung, J.-H. (2007). Immersed electrokinetic finite element method. *International Journal for Numerical Methods in Engineering*, 71(4):379–405.

[67] López-Herrera, J., Popinet, S., and Herrada, M. (2011). A charge-conservative approach for simulating electrohydrodynamic two-phase flows using volume-of-fluid. *Journal of Computational Physics*, 230(5):1939–1955.

[68] Maehlmann, S. and Papageorgiou, D. T. (2009). Numerical study of electric field effects on the deformation of two-dimensional liquid drops in simple shear flow at arbitrary reynolds number. *Journal of fluid mechanics*, 626:367–393.

[69] Mandal, S. and Chakraborty, S. (2017). Effect of uniform electric field on the drop deformation in simple shear flow and emulsion shear rheology. *Physics of Fluids*, 29(7):072109.

[70] Markx, G. H., Huang, Y., Zhou, X.-F., and Pethig, R. (1994). Dielectrophoretic characterization and separation of micro-organisms. *Microbiology*, 140(3):585–591.

[71] McDonald, J. C., Duffy, D. C., Anderson, J. R., Chiu, D. T., Wu, H., Schueller, O. J., and Whitesides, G. M. (2000). Fabrication of microfluidic systems in poly (dimethylsiloxane). *ELECTROPHORESIS: An International Journal*, 21(1):27–40.

[72] Melcher, J. (1969). Electrohydrodynamics: a review of the role of interfacial shear stresses. *Ann. Rev. Fluid Mech.*, 1:111–146.

[73] Merriman, B., Bence, J. K., and Osher, S. J. (1994). Motion of multiple junctions: A level set approach. *Journal of computational physics*, 112(2):334–363.

[74] Mhatre, S. and Thaokar, R. M. (2013). Drop motion, deformation, and cyclic motion in a non-uniform electric field in the viscous limit. *Physics of Fluids*, 25(7):072105.

[75] Muschiolik, G. (2007). Multiple emulsions for food use. *Current Opinion in Colloid & Interface Science*, 12(4-5):213–220.

[76] Niepa, T. H., Hou, L., Jiang, H., Goulian, M., Koo, H., Stebe, K. J., and Lee, D. (2016). Microbial nanoculture as an artificial microniche. *Scientific reports*, 6(1):1–10.

[77] Notz, P. K. and Basaran, O. A. (1999). Dynamics of drop formation in an electric field. *Journal of Colloid and Interface Science*, 213(1):218–237.

[78] Ogata, J. and Yabe, A. (1991). Augmentation of nucleate boiling heat transfer by applying electric fields. In *Proceedings of the 1991 ASME JSME thermal engineering joint conference*.

[79] Ogata, J. and Yabe, A. (1993). Basic study on the enhancement of nucleate boiling heat transfer by applying electric fields. *International journal of heat and mass transfer*, 36(3):775–782.

[80] O'Konski, C. T. and Thacher Jr, H. C. (1953). The distortion of aerosol droplets by an electric field. *The Journal of Physical Chemistry*, 57(9):955–958.

[81] Osher, S. and Fedkiw, R. P. (2005). *Level set methods and dynamic implicit surfaces*, volume 1. Springer New York.

[82] Osher, S. and Sethian, J. A. (1988). Fronts propagating with curvature-dependent speed: Algorithms based on hamilton-jacobi formulations. *Journal of computational physics*, 79(1):12–49.

[83] Paknemat, H., Pishevar, A., and Pournaderi, P. (2012). Numerical simulation of drop deformations and breakup modes caused by direct current electric fields. *Physics of Fluids*, 24(10):102101.

[84] Parikesit, G. O., Markesteijn, A. P., Piciu, O. M., Bossche, A., Westerweel, J., Young, I. T., and Garini, Y. (2008). Size-dependent trajectories of dna macromolecules due to insulative dielectrophoresis in submicrometer-deep fluidic channels. *Biomicrofluidics*, 2(2):024103.

[85] Park, J., Jung, J. H., Park, K., Destgeer, G., Ahmed, H., Ahmad, R., and Sung, H. J. (2018). On-demand acoustic droplet splitting and steering in a disposable microfluidic chip. *Lab on a Chip*, 18(3):422–432.

[86] Park, J., Kim, B., Choi, S. K., Hong, S., Lee, S. H., and Lee, K.-I. (2005). An efficient cell separation system using 3d-asymmetric microelectrodes. *Lab on a Chip*, 5(11):1264–1270.

[87] Poddar, A., Mandal, S., Bandopadhyay, A., and Chakraborty, S. (2018). Electrohydrodynamic migration of a surfactant-coated deformable drop in poiseuielle flow. *arXiv preprint arXiv:1806.10006*.

[88] Pohl, H. A. (1978). Dielectrophoresis. *The behavior of neutral matter in nonuniform electric fields*.

[89] Popinet, S. (2003). Gerris: a tree-based adaptive solver for the incompressible euler equations in complex geometries. *Journal of computational physics*, 190(2):572–600.

[90] Puckett, E. G., Almgren, A. S., Bell, J. B., Marcus, D. L., and Rider, W. J. (1997). A high-order projection method for tracking fluid interfaces in variable density incompressible flows. *Journal of computational physics*, 130(2):269–282.

[91] Romero, P. A., Tran, T. M., and Abate, A. R. (2015). Dissecting enzyme function with microfluidic-based deep mutational scanning. *Proceedings of the National Academy of Sciences*, 112(23):7159–7164.

[92] Russo, G. and Smereka, P. (2000). A remark on computing distance functions. *Journal of computational physics*, 163(1):51–67.

[93] Salipante, P. F. and Vlahovska, P. M. (2010). Electrohydrodynamics of drops in strong uniform dc electric fields. *Physics of Fluids*, 22(11):112110.

[94] Santra, S., Mandal, S., and Chakraborty, S. (2019). Confinement effect on electrically induced dynamics of a droplet in shear flow. *Physical Review E*, 100(3):033101.

[95] Saville, D. (1997). Electrohydrodynamics: the taylor-melcher leaky dielectric model. *Annual review of fluid mechanics*, 29(1):27–64.

[96] Schnelle, T., Müller, T., and Fuhr, G. (2000). Trapping in ac octode field cages. *Journal of Electrostatics*, 50(1):17–29.

[97] Schnitzer, O. and Yariv, E. (2015). The taylor-melcher leaky dielectric model as a macroscale electrokinetic description. *Journal of Fluid Mechanics*, 773:1.

[98] Sethian, J. A. (1999). *Level set methods and fast marching methods: evolving interfaces in computational geometry, fluid mechanics, computer vision, and materials science*, volume 3. Cambridge university press.

[99] Setiawan, E. and Heister, S. (1997). Nonlinear modeling of an infinite electrified jet. *Journal of Electrostatics*, 42(3):243–257.

[100] Sherwood, J. (1988). Breakup of fluid droplets in electric and magnetic fields. *Journal of Fluid Mechanics*, 188:133–146.

[101] Shin, D.-Y., Grassia, P., and Derby, B. (2004). Numerical and experimental comparisons of mass transport rate in a piezoelectric drop-on-demand inkjet print head. *International journal of mechanical sciences*, 46(2):181–199.

[102] Shrimpton, J. and Yule, A. (1999). Characterisation of charged hydrocarbon sprays for application in combustion systems. *Experiments in fluids*, 26(5):460–469.

[103] Singh, R., Bahga, S. S., and Gupta, A. (2019). Electric field induced droplet deformation and breakup in confined shear flows. *Physical Review Fluids*, 4(3):033701.

[104] Song, H., Mulukutla, V., James, C. D., and Bennett, D. J. (2008). Continuous-mode dielectrophoretic gating for highly efficient separation of analytes in surface micromachined microfluidic devices. *Journal of Micromechanics and Microengineering*, 18(12):125013.

[105] Sui, Y. and Spelt, P. D. (2013). Validation and modification of asymptotic analysis of slow and rapid droplet spreading by numerical simulation. *Journal of Fluid Mechanics*, 715:283–313.

[106] Sui, Y. and Spelt, P. D. (2015). Non-isothermal droplet spreading/dewetting and its reversal. *Journal of Fluid Mechanics*, 776:74–95.

[107] Sussman, M. and Fatemi, E. (1999). An efficient, interface-preserving level set redistancing algorithm and its application to interfacial incompressible fluid flow. *SIAM Journal on scientific computing*, 20(4):1165–1191.

[108] Sussman, M. and Puckett, E. G. (2000). A coupled level set and volume-of-fluid method for computing 3d and axisymmetric incompressible two-phase flows. *Journal of computational physics*, 162(2):301–337.

[109] Sussman, M., Smereka, P., and Osher, S. (1994). A level set approach for computing solutions to incompressible two-phase flow. *Journal of Computational physics*, 114(1):146–159.

[110] Tan, Y.-C., Fisher, J. S., Lee, A. I., Cristini, V., and Lee, A. P. (2004). Design of microfluidic channel geometries for the control of droplet volume, chemical concentration, and sorting. *Lab on a Chip*, 4(4):292–298.

[111] Taylor, G. I. (1964). Disintegration of water drops in an electric field. *Proceedings of the Royal Society of London. Series A. Mathematical and Physical Sciences*, 280(1382):383–397.

[112] Taylor, G. I. (1966). Studies in electrohydrodynamics. i. the circulation produced in a drop by an electric field. *Proceedings of the Royal Society of London. Series A. Mathematical and Physical Sciences*, 291(1425):159–166.

[113] Taylor, G. I. (1969). Electrically driven jets. *Proceedings of the Royal Society of London. A. Mathematical and Physical Sciences*, 313(1515):453–475.

[114] Teigen, K. E. and Munkejord, S. T. (2009). Sharp-interface simulations of drop deformation in electric fields. *IEEE Transactions on Dielectrics and Electrical Insulation*, 16(2):475–482.

[115] Tomar, G., Gerlach, D., Biswas, G., Alleborn, N., Sharma, A., Durst, F., Welch, S. W., and Delgado, A. (2007). Two-phase electrohydrodynamic simulations using a volume-of-fluid approach. *Journal of Computational Physics*, 227(2):1267–1285.

[116] Torza, S., Cox, R., and Mason, S. (1971). Electrohydrodynamic deformation and bursts of liquid drops. *Philosophical Transactions of the Royal Society of London. Series A, Mathematical and Physical Sciences*, 269(1198):295–319.

[117] Tsori, Y., Tournilhac, F., and Leibler, L. (2004). Demixing in simple fluids induced by electric field gradients. *Nature*, 430(6999):544.

[118] Tsukada, T., Katayama, T., Ito, Y., and Hozawa, M. (1993). Theoretical and experimental studies of circulations inside and outside a deformed drop under a uniform electric field. *Journal of chemical engineering of Japan*, 26(6):698–703.

[119] Unger, M. A., Chou, H.-P., Thorsen, T., Scherer, A., and Quake, S. R. (2000). Monolithic microfabricated valves and pumps by multilayer soft lithography. *science*, 288(5463):113–116.

[120] Vizika, O. and Saville, D. (1992). The electrohydrodynamic deformation of drops suspended in liquids in steady and oscillatory electric fields. *Journal of fluid Mechanics*, 239:1–21.

[121] Vlahovska, P. M. (2011). On the rheology of a dilute emulsion in a uniform electric field. *Journal of fluid mechanics*, 670:481–503.

[122] Voldman, J., Toner, M., Gray, M., and Schmidt, M. (2003). Design and analysis of extruded quadrupolar dielectrophoretic traps. *Journal of electrostatics*, 57(1):69–90.

[123] Welch, S. W. and Biswas, G. (2007). Direct simulation of film boiling including electrohydrodynamic forces. *Physics of fluids*, 19(1):012106.

[124] Windbergs, M., Zhao, Y., Heyman, J., and Weitz, D. A. (2013). Biodegradable core–shell carriers for simultaneous encapsulation of synergistic actives. *Journal of the American Chemical Society*, 135(21):7933–7937.

[125] Yang, L., Banada, P. P., Bhunia, A. K., and Bashir, R. (2008). Effects of dielectrophoresis on growth, viability and immuno-reactivity of listeria monocytogenes. *Journal of biological engineering*, 2(1):1–14.

[126] Zhang, H., Chang, H., and Neuzil, P. (2019). Dep-on-a-chip: Dielectrophoresis applied to microfluidic platforms. *Micromachines*, 10(6):423.

[127] Zhang, J. and Kwok, D. Y. (2005). A 2d lattice boltzmann study on electrohydrodynamic drop deformation with the leaky dielectric theory. *Journal of Computational Physics*, 206(1):150–161.

[128] Zhang, Y., Ho, Y.-P., Chiu, Y.-L., Chan, H. F., Chlebina, B., Schuhmann, T., You, L., and Leong, K. W. (2013). A programmable microenvironment for cellular studies via microfluidics-generated double emulsions. *Biomaterials*, 34(19):4564–4572.

[129] Zheng, B., Tice, J. D., and Ismagilov, R. F. (2004). Formation of droplets of alternating composition in microfluidic channels and applications to indexing of concentrations in droplet-based assays. *Analytical chemistry*, 76(17):4977–4982.

[130] Zhu, Y. and Fang, Q. (2013). Analytical detection techniques for droplet microfluidics—a review. *Analytica chimica acta*, 787:24–35.

[131] Zhu, Y., Zhu, L.-N., Guo, R., Cui, H.-J., Ye, S., and Fang, Q. (2014). Nanoliter-scale protein crystallization and screening with a microfluidic droplet robot. *Scientific reports*, 4(1):1–9.